Applications of Aminated cellulose

By:

Jane Ebosetale Eiyegbenin

Department of Chemistry

McGill University

Montreal, Quebec, Canada

March 2024

A thesis submitted to McGill University in partial fulfillment of

the requirements of the degree of

Doctor of philosophy

Abstract

In this thesis, a new chemical modification of cellulose on the macro, nano and molecular scale was performed and various applications of the modified celluloses were explored. On the macroscale, we synthesized a new cationic cellulose derivative fiber called diaminocellulose fiber (DAmF). DAmF was prepared by a two-step process; first by oxidizing the polymeric chains of pulp by a periodate reaction, followed by a reductive amination reaction to convert aldehyde groups to primary amine. The resulting fiber had a dark brown color, and its amine content was double that of chitosan (a well-known bio-renewable cationic polymer). Like chitosan, DAmF can also be solubilized at low pH which gives the molecular scale form, diaminocellulose (DAmC)

On the nano scale, a new member of the hairy nanocellulose (HNC) family was developed. We refer to this new HNC as aminated nanocrystalline cellulose (ANCC). ANCC consists of a crystalline rod-like body and amorphous cellulose chains (“hairs”) at both ends that contain primary amine groups. To synthesize ANCC, dialdehyde modified cellulose (DAMC) was prepared by partial periodate oxidation of cellulose and subsequently the aldehyde groups of DAMC were converted into primary amines by reductive amination reaction, which yielded diamine modified cellulose fiber (DAmMF). DAmMF were subjected to an acidic hot-water treatment to isolate amine-functionalized hairy nanocellulose.

Finally, DAmF and DAmC were used in the purification of dyed wastewater and in the removal of lead from water and ANCC was used for its anti-microbial property.

Résumé (French abstract)

Dans cette thèse, une nouvelle modification chimique de la cellulose à l'échelle macro, nano et moléculaire a été réalisée et diverses applications des celluloses modifiées ont été explorées. À l’échelle macro, nous avons synthétisé une nouvelle fibre dérivée de cellulose cationique appelée fibre de diaminocellulose (DAmF). Le DAmF a été préparé selon un processus en deux étapes ; d'abord en oxydant les chaînes polymères de la pâte par une réaction au périodate, suivie d'une réaction d'amination réductrice pour convertir les groupes aldéhyde en amine primaire. La fibre résultante avait une couleur brun foncé et sa teneur en amine était le double de celle du chitosane (un polymère cationique bio-renouvelable bien connu). Comme le chitosane, le DAmF peut également être solubilisé à faible pH, ce qui donne la forme à l'échelle moléculaire, la diaminocellulose (DAmC).

À l’échelle nanométrique, un nouveau membre de la famille des nanocelluloses poilues (HNC) a été développé. Nous appelons ce nouveau HNC cellulose nanocristalline aminée (ANCC). L'ANCC se compose d'un corps cristallin en forme de bâtonnet et de chaînes de cellulose amorphes (« poils ») aux deux extrémités qui contiennent des groupes amine primaire. Pour synthétiser l'ANCC, de la cellulose modifiée par du dialdéhyde (DAMC) a été préparée par oxydation périodate partielle de la cellulose, puis les groupes aldéhyde de la DAMC ont été convertis en amines primaires par réaction d'amination réductrice, ce qui a donné une fibre de cellulose modifiée par une diamine (DAmMF). Les DAmMF ont été soumis à un traitement acide à l'eau chaude pour isoler la nanocellulose poilue fonctionnalisée par une amine.

Enfin, le DAmF et le DAmC ont été utilisés dans la purification des eaux usées teintes et dans l'élimination du plomb de l'eau et l'ANCC a été utilisé pour ses propriétés antimicrobiennes.

Table of Contents

Acknowledgements

I will first thank God for seeing me through this process because this would not have been possible without his love and guidance (what is hard for you to do, it can never exist!).

Professor Theo van de Ven, my supervisor, has been tremendously helpful to me over the years. Because of your positive attitude and can-do attitude toward my work, I was able to reach my full potential and gain scientific self-assurance. Your direction kept me on course, and your confidence in me pushed me to assured greatness. I also want to thank my committee members, Professors Ashok Kakkar and Matthew J. Harrington who provided me with invaluable research advice and insight that greatly aided my approach to problem solving. Your passion for discovery and innovation is contagious.

Over the years, many brilliant researchers worked in the van de Ven lab, and their contributions informed my own. Chouchou Nguyen, who helped me get started and contributed many great ideas, deserves special recognition. Despite your busy schedule, you put in a lot of time and attention into my project. The van de Ven lab would not be the same without the contributions of Md Shahidul Islam, Md Nur Alam, Mohammadhadi Moradian, Kayrel Edwards, Sierra Crammer-Smith, Yiwei Jiang, and Mandana Tavakolian. Your help has been much appreciated.

I am also incredibly appreciative of Roya Koshani and Martin Sichinga. You guys are wonderful, and I thank you so much for all your help and encouragement. You cannot imagine what you have done for me, and words cannot express my gratitude.

Thank you to the McGill Chemistry Department, the NSERC Sustainable Resource Network (SRN) on Green Fibers, the NSERC Strategic Priorities Group (SPG) Centre for Advanced Materials (QCAM/CQMF), and FPInnovations for supporting my research. It is an honour to have

received support from your organisation; institutions like yours are vital to Canada's scientific community.

The Chemistry Department administrative staff, Chantal Marotte, Jennifer Marleau, Lina Alvarez, Chelsea Briand-Pitts provided great help in many instances, especially with the smooth running of my laboratory administrative duties and with the completion of this. I also want to thank prof. Mark Andrew, the internal examiner for taking the time to analyze and correct my initial thesis submission. And thank you for McGill and the chemistry department for giving me a second chance in rewriting.

Finally, I want to thank my family. I would forever be grateful to my mum and dad for their spiritual, financial, and mental support during the course of my studies. Special thanks to my sister Susan, for your unwavering faith in me. You are a real G! and I am lucky to have you. Also, thanks to Iby, my dearest friend. I will forever love you and keep you close to my heart. You started this journey with me, and I am happy to have you end this journey with me. To my partner Ehi, thank you for holding my hands through this process. Special thanks to Isreal, Stephanie Oni, Makan, Omon, Joy, Junior, Stephen, Jennifer, Aunty DD, Silas, Clinton, Henry, Nelson, Chidinma, etc. For all the people I could not mention, thank you for the patience, prayers, love, and support through this journey. I really could not have pulled through without you guys. I will love you and you shall reap the fruits of your investments in me.

Contribution to Original Knowledge

1. Synthesis of Diaminocellulose

   Here we developed a new protocol for functionalizing cellulose with primary amine groups. This involves the periodate oxidation of cellulose pulp followed by a reductive amination reaction in the presence of excess ammonia and absence of water. With this process, we were able to produce diaminocellulose fiber (DAmF) and Diaminocellulose (DAmC) with amine content of 9.5 mmol g^{-1}. We explored their application in wastewater treatment and discovered that DAmF is a green alternative to petroleum-based reusable adsorbent.

2. An addition to hairy nanocellulose - Aminated nanocrystalline cellulose (ANCC)

   Animated nanocrystalline cellulose (ANCC) is a new type of hairy nanocellulose (HNC) that we synthesized. ANCC has polymeric chains sticking out of the ends like "hairs" that contain primary amine groups. This process involves partial periodate oxidation and subsequent reductive amination of cellulose fibers, followed by acidic hot-water treatment and addition of cosolvent to isolate the particles. ANCC is confirmed to be electrosterically stable and shows antibacterial activity, significantly higher against Gram-negative bacteria than Gram-positive ones.

List of Figures

List of Tables

List of Abbreviation

ANCC	Aminated nanocrystalline cellulose
AFM	Atomic force microscopy
AGU	Anhydroglucose units
CFU	Colony-forming units
CNCC	Cationic nanocrystalline cellulose
DAC	Dialdehyde cellulose
DAmC	Diaminocellulose
DAmF	Diaminocellulose fiber
DAmMF	Diamino modified cellulose fiber
DAMC	Dialdehyde modified cellulose
DAMF	Dialdehyde modified cellulose fiber
DCC	Dicarboxylated cellulose
DImF	Diiminocellulose fiber
DLS	Dynamic light scattering
DO	Degree of oxidation
DS	Degree of substitution
eHNC	Electrosterically Hairy nanocrystalline cellulose

ENCC	Electronically stabilized nanocrystalline cellulose
FTIR	Fourier transform infrared spectra
HENCC	Hydrolyzed Electrosterically nanocrystalline cellulose
HNC	Hairy nanocrystalline cellulose
NCC	Nanocrystalline cellulose
NMR	Nuclear magnetic resonance spectroscopy
SEM	Scanning electron microscopy
sHNC	Sterically stabilized hairy nanocrystalline cellulose
SNCC	Sterically stabilized nanocrystalline cellulose
TEM	Transmission electron microscopy
UV-vis	Ultraviolet-visible spectroscopy
XPS	X-ray photoelectron spectroscopy

Chapter 1

THESIS RATIONALE

In materials science, the availability, reusability, and biodegradability of cellulose have provided researchers motivation to investigate this organic biopolymer. Cellulose has frequently been studied for its utility in various industries because of the ever growing need to manufacture materials in a sustainable way. It has gained a lot of attention due to its distinctive physical characteristics, which include high mechanical strength, low mass density, and excellent stability in harsh environments (such as acid or high temperature). Additionally, because cellulose has accessible functional groups, it is easy to functionalize it, in order to modify its chemical properties to suit the required application. Many parts of the world have easy access to various types of carbohydrates and cellulose, which are produced in high abundance by plants, bacteria, and marine life. Due to these outlined reasons, researchers have shown interest in modifying and exploring carbohydrates in various forms in order to employ them for a wide range of unique applications. This thesis contributes to novel derivatives and applications of cellulose.

1.1. Research Objectives

The main goal of this thesis is to develop a protocol for synthesizing aminated cellulose with high amine content and to explore some of its potential applications.

To achieve the main objective, the project was divided into sub objectives as follows:

(a) Develop a protocol for the functionalization of cellulose with primary amine groups

(b) Synthesize the various forms of aminated cellulose and study its properties. The forms of cellulose are cellulose fiber, dissolved cellulose, and cellulose nanocrystals.

(c) Utilize aminated cellulose by taking advantage of its high primary amine content for water purification.

1.2. Outline and Scope of the thesis.

This is a manuscript-based thesis consisting of 1 published paper (Chapters 5)

Chapter 2 provides some information about cellulose and its various derivatives, the main chemical modifications that were used in this thesis, a brief literature review on the use of fibers, dissolved cellulose and nanocellulose for biomedical and industrial applications and some chemical analytical techniques employed to characterize the materials qualitatively and quantitatively.

Chapter 3, we demonstrate the development of the protocol in synthesizing aminated cellulose. Here we synthesized DAmF and DAmC and utilized them in dye removal. We studied the effect of various environmental conditions on dye removal such as ionic strength, pH, etc.

Chapter 4, we used DAmF and its precursor diiminocellulose (DImC) to adsorb lead ions form solution. We studied the effects of pH, time, and concentration on adsorption.

Chapter 5 We employed the protocol in synthesizing a new type of hairy nanocellulose, ANCC and study its properties such as size, morphology, zeta-potential and antimicrobial property against Gram-positive and Gram-negative bacteria.

This chapter has been published (Koshani, R.; Eiyegbenin, J. E.; Wang, Y.; van de Ven, T. G. M., Synthesis, and characterization of hairy aminated nanocrystalline cellulose. *J Colloid Interface Sci* **2022***, 607*, 134-144). The first two authors contributed equally to the paper as evidenced by the attached letter of Roya Koshani.

Chapter 6 provides concluding remarks on the three manuscripts and protocols developed, with suggestions on future work to be done.

1.3. Contribution of Authors.

Chapter 2: Introduction and literature review of cellulose, modifications, and utilization of cellulose-based materials.

Chapter 2 was researched and written entirely by Jane E. Eiyegbenin, with prof. van de Ven helping with final editing of text.

Chapter 3: The removal of anionic dye in wastewater treatment by adsorption on diaminocellulose.

Eiyegbenin, J. E.; Nguyen C.; and van de Ven, T. G. M., The removal of anionic dye in wastewater by treatment by adsorption on diaminocellulose. (To be submitted)

Contributions: Jane Ebosetale Eiyegbenin designed and performed all experiments, characterization, data analysis, wrote the manuscript and supervised Chouchou Nguyen, an undergraduate student who helped in performing the experiment. Theo van de Ven supervised the author, provided input during the research, and edited the manuscript.

Chapter 4: Sorption of lead using diimino- and diaminocellulose.

(b) Eiyegbenin, J. E.; and van de Ven, T. G. M., Sorption of lead using diiminocellulose and diaminocellulose. (To be submitted)

Contributions: Jane Ebosetale Eiyegbenin performed all experiments, characterization, data analysis and wrote the manuscript. Theo van de Ven supervised the author, provided input during the research, and edited the manuscript.

Chapter 5: Synthesis and characterization of hairy aminated nanocrystalline cellulose

Reprinted (adapted) with permission from: Koshani, R.; Eiyegbenin, J. E.; Wang, Y.; van de Ven, T. G. M., Synthesis, and characterization of hairy aminated nanocrystalline cellulose. *J Colloid Interface Sci* **2022**, *607*, 134-144.

Contributions: Jane Ebosetale Eiyegbenin developed the protocol for aminating cellulose, Roya Koshani is the expert in nanocellulose. Jane and Roya Koshani performed all experiments except the antibacterial tests, wrote, and edited the manuscript. Yixiang Wang reviewed and edited the manuscript and Theo G. M. van de Ven supervised the project, provided input during research, and edited the manuscript.

Chapter 6. Conclusions and future work.

Chapter 6 was researched and written entirely by Jane E. Eiyegbenin, with prof. van de Ven helping with final editing of text.

Chapter 2

INTRODUCTION AND LITERATURE REVIEW OF CELLULOSE, MODIFICATIONS, AND UTILIZATION OF CELLULOSE BASED MATERIALS

Cellulose has been extensively researched and modified for industrial, medical, food, etc. applications. Depending on the type of chemical modification and degree of substitution, different forms of cellulose can be obtained and utilized for several applications, namely, fibers (macroscale), cellulose microfibrils (microscale), nanocellulose (nanoscale), and dissolved cellulose (molecular scale). These materials will be discussed below.

2.1. Cellulose fibers – The macroscale

In this section, we discuss cellulose fibers extracted from wood fibers because we used Domtar softwood kraft pulp sheets with 86.8 % Alpha cellulose, 12 % Gamma cellulose, 0.9 % hemicellulose, 0.15 % lignin, and 0.2 % ash in the development of the thesis. This can and will be used interchangeably with pulp.

Wood fibres are long slender hollow cylinders with lengths, widths and wall thickness ranging from 0.5-4 mm, 20-50 µm, and 2-10 µm respectively[1]. They are mostly obtained from branches and tree trunks are composed of 40–60% cellulose, 20–30% lignin, and 10–30% hemicellulose depending on the source[2]. Cellulose serves as the fibre backbone in a hemicellulose and lignin matrix and is primarily responsible for the mechanical strength of wood fibres. Hemicelluloses are branched carbohydrates while lignin is a complex biopolymer composed of varying amounts of three monolignols (p-coumarylalcohol, coniferyl alcohol, and sinapyl alcohol) depending on the source[3]. As illustrated in Fig. 2- 1, wood fibers are composed of bundles of cellulose microfibrils which are bundles of cellulose nanofibrils.

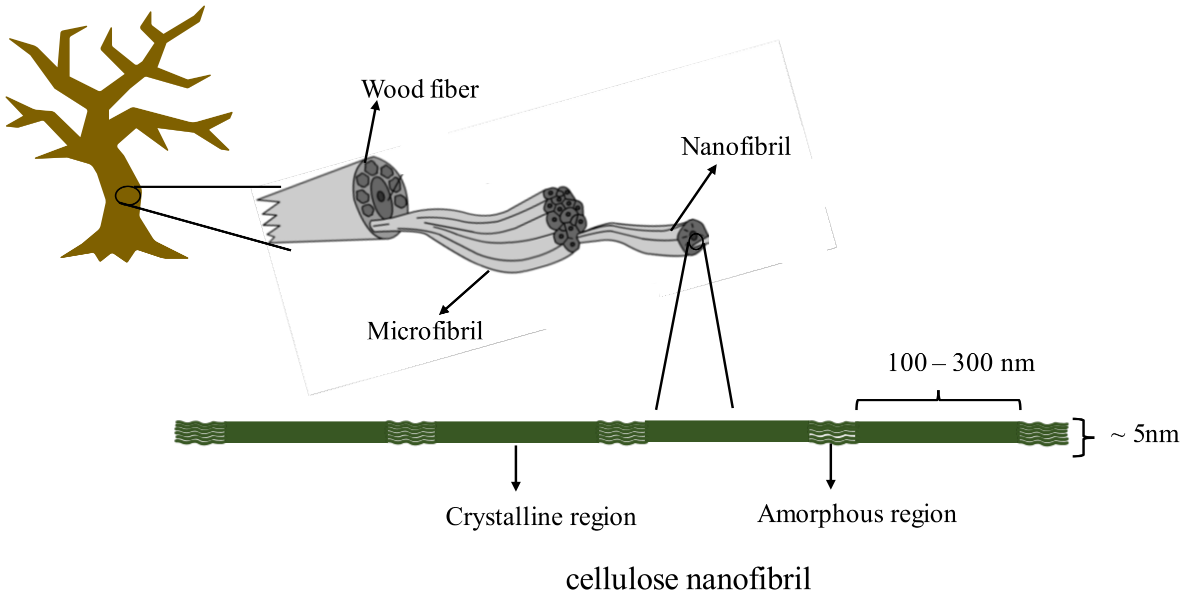

Fig. 2- 1. Schematic representation of the hierarchy of cellulose from macroscopic down to the nano level (nanofibrils (4-10 nm), microfibrils (50-100 μm), and wood fiber (2-3 μm)). Ref[4] with some modifications

In wood fiber as shown in Fig. 2- 2, there are three layers that surround the lumen (the hollow cavity inside the fibre). Moving outward from the lumen, the secondary layer (S) is the first layer that consist mostly of cellulose and hemicellulose and this layer is subdivided into S1, S2 and S3. The outer most layer is the primary wall that contains predominantly lignin. The fibers in wood are separated by the middle lamella, which is almost entirely lignin and binds the neighbouring cells.

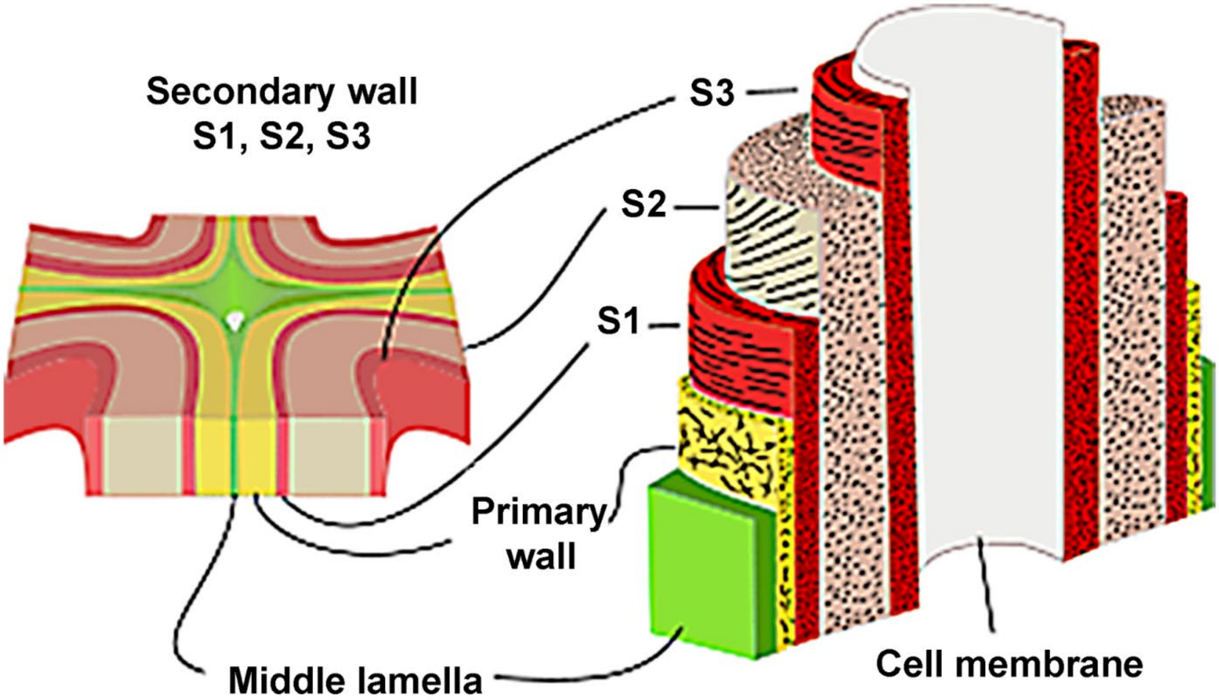

Fig. 2- 2. Different layers in cell wall of a wood fiber[5]. Copyright © 2022 American Society of Plant Biologists

One of the most common methods for producing cellulose fibres (a.k.a. pulp) is by kraft pulping and bleaching process. Kraft pulping is a process of treating wood fibers with sodium hydroxide and sodium sulfide under pressure to dissolve lignin without disrupting the cellulose backbone as much as possible[6]. A bleaching step is then performed to remove any residual lignin and achieve brightness. This results in a loss of 20-30% in total weight of the original fiber and a more porous structure is attained, considerably improving chemical accessibility. After the pulping process, only the S layers survive, and consequently, when kraft fibres are utilised as a starting material like in this thesis, it is only the S layer that is being studied[7]. This S layer consists of microfibrils which are bundles of nanofibrils with alternating amorphous and crystalline regions with a degree of polymerization up to 20,000 units and varying crystalline sizes depending on the source[8]. At room temperature and pressure, its high degree of H-bonding makes cellulose fiber insoluble in water or dilute acids and alkalis.

2.2. Cellulose Microfibrils – The microscale

Cellulose microfibrils are hierarchical structures formed by the aggregation of cellulose nanofibrils[9]. They have lateral dimensions of up to 100 nanometers and axial dimensions of micrometers[10]. Within plant cell walls, cellulose microfibrils provide the structural framework that contributes to the mechanical integrity of the plant. These microfibrils consist of bundled nanofibrils, held together by hydrogen bonding, and van der Waals forces (nanofibrils is discussed in section 2.3.1). The arrangement of cellulose microfibrils contributes to the unique properties of various natural materials, including wood, cotton, and other fibrous plant tissues.

2.3. Nanocellulose – The nanoscale

Nanocellulose is a fibrous material with at least one dimension on the nanometric scale (1-100 nm), with interesting properties such as large specific surface area (typically >30 m^2g^{-1} depending on the type[11]), aspect ratios, and simple surface functionalization[12]. With the advancement in nanotechnology, nanocellulose has attracted the interest of researchers all over the world due to its low cost, biocompatibility, renewability, exceptional reactivity, and ideal physical properties such as light weight, high stiffness, tensile strength, strength-to-weight ratio, optical transparency, and low thermal expansion[13, 14]. Depending on the source of cellulose and processing conditions, cellulose nanostructures have been classified into four distinct groups: cellulose nanofibrils also called cellulose nanofibers (CNFs)[15], Cellulose nanocrystals (CNCs)[16], bacterial nanocellulose (BNC)[17], and hairy nanocellulose (HNC)[18]. However, we only discuss CNFs, CNCs and HNCs as they can all be produced from cellulose fibers. In BNCs synthesis, it is a bottom-up approach with the use of bacteria such as *Acetobacter* to synthesize pure nanocellulose unlike the others which are plant derived and the focus of this thesis [19].

2.3.1. Cellulose Nanofibrils

Cellulose nanofibrils (CNFs) also known as nanofibrillar cellulose or cellulose nanofibers are micron-sized fibres with nano-dimension cross sectional structures or nano-sized fibres that are less than 100 nm wide, but typically around 5nm[20]. Due to CNFs retaining both its crystalline and amorphous regions, they have longer length with high aspect ratios (length to diameter) in comparison to CNCs or HNCs[21]. CNFs has been used in different applications such as additives in coating[22], hydrogels[23], rheological modifiers[24], etc. They can be extracted through mechanical disintegration of cellulose fibers by high pressure homogenization[25, 26], ultra-fine friction grinding[27], refining process[28], twin-screw extrusion[29] high speed grinding[30], ultrasonication[31], cyrocrushing[32], ball milling[33] or aqueous counter collision (ACC)[34].

They can also be manufactured chemically. Chemical processes involve first loosening the crystalline domains and interfibrillar interactions in cellulose raw materials before facile mechanical separation into nanofibrils[35]. The most common chemical process, TEMPO (2,2,6,6-tetramethylpiperidin-1-oxyradical) catalytic oxidation is performed with a combination of TEMPO, NaBr and NaClO in water at pH 10 – 11. This reaction selectively oxidizes the hydroxyl groups on the C_6 position to carboxylate salt via aldehydes on the surface of the crystalline regions of the fibrils[36]. The introduction of carboxylate salts creates negative charges on the fibril surface which helps to repel and stabilize fibrils in suspension when they are separated from the fibril bundles through subsequent mechanical refining such as blending or high-pressure homogenization[37]. The resulting nanofibrils have a narrow size distribution. Other chemical processes similar to TEMPO to produce CNFs is by carboxymethylation[38] and periodate-chlorite oxidation[39] that also introduces carboxylates on the fibril surface. Other chemical processes include sulfonation[40], quaternization[41], solvent-assisted pretreatments[42-44]

2.3.2. Cellulose nanocrystals (CNCs)

Cellulose nanocrystals (CNCs) also called nanocrystalline cellulose (NCC) are rigid cellulose nanorods measuring 3-10 nm in width and 100-200 nm in length[45]. CNCs are synthesised through the hydrolysis of the amorphous regions in the cellulose chains leading to the liberation of nanocrystals[46]. The synthesis of CNC is most commonly achieved through sulfuric acid-mediated hydrolysis. This method involves the use of sulfuric acid to break down the amorphous cellulose segments and hydrolyze the glycosidic bonds, while simultaneously esterifying the surface hydroxyl groups to form sulfate half-ester groups. A study by Mukherjee and Woods identified the concentration of sulfuric acid (specifically 64 wt. %) as an important factor in producing sulfated cellulose nanocrystals (sCNC, see Fig. 2- 3a)[47]. Other acids have also been used for this process such as phosphoric acid[48], hydrobromic acid[49], hydrochloric acid[50], maleic acid[51], etc. Currently, several companies produce sCNC using forestry pulp feedstocks. Some notable ones include Alberta-Pacific Forest Industries, GranBio, and the industry-leading Celluforce. These companies utilize sulfuric acid hydrolysis to produce sCNCs on a large scale. In Canada, Anomera and Blue Goose Biorefineries are the leading industrial producers of CNCs specifically carboxylated cellulose nanocrystals (cCNCs – see Fig. 2- 3d). Anomera utilizes a hydrogen peroxide-assisted method while Blue Goose Biorefineries uses a transition-metal-catalyzed process[52, 53]. Carboxylated cellulose nanocrystals (cCNCs) exhibit comparable colloidal stability, uniform nanoscale lengths, and high crystallinity to sulfated cellulose nanocrystals (sCNCs). Like the sulfate half-ester groups found in sCNCs, cCNCs possess carboxyl groups that enhance the electrostatic repulsion between neighboring CNCs, preventing their aggregation. An intriguing characteristic of cCNCs is the potential for these carboxyl groups to undergo further reactivity, allowing for surface modifications that can customize the properties of the nanomaterial to suit specific downstream applications[54]. Some other non-acid hydrolysis methods to produce CNCs include the use of TEMPO-H_2O_2[55], ammonium persulfate[56], ionic liquids[57-59], enzyme[60], and deep eutectic solvents (DES)[61].

In our lab, we developed a new class of nanocellulose known as hairy nanocellulose (HNC). Unlike the CNCs described in the previous paragraphs, HNCs consist of crystalline rods (which we refer to as NCC) with amorphous regions protruding from both ends. HNCs are produced via a partial oxidation of cellulose fibers using periodate followed by either chlorite oxidation or reductive amination [62].

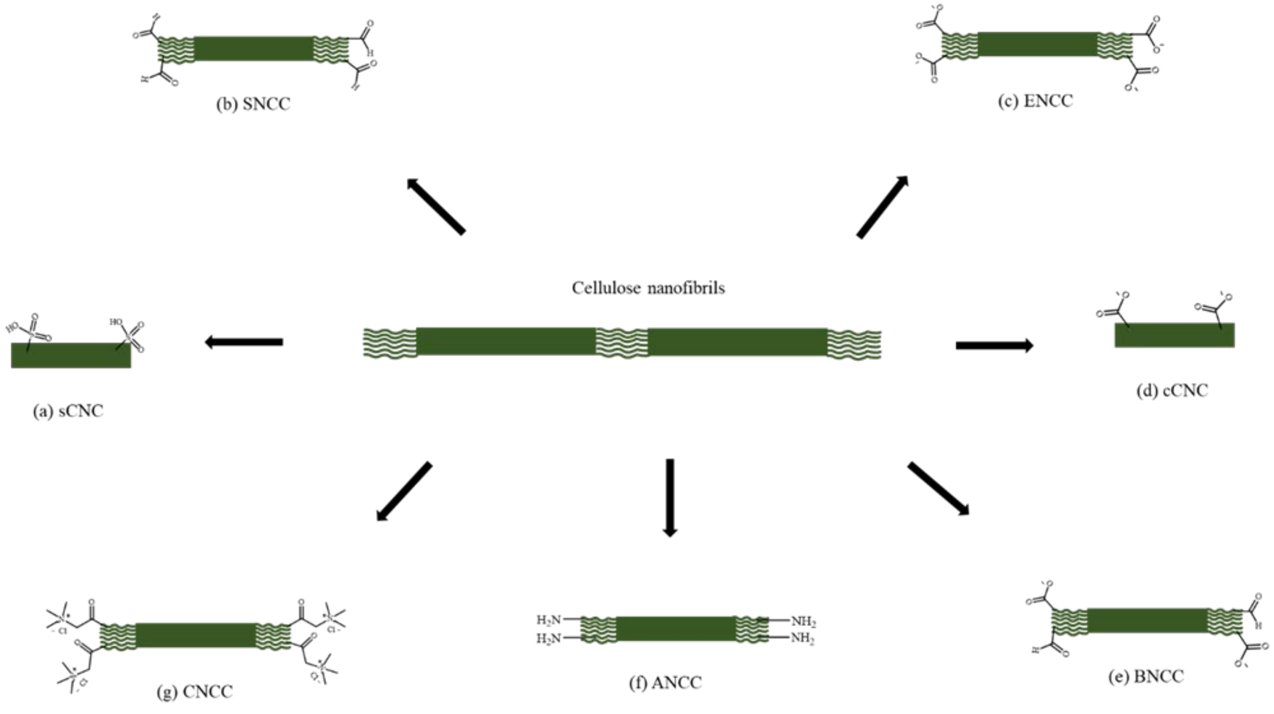

Fig. 2- 3. Diagram showing the different types of CNCs and HNCs made from cellulose nanofibril. The various HNCs are discussed in the text below.

2.3.3. Hairy nanocrystalline cellulose (HNC)

The van de Ven research group developed a new class of nanocellulose called hairy nanocellulose (HNC). HNCs can also be considered as nanocrystalline cellulose (NCC) because these particles contain both a crystalline region with polymeric amorphous chains sticking out its ends like "hairs"[63]. Hairy nanocelluloses are rod-shaped particles that are 100-200 nm long and 5-10 nm wide and can withstand high ionic strength without flocculation[64]. HNC synthesis involves partial sodium periodate oxidation of pulp in which the C_2-C_3 bonds of the glucose chains are broken, thereby cleaving the cellulose chains in the amorphous region. These amorphous chains are kinetically accessible and can be functionalized with different functional and charge groups.

The types of HNCs that have been synthesized so far are illustrated in Fig. 2- 3: (b) sterically stabilised hairy nanocellulose (SNCC) is a neutral HNC functionalized with aldehyde groups, which are highly reactive and can be used as an intermediate to react with other compounds or functional groups[65]; (c) electrosterically stabilised hairy nanocellulose (ENCC) is functionalized with carboxyl group which has a negative charged and a carboxylic content of about 6 mmol per gram[63]; (e) bifunctional nanocrystalline cellulose (BNCC) is functionalized with both carboxyl and aldehyde groups[66]; (f) aminated nanocrystalline cellulose (ANCC) is functionalized with primary amine groups and has an amine content of 5.5 mmol per gram[67]; (g) cationic nanocrystalline cellulose (CNCC) is functionalized with quaternary amine[68]. SNCC in solution is stabilized by the steric repulsion between the polymeric chains while ENCC, CNCC, BNCC and ANCC are stabilised by both steric and electrostatic repulsions (a.k.a. electrosterically stabilized HNCs (eHNC)). Fibres functionalized with carboxyl groups must have a minimum charge content of 3 meq per gram to spontaneously disintegrate into nanocellulose without mechanical or heat treatment, while fibres functionalized with aldehyde or amine groups need heat treatment [69]. It must be emphasized that the charge content of HNCs can be tuned by trimming the hairs via acid hydrolysis.

In comparison to CNCs, HNCs show a higher stability at high ionic strengths as shown by Lenfant, et al. (2017)[70]. In this study, the stability of sCNC and ENCC suspensions (both negatively charged) were studied at various monovalent (Na^+) and divalent (Ca^{2+}) salt concentrations. It was demonstrated at sCNCs form gels at low salt concentrations (ionic strength I = 20 mM) due to agglomeration while ENCC could withstand much higher salt concentrations. Precipitation occurred with Na^+ at I = 200 mM and gelation with Ca^{2+} due to bridging of the carboxyl groups when $[Ca^{2+}] = [COOH]/2$.

We can measure the size and morphology of HNCs by AFM and TEM, but the protruding hairs on HNCs cannot be detected by these techniques. The presence of the hairs can be concluded from the hydrodynamic size variations of these particles under specific conditions. When electrosterically stabilized HNCs (ENCC, CNCC, ANCC) are placed in varying ionic strengths solutions,[64, 67, 68] or a cosolvent (e.g. propanol) is added to sterically stabilized HNC (SNCC) solution[65], we can measure the change in particle size by dynamic light scattering (DLS). For example, when salt is added to ENCC, the ions partially screen the charges and "folds" the hairs of these particles (reduces their expanded state), thereby decreasing their effective diameter. After full charge screening, ENCC starts to aggregate at a specific salt concentration (~2 M). This method can confirm the presence of hairs, but not their position, therefore, a few studies have been performed on hydrolyzed ENCC (HENCC). HENCC, when cross-linked with diamine or azide–alkyne showed that the particles formed end-to-end linkages, thus proving that the carboxyl groups were located in the protruding hairs[71]. In another study, a micro-sized network was formed from covalently linking positively charged PAMAM dendrimers to HENCC particles, to which negatively charged latex beads were attached. AFM images showed the latex beads were predominantly located at the extremities of HENCC particles where PAMAM dendrimers resided, confirming again that the hairs are located at both ends of the particle[72].

2.4. Dissolved cellulose – The molecular scale

In this thesis, we define dissolved cellulose as a cellulose derivative that is completely soluble in water and has no crystallinity, we consider this as "cellulose at the molecular scale". As earlier mentioned, cellulose is insoluble in water and in most solvents, but can be made soluble with chemical treatment or modifications. Dissolved celluloses are useful in numerous applications such as making of gels (hydrogels, sol-gels or aerogels)[73], as natural dispersants, flocculants[74], emulsifiers[75], thin film fabrication[76], etc.

Solubilization of cellulose can be done in three ways; solubilization in solvent (such as ionic liquid[77]), solubilization of cellulose chains as a by-product of nanocellulose synthesis[78] and solubilization by chemical modification of cellulose pulp. We would only emphasize solubilization by chemical modification as that is the focus of this thesis.

One of the most successful ways to dissolve cellulose is via the viscose process. This process developed by Cross et al. converts cellulose to cellulose xanthate by a reaction with carbon disulfide in sodium hydroxide, and this derivative is soluble in a NaOH solution[19]. Although the process is widely used today, the process is environmentally tasking and harmful to human health due to the liberation of CS_2 which has led to documented hysteria[79], developments of coronary heart disease[80], strokes[81], leukemia[82], etc. among factory workers. In addition, it has been uncovered that the main viscose suppliers, who are primarily located in Asia, dump untreated CS_2 wastewater into neighbouring lakes and rivers, jeopardising the livelihoods of residents[83].

Therefore, extensive research has been done on environmentally friendlier methods of dissolving cellulose.

Introducing hydrophilic groups on cellulose can result in dissolution but to achieve amorphization of cellulose, the degree of substitution has to be high so as to completely disrupt the intra- and inter- hydrogen bonds holding the polymeric chains together. Such modifications are mentioned in section 2.6.

2.5. Cellulose – The building block

In this section, we will discuss the biopolymer, cellulose, which serves as the building block for the materials discussed in sections 2.1 - 2.5. Cellulose is a natural, highly insoluble polymer consisting of repeating units of cellobiose as shown in Scheme 2- 1. This monomer is 1.03nm in length and is a dimer of glucose (also called D-anhydroglucopyranose unit (AGU)) linked via a β (1→4) glycosidic bond[84]. The number of β 1-4 glycosidic bonds determines the degree of polymerization (DP), which is in the range of 10, 000 and 15,000 depending on the material from which the cellulose is sourced [85].

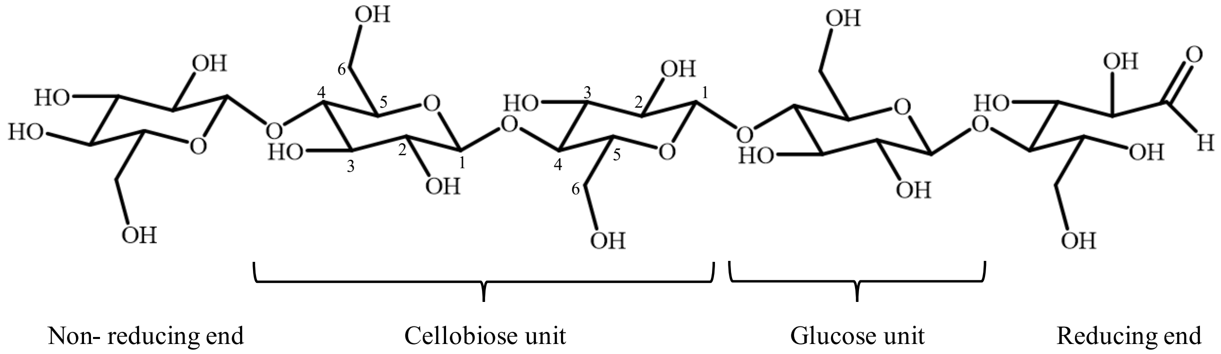

Scheme 2- 1. Molecular structure of a cellulose unit, showing the cellobiose repeat unit, the glucose monomer and reducing and non-reducing end. Ref[86] with some modifications

The ends of the cellulose chain are chemically distinct with one end having a free OH-group at C4 (nonreducing end), while the other end has reducing properties and a free hemiacetal or aldehyde group at the C1 position[87]. The hydroxyl groups on C2, C3 and C6 give the structure chemical reactivity and hydrogen bonding (inter- and intramolecular), in addition to self assembly in crystalline and amorphous regions, which is taken advantage of in both chemical and physical modifications[88-90]. Infrared and C-Nuclear Magnetic Resonance investigations of native cellulose indicated that intramolecular H-bonds are formed between the OH-group at C3 and the neighbouring ether oxygen (O5) of the AGU, and between the OH-group at C6 and the adjacent OH-group of C2. Intermolecular bonds, on the other hand, are generated primarily between the OH-group at C6 and the oxygen atom in C3 of nearby cellulose chains[91]. These bonds are illustrated in Scheme 2- 2.

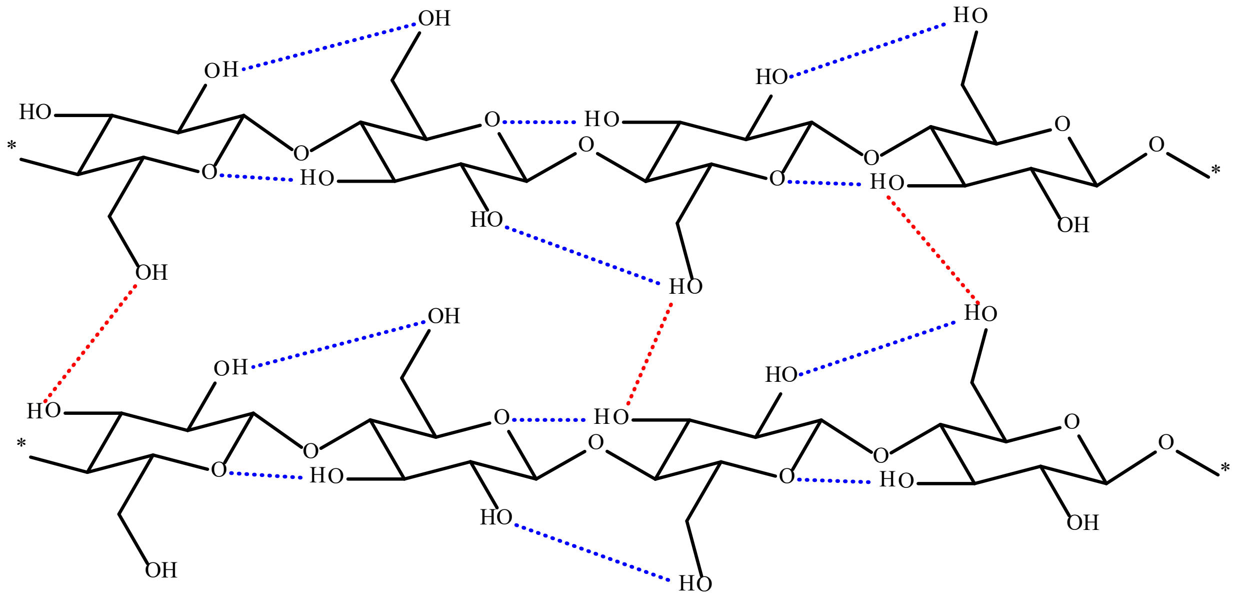

Scheme 2- 2. Intramolecular (- - - -) and intermolecular (- - - -) hydrogen bonding networks in cellulose structure. Ref[12] with some modifications.

This biopolymer can be found in nature in wood, plants, animals, algae, fungi, and bacteria, with wood and cotton being the two most abundant sources of cellulose[92]. It is also one of the most abundant material on earth and the most common organic polymer, representing about 1.5 x 10^{12} tons of the annual biomass production. Cellulose is considered an almost inexhaustible source of raw material for the increasing demand for environmentally friendly and biocompatible products [93, 94]. As a naturally important material, cellulose has been the subject of extensive research into its formation, chemical and physical structures, isolation and purification, and chemical modifications. These studies have resulted in a better knowledge of its nature, behaviour, and the development of value-added products in modern society.

Modification of cellulose is usually done on the hydroxyl groups on carbons at positions 2, 3, and 6 which have different reactivities. The extent to which these are modified greatly influences the chemical and physical properties of the cellulose derivative. As a result, a method for determining the average degree of substitution (DS) based on polymerization degree and probability of attaching to C2, C3, and C6 atoms was developed. The degree of substitution (DS) in cellulose refers to the average number of substituent groups attached per base unit of cellulose (substitution of OH group at the three positions). It provides information about the extent of chemical modification or derivatization of cellulose[95]. The maximum DS that can be achieved is 3 (~18.5 mmol g^{-1}), this implies that all three OH groups have been substituted. When oxidation reaction is performed on cellulose, the degree of oxidation (DO) can be used in place of DS.

2.6. Modifications of Cellulose

Chemical modification can be done to an extent to which the fibers are intact and insoluble in water, and this can be advantageous in textile making, paper making, manufacture of water purification adsorbent, wood and metal coating, thin film fabrication, antimicrobial wound dressing etc. Some of these modifications include.

1. Carboxylation by carboxymethylation[15], periodate-chlorite oxidation[16], TEMPO-mediated oxidation[17], etc. This introduces negative charges on pulp because carboxylic acids have pK_a in the range of 1.5-5[96]; therefore, DS should be less than 0.5 to prevent the dissolution of fibers at room temperature and neutral pH.
2. Amination by grafting[18] or direct synthesis (to be discussed later on). This introduces positively charged amines on the fibers, but DS can be higher because simple alkyl amines are generally weak bases (pK_aH in the range of 9.5-11)[97] and therefore would not have a high charge content at neutral pH.
3. Other modifications include esterification[98], etherification[99], nitrification[100], silylation[101], polymer grafting[102], phosphorylation[103], thiolation[104], etc.

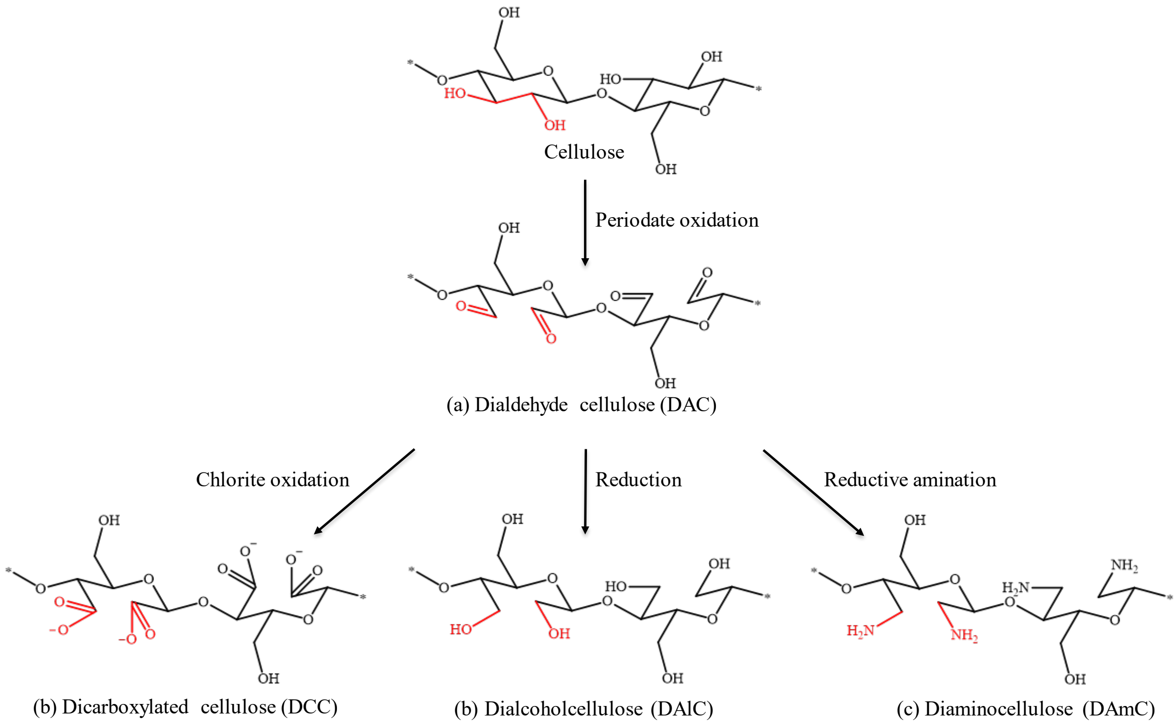

Scheme 2- 3. Flow diagram showing some modification on the cellobiose monomer of cellulose.

2.6.1. Periodate oxidation

The base reaction for the amination reactions performed on cellulose in this thesis is the periodate reaction. This reaction is a stereospecific oxidative cleavage of 1,2-diols that results in the creation of two carbonyl compounds, aldehydes or ketones, by the formation of a cyclic intermediate that results in the cleavage of the C-C bond[105]. Scheme 2- 4 depicts the simplified mechanism of the oxidation of cellulose (carbohydrates) by acting on the hydroxyl groups in the 2,3-positions, resulting in anhydro D-glucopyranose ring opening and the formation of 2,3-dialdehyde cellulose (DAC). The degree of oxidation (DO) is controlled by the amount of periodate used and/or the time of reaction. The DO determines the physical and chemical properties of the produced DAC. The more reactive aldehyde groups are further explored to make various products for different applications, i.e., water purification and textiles [88, 89].

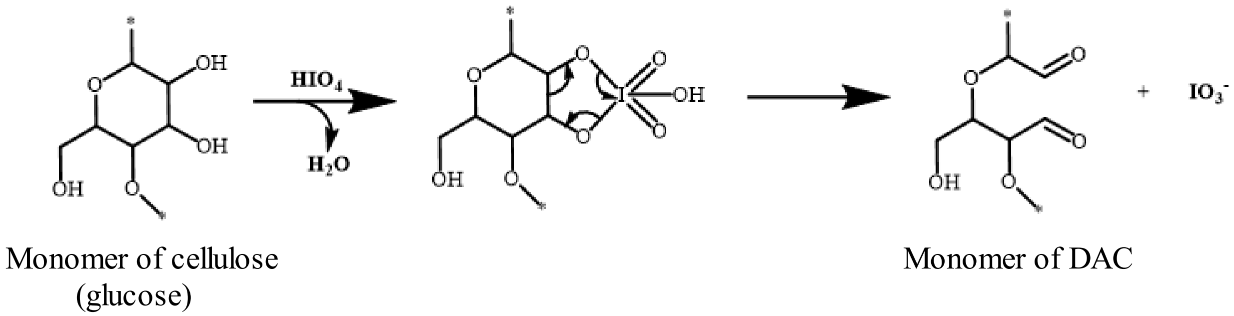

Scheme 2- 4. Mechanism for periodate oxidation reaction of a glucose monomer of cellulose

One major drawback of this reaction is the high cost of periodate. This can be combated by regenerating periodate chemical by secondary oxidation agents or electrochemical reactions. The electrochemical regeneration of periodate has been explored in production of dialdehyde starch[106]. Electrochemical oxidation is not ideal for periodate regeneration due to high operating costs and electrode sensitivity. Electrode sensitivity may also be related to the partial breakdown and degradation of cellulose (and other polysaccharides) during periodate oxidation, resulting in regeneration difficulties. It has been shown that under mild oxidation conditions (A.C ≈ 0.4 mmol/g) hypochlorite has been used as a secondary oxidation agent to regenerate 100 % of used periodate[107]. The regenerated periodate had the same oxidation capability as in the first cycle. However, when the oxidation duration (and hence the aldehyde concentration) was increased, regeneration efficiency declined significantly. It was thought that the loss in regeneration efficiency was related to the production of a small fraction of dissolved cellulose degradation that could not be eliminated by ultrafiltration. However, hypochlorite was shown to be a good chemical for periodate regeneration and might reduce the cost of the oxidation phase from around 16,500 €/ton to approximately 450 €/ton. The study using ozone was also very promising as it was able to regenerate 90% periodate quite rapidly at high pH (pH ≥ 13)[108].

Periodate reaction of cellulose can be used to produce DAC fiber on a macro scale, SNCC on a nano scale and dissolved DAC on a molecular scale.

2.6.1.1. Dialdehyde cellulose (DAC) and dialdehyde modified cellulose (DAMF) fibers.

The periodate oxidation reaction product, 2,3-dialdehyde cellulose is fibrous and insoluble in water at room temperature and its look and texture is similar to pulp. Fully oxidized product has a degree of oxidation (DO) = 2 which translates to an aldehyde content of 12.5 mmol g^{-1}. This means that the two hydroxyl groups on C_2 and C_3 of each monomer in the polymeric chain have been converted to aldehyde groups (see (a) in Scheme 2- 3). Depending on the degree of oxidation, the product can be referred to as DAC with an aldehyde content (AC) ≥ 9.0 mmol g^{-1} or dialdehyde modified cellulose fiber (DAMF) with AC of 3 - 8 mmol g^{-1}. Due to the higher aldehyde content, DAC fiber has reduced hydrogen bonding, is more reactive than cellulose, highly soluble at > 60 °C and cannot be mercerized. Mercerization is a process that involves treating cellulose with a strong alkali solution to improve tensile strength, luster, hygroscopic property, dye uptake, etc. of the fabric[109]. During periodate reaction, severe depolymerization occurs which leads to a decrease in crystallinity and structural integrity which is integral for mercerization[110, 111]. DAMF with low DO (~3 mmol/g) has a very low solubility at >60 °C and retains similar chemical properties to cellulose due to a low degree of modification. Solubility via mercerization can be achieved without decomposition[88]. From now on, wherever DAMF is mentioned, we mean DAMF with an AC ~6.5 - 8 mmol g^{-1} (DO ~ 1-1.3)

The ability to further modify DAC and DAMF fibres to incorporate carboxylic acid, alcohol, and primary amine groups is just one benefit of the aldehyde groups' reactivity, which is further discussed in this chapter. The fibres have also been used to remove dyes.[112]

2.6.1.2. Sterically stabilized nanocrystalline cellulose (SNCC)

SNCC is a type of hairy nanocellulose that has aldehyde groups on the hairs protruding from its ends. DAMF is synthesized and solubilized at high temperature after which propanol is added into the solution to precipitate out SNCC[65]. This HNC is sterically stable in water because the protruding polymeric chains creates an entropic repulsion between the nanoparticles. SNCC has been successfully used to develop antibacterial wound dressing[113].

2.6.1.3. Dissolved dialdehyde cellulose (DDAC)

Dissolved DAC is produced by heating DAC with high DO at 80 °C for 1 hour at which all the fibers go into solution. The process is irreversible upon cooling, as the solubilized product is thermodynamically stable [114]. DDAC is a robust polymer with a wide variety of applications. It has been studied as a natural based adhesive for wood to replace fossil based adhesives[115]. With the ability to form cross-linked structures, DDAC has also been used in fabricating thin films[116], vitrimers[117], hydrogels[118] and aerogels[119].

2.6.2. Periodate oxidation - chlorite oxidation reactions

After periodate oxidation on cellulose pulp to produce DAC fiber, an oxidation reaction with sodium hypochlorite can be used to convert the aldehyde groups to carboxylate groups. Scheme 2- 3(b) shows this modification on the cellobiose monomer. This reaction produces HCl as a byproduct as shown in mechanism in Scheme 2- 5 below, therefore the pH of the solution has to be monitored and maintained above 5 to ensure that the reaction goes to completion.

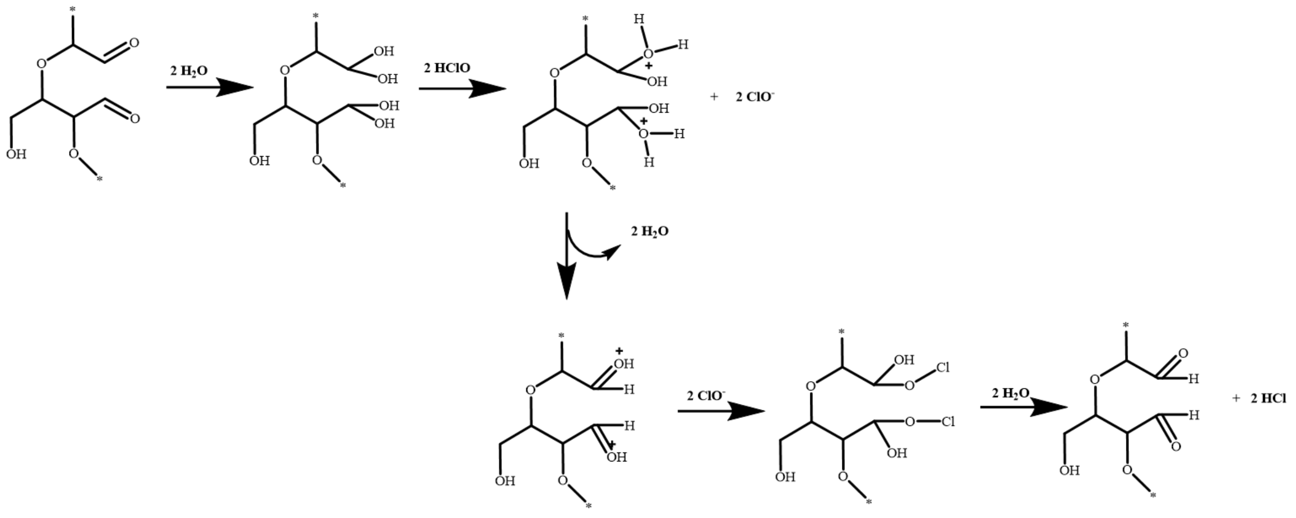

Scheme 2- 5. Mechanism for chlorite oxidation reaction

Because this reaction introduces negative charges in the fiber, dissolution occurs and therefore we can produce ENCC on a nanoscale and DCC on a molecular scale.

2.6.2.2 Electrostatically stabilized nanocrystalline cellulose (ENCC)

Chlorite oxidation of DAMC fibers lead to the introduction of negative charges on the fiber leading to dissolution. ENCC is produced when a cosolvent such as ethanol is added to the solution to precipitate ENCC[120]. ENCC is a type of HNC that has carboxylic groups in the amorphous chains protruding from its ends (see (c) in Fig. 2- 3). This HNC is electrosterically stabilized by steric repulsion of the polymeric chains and electrostatic repulsion via the negatively charged carboxyl groups.

2.6.2.1. Dicarboxylated cellulose (DCC)

DCC is an anionic soluble polymer synthesized from the chlorite oxidation of DAC fibers. DCC is completely amorphous, as this modification causes a decrease in crystallinity and molecular weight which can be advantageous[121]. Structure-property relationship of polymer studies show that amorphous and low molecular polymers are more biodegradable than crystalline and high molecular weight polymers[122]. DCC has been used to make functionalized hydrogels and aerogels. Its anionic property makes it useful in absorbing positively charged compounds such as cationic dyes[123], heavy metals[124], clay[125], etc.

2.6.3. Periodate oxidation - reductive amination

Here in lies the focus of this thesis, where we introduce primary amine groups on cellulose. To the best of our knowledge, this type of diaminocellulose has never been synthesized before. In previous research, primary and secondary amine compounds underwent successive oxidation and reductive amination processes to successfully link secondary and tertiary amines to cellulose strands. However, primary amines are more useful because they are more reactive and easily functionalized[126, 127]. As previously documented, attaching primary amines to cellulose chains with diamine-compounds is inefficient in creating primary amines since it results in low primary amine content due to cross-linking[128].

After periodate oxidation of pulp to DAC, the aldehyde groups are reacted with excess ammonia through a Schiff base reaction to produce imine groups. After which a reduction reaction with $NaBH_4$ converts the imine bonds to amine, thereby producing primary amine groups. A simplified reaction scheme is shown in Scheme 2- 6 below.

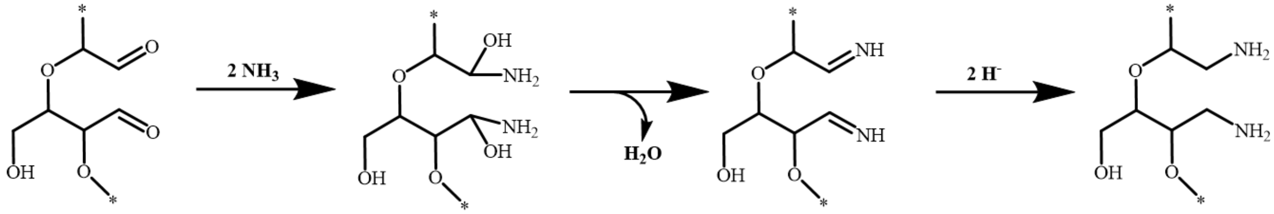

Scheme 2- 6. Mechanism for reductive amination reaction

This reaction can be used in producing DAmF on a macroscale, ANCC on a nano scale and DAmC on a molecular scale.

2.6.3.1. Diaminocellulose fiber (DAmF)

DAmF is made from the reductive amination of DAC and the resulting fiber is a brown and insoluble in water at room temperature. Like chitosan, the solubility can be increased by acid and/or heat treatment. It is soluble at low pH when charges are introduced via the protonation of the amine groups.

2.6.3.2. Aminated nanocrystalline cellulose (ANCC)

ANCC is a type of hairy nanocellulose that has amine groups on the hairs protruding from its ends. DAMF is synthesized followed by a reductive amination reaction. The product diamino modified cellulose fiber (DAmMF) is solubilized at 60 °C and pH 3, after which propanol is added into the solution to precipitate out ANCC[67]. ANCC is electrosterically stable in water because the polymeric chains coupled with cationic amine groups create entropic and electrostatic repulsion between the nanoparticles.

2.6.3.3. Dissolved diaminocellulose (DAmC)

DAmC is produced by heating DAmF at 60 °C for 1 hour at pH 3 at which all the fibers go into solution. The process is irreversible upon cooling, as the solubilized product is thermodynamically stable via electrostatic stabilization. DAmC is a robust polymer that can be used in fabricating thin films and gels.

2.7. Applications of cellulose-based materials.

Going forward, the term cellulose-based materials refer to every form of cellulose including cellulose fiber, nanocellulose, cellulose composites, hydrogels, aerogels, etc.

2.7.1. Water treatment

Water is one of the most basic necessities for life to exist. According to the United Nations, the world's estimated population of 8 billion in 2022 is putting increasing strain on the world's limited water resources[129]. However, even as more water is consumed, the quality of water is deteriorating due to the massive amounts of pollutants dumped into the world's river systems, lakes, and oceans every day. Heavy metals, dyes, and oils are some of the contaminants that are contributed by industries[130]. It is imperative that treatments are developed to adequately remove these toxic substances.

Wastewater treatment technology was designed to treat and clean wastewater based on type and extent of contamination while being cost-effective. Water treatment systems have evolved from conventional media filters to high-efficiency centrifuge filters, disc filters, membrane filtration (micro and ultra-filtration), and non-membrane filtration systems[131]. However, traditional materials and wastewater treatments have failed to meet environmental standards and have been ineffective in removing heavy metals at low concentrations in some instances[132].

The use of natural fibres as raw materials is becoming increasingly popular as people become more concerned about environmental sustainability. In recent years, bio-based materials have seen increased demand in the market and industries[133]. Natural fibers are non man-made fibers that are derived from plant or animal sources such as lignocellulose, chitin, etc[134]. One of the most utilized natural fibers is cellulose due to its abundance, high porosity, non-toxicity, good mechanical properties, biocompatibility, and biodegrability[135].

2.7.1.1. Dye adsorption.

Dyes are a significant category of pollutants that have a detrimental impact on the environment, particularly when they enter aquatic systems[136],[137]. The complex molecular structure of dyes, along with their synthetic origins, makes them highly stable and resistant to degradation[138]. As a result, the presence of dyes in water bodies can render it unsuitable for use and poses challenges for water treatment processes. Dyes are extensively used in industries such as textiles, cosmetics, printing, and plastics to add color to products, resulting in the generation of a large volume of colored wastewater[139]. The persistence of dye molecules in aquatic environments can be attributed to their low biodegradability, resistance to photolysis and oxidizing agents[140]. This persistence further contributes to the environmental impact of dyes.

Dyes can be broadly classified into two types: natural and synthetic. Natural dyes are derived from sources such as plants, animals, minerals, and insects without undergoing chemical treatment[141]. On the other hand, synthetic dyes are chemically synthesized and are highly stable and toxic to living organisms[142]. Commercial synthetic dyes can be classified in various ways, such as based on color, chemical structure, or application methods[143]. One method of classification is based on their charge after dissolution in aqueous medium. Dyes can be categorized as cationic (positively charged), anionic (negatively charged), or non-ionic (no charge). This classification helps understand the affinity of different dyes towards different types of fibers and the dyeing process conditions. Fig. 2- 4 shows some toxic effects of these dyes on human health.

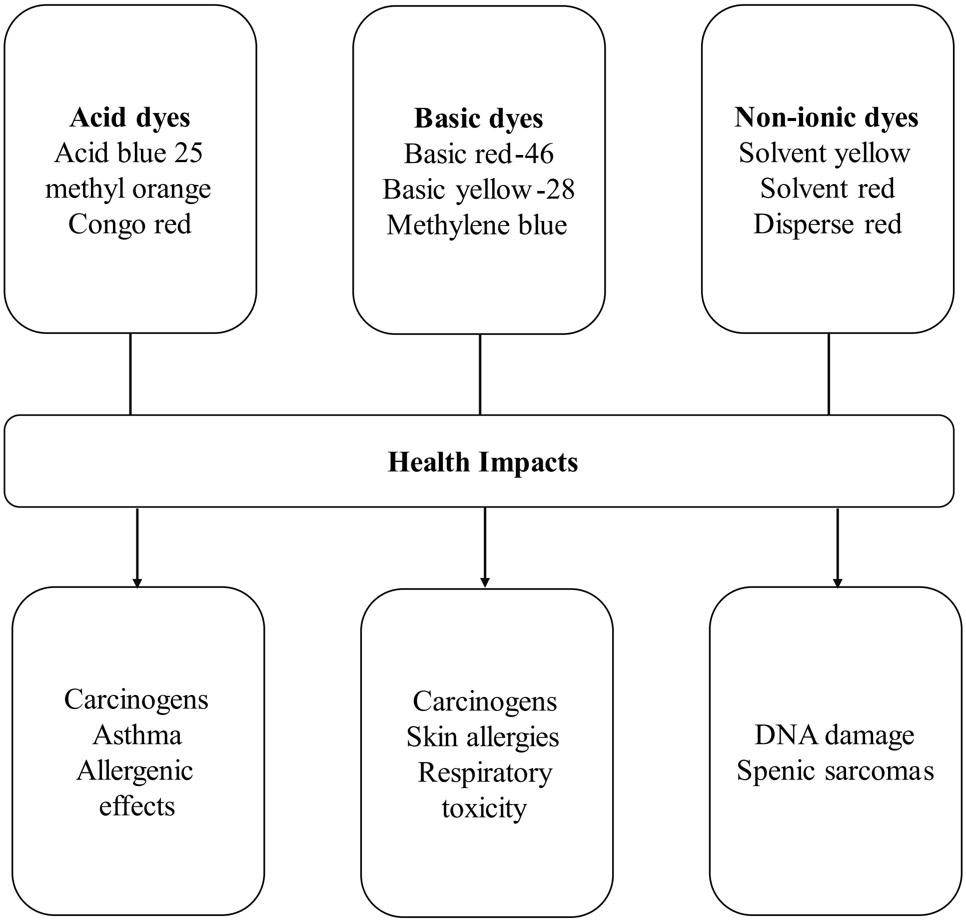

Fig. 2- 4. Hazardous effects caused by different classes of dyes (modified from on[137])

The dyes are non-biodegradable. Therefore, neither primary nor secondary conventional systems are suitable for the treatment of these effluents[137, 144]. Scientists have explored alternative treatment processes for dye wastewater, including advanced oxidation and biological processes. Advanced oxidation processes (AOPs) have shown some effectiveness in reducing chemical oxygen demand (COD) and removing suspended solids but are ineffective in removing color from wastewater. On the other hand, biological processes face challenges due to the complex composition and high organic load of dye wastewater, leading to inefficiency in treatment and purification. To address these limitations, various treatment techniques have been employed, including flocculation/coagulation, biological treatment, advanced oxidation processes, ozonation, adsorption, and membrane filtration. However, these methods have their limitations in terms of high operating costs, limited performance, and environmental impact, making them unsuitable for industrial applications[145, 146].

Among these methods, adsorption has proven to be the most suitable due to several advantages. Adsorption techniques offer high efficiency in removing a wide range of dyes from wastewater. They are versatile and can be applied to different types of wastewater with various dye compositions. Adsorption is also cost-effective, with some adsorbents being readily available and inexpensive[147]. The simplicity of the adsorption process allows for straightforward implementation in existing wastewater treatment systems, and certain adsorbents can be regenerated and reused multiple times, reducing overall costs and environmental impact. Moreover, adsorbents can exhibit selectivity towards specific dyes, allowing for targeted removal in complex dye mixtures. The high adsorption capacity of many adsorbents ensures efficient removal, even at low concentrations of dyes[148]. A detailed compilation of cellulose based materials and their adsorption removal efficiency of different dyes has been reported by Kausar et al[137].

2.7.1.2. Heavy Metal scavengers

Since the 1990s, researchers have focused on investigating the potential of cellulose-based materials for metal ion adsorption[149]. While cellulose itself has limited capacity to adsorb metal ions, it can be modified either physically or chemically to produce nanoscale materials or surface-functionalized variants that are environmentally friendly and possess enhanced metal ion adsorption capabilities. Chemical modification and surface functionalization techniques are employed to modify the properties of cellulose-based materials. Common methods include esterification[150], halogenation[151], oxidation[152], silylation[152], amination, sulfonation, and phosphorylation[153]. These modifications introduce functional groups, resulting in increased metal ion absorption and adsorption capacities. The interaction between metal ions and the modified cellulose-based adsorbents occurs through both chemical and physical mechanisms.

The sorption capacity of cellulose-based materials is influenced to a greater extent by the size and characteristics of the surface groups rather than the specific surface areas. Table 2- 1 summarizes the functional groups of cellulose-based adsorbents that have been reported to bind to heavy metals and haven been classified into hard, soft or intermediate bases[149, 154]. Promotion of adsorption is facilitated by the formation of covalent bonds or coordination complexes between specific groups and metal ions. These groups, such as those containing chelating atoms like N, P, O, and S, play a key role in enhancing adsorption processes.

Table 2- 1. Principal binding groups of cellulose-based adsorbents. Reprinted from ref[155] Copyright (2022), with permission from Elsevier.

Binding groups	**Structural formula**	**HSAB classification**
Oxygen (O) containing functional groups		
Hydroxyl	—OH	hard base
Carbonyl	>C = O	hard base
Carboxyl	—COOH	hard base
Nitrogen (N) containing functional groups		
Amine	$—NH_2$	intermediate base
Amide	$—CONH_2$	intermediate base
Acrylamide	$>C = C—C(=O)—NH_2$	intermediate base
Imine	=NH	intermediate base

Imidazole	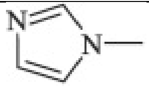	soft base
Amidoxime	—C(=N—OH)—H	intermediate base
Sulfur (S) and Phosphorus (P) containing functional groups		
Thiol	—SH	soft base
Sulfonate	—SO_3	hard base
Thiocarbamate and Dithiocarbamates	>N—C(=S)—S—	soft base
Thioether	—S—	soft base
Xanthate	—O—C(=S)—SNa	soft base
Phosphonate	—$P(OH)_2 = O$	hard base

Pearson's hard and soft acids and bases (HSAB) theory categorizes metals based on their preference for association with hard or soft bases. According to this theory, metals can be classified as hard, soft, or borderline/ intermediate[156]. This classification is shown in Table 2- 2. Tsezos et al. applied this classification to examine the binding preferences of metal ions for sites and found that hard acids tend to associate with hard bases, while soft acids prefer to associate with soft bases[157]. Its been reported that the mechanisms of adsorption in biosorbents can occur through various processes including chemisorption, complexation, adsorption on surfaces and pores, ion exchange, chelation, adsorption by physical forces, and entrapment in inter- and intra-fibrillar capillaries and spaces[158, 159].

Table 2- 2. Classification of metal ions as hard, soft, and borderline acids. Reprinted from ref[155] Copyright (2022), with permission from Elsevier.

Types	**Metal ions**
Hard acids	Li^+, Na^+, K^+, Be^{2+}, Mg^{2+}, Ca^{2+}, Sr^{2+}, Al^{3+}, Cr^{3+}, Cr^{6+}, Sc^{3+}, Ce^{3+}, Lu^{3+}, Ti^{4+}, Zr^{4+}, UO_2^+, etc.
Soft acids	Cu^+, Ag^+, Cd^{2+}, Pd^{2+}, Pt^{2+}, Pt^{4+}, Au^+, Hg^{2+} etc.
Borderline acids	Fe^{2+}, Co^{2+}, Ni^{2+}, Cu^{2+}, Zn^{2+}, Ru^{2+}, Rh^{2+}, Sn^{2+}, Sb^{3+}, Rh^{3+}, Ir^{3+}, Pb^{3+}, Pb^{2+}, Bi^{3+}, etc.

In the interaction between metal ions and adsorbents, both physical and chemical forces come into play. Metal ions can be adsorbed onto the surface of the adsorbent through physical mechanisms such as ion exchange, electrostatic attraction, and van der Waals forces. Chemically, metal ions can form coordination complexes with functional groups on the adsorbent surface such as thiol, phenolic, carboxyl, methoxy, and/or carbonyl groups[160]. The lone pairs of electrons on N, P, O, and S act as electron donors and can form coordinate covalent bonds with metal ions. The presence of these lone pairs facilitates the formation of relatively stable complexes between the derivatives and metals[161]. The detailed mechanism of the metal adsorption process is discussed in the literature by different authors[162, 163]. Surface complexation and ion exchange are common mechanisms mentioned in these discussions. Surface complexation involves the interaction between metal ions and functional groups on the adsorbent surface, forming strong bonds through coordination[164]. Ion exchange occurs when metal ions in solution replace exchangeable ions on the adsorbent surface. It is important to note that the specific mechanisms of metal adsorption can vary depending on various factors such as pH, temperature, concentration of metal ions, and the characteristics of the adsorbent material[165]. A synopsis of some cellulose modifications that have been implemented to adsorb heavy metals is provided in Table 2- 3.

Table 2- 3. Source, modification methods, and adsorption capacity of chemically modified cellulose (reprinted with some modifications from Ref[166]).

Bio-adsorbents	**Source of cellulose**	**Methods for chemical modification on cellulose**	**Metal ions**	**Optimum pH**	**Maximum adsorption capacity (mg g^{-1})**	**Ref.**
Grafted cellulose (AGCS-Cell)	Raw corn stalk	Keto-alcohol free-radical initiation by $KMnO_4$, graft-copolymerization with acrylonitrile monomer and N,N′-methylenebis (acrylamide) as cross-linker	Cd	7	Cd 21.37	[167]
Carboxylated cellulose (Cell-EDTA)	Pineapple leaf fiber, cellulose extracted by soda process	Modified with EDTA dianhydride at C-6 atom	Cd	6	Cd 33.2	[168]
			Pb		Pb 41.2	
Carboxymethyl cellulose (Cell-CM)	Pineapple leaf fiber, cellulose extracted by soda process	Modified with carboxymethyl group using sodium monochlorite and acetic acid C-6 atom	Cd	6	Cd 23.0	[168]
			Pb		Pb 63.4	
Schiff base cellulose (Cell-Hy)	Natural cellulose	$NaIO_4$ oxidation followed by acid-catalyzed condensation of dialdehyde	Cu	6	Cu 80.35	[169]
			Pb		Pb 81.32	

		cellulose with p-aminophenol				
Schiff base cellulose (Gu-Mc)	Cellulose powder	KIO_4 oxidation and condensation with alcoholic N-aminoguanidine hydrochloride in presence of triethylamine	Cu	6	Cu 83.0	170
			Cd		Cd 68.0	
			Pb		Pb 52.0	
Schiff base cellulose (MTC)	Cotton (*Gossypium hirsutum* L)	KIO_4 oxidation followed by condensation with N(4)-morpholino thiosemicarbazide	Cu	6	Cu 106.38	171
Grafted cellulose (pAHA-cellulose)	Cotton fibers	Keto-alcohol free-radical initiation by CAN, grafting with EMCA monomer followed by oximation with hydroxylamine and sodium hydroxide	Cu	5.5 (Cu)	Cu 395.3	172
			Pb	5.4 (Pb)	Pb 333.3	
Grafted cellulose (CMC)	Cellulose	CAN initiation grafting with vinyl monomer glycidyl methacrylate to form epoxy cellulose functionalized with thiosemicarbazide	Cd	5.2 (Cd)	Cd 279.33	173
			Cd	5.6 (Cd)	Cd 217.39	174

Grafted cellulose (PEI/SA-MCC$_{MV}$)	Microcrystalline cellulose (25 mm)	Grafting succinic anhydride on pretreated MCC with microwave H_2O_2 and then with polyethyleneimine	Pb	5.0 (Pb)	Pb 357.14	
Cross-linked cellulose (PEI-RCSA)	Native Cellulose (cotton linter, alpha-cellulose)	Cross-linked cellulose–sodium alginate modified with polyethylene imine via glutaraldehyde cross-linking	Cu	5.5	Cu 177.1	175
			Pb		Pb 234.2	
Cross-linked cellulose (CSECM)	Commercial carboxymet-hyl cellulose	Derived from chitosan-carboxymethyl cellulose cross-linked with EDTA	Cu	5.5	Cu 142.95	176
Multifunctionalized cellulose	Commercial cellulose	Multifunctional group insertion	Cd	4	Cd 401.1	177
Multifunctionalized cellulose (TMCS)	Raw corn stalk	Etherification followed by amination, sodium sulfide/DMF	Cd	5.1	Cd 54.71	178
Multifunctionalized cellulose (PEI-g-OC)	Corncob	Schiff base formation by grafting polyethylenimine on oxidized corncob and reduced with $NaBH_4$	Cu	5.0 (Pb)	Cu 159.5	179
			Cd	5.5 (Cu, Cd)	Cd 212.6	
			Pb		Pb 224.0	
Carboxylated cellulose (Cellulose-EDTA)	Filter paper–Whatman grade 6 (42.5 mm)	Modified with EDTA dianhydride	Cd	7	Cd 102.0	180
			Pb		Pb 227.3	

Carboxylated cellulose (MMCC)	Microcrystalline cellulose (50 mm)	Modified with BTCA at high temperature	Pb	5	Pb 1155.0	181
Carboxymethylated cellulose (CMF)	Softwood kraft pulp fibers	Modified with carboxymethyl group	Cu	–	Cu 64.15	182
Carboxylated cellulose (CWH)	Water hyacinth	Citric acid-modified cellulose	Cu	6.0	Cu 77.98	183

2.7.2. Anti-bacterial applications

Infectious diseases generated by germs such as bacteria, viruses, and fungi remain the principal health hazards that can cause widespread socio-economic difficulties, despite significant advancements in the healthcare profession and medical technology standards. Also, conventional antibiotics promote the development of drug-resistant bacteria[184, 185]. To address these issues, researchers have been developing and manufacturing novel antibacterial compounds[186]. Several novel materials, such as antibacterial nanoparticles[187, 188], antibacterial peptides[189], and natural and synthetic cationic polymers[190], have been created to replace conventional antibiotics. Furthermore, conventional antibiotics act on specific targets, such as inhibiting microbial protein synthesis, whereas these new antimicrobial materials electrostatically act on the entire cellular membrane, resulting in the insertion of their component into the cell membrane and the formation of pores in the microbial cell that finally results in cell rupture, cytoplasmic leakage, and cell death[191].

However, there are limitations to modern antibacterial agents. Some metal nanoparticles used as antibacterial agents can have cytotoxic effects on mammalian cells[192]. Also, proteins in free form can undergo changes and aggregation, diminishing their antibacterial properties over time[193].

Covalently attaching these antibacterial agents to surfaces can also hinder their effectiveness by impacting certain functional groups. To address these issues, some antibacterial agents are non-covalently attached to carriers and released in specific areas. However, long-term use is hampered by the gradual release of the grafted antibacterial agent, as its concentration in the substrate decreases below the threshold value, rendering it ineffective against bacteria[194]. Additionally, conventional antibacterial drugs, including synthetic antibiotics, raise concerns about their environmental impact when they enter municipal wastewater, threatening humans and aquatic organisms. Antibacterial agents can leach from carriers and end up in wastewater, necessitating further filtration and treatment processes to mitigate the potential risks[195]. To address the challenges mentioned above, an alternative strategy is to focus on developing biomaterials that exhibit long-lasting antibacterial activity without leaching of the antibacterial agents. This approach involves creating materials with a non-leaching mechanism of action, ensuring the preservation of antibacterial efficacy over extended periods of time.

Cellulosic-based antibacterial materials are one of the innovative applications of cellulose. Unlike certain other biopolymers with intrinsic biocidal activity (e.g., chitosan[196]), cellulose is not biocidal by nature[197]. Therefore, cellulose has been chemically modified or grafted with organic or inorganic antibacterial agents such as metal nanoparticles (silver[198], zinc[199], etc.), antibiotics[200], and proteins[201] for this purpose. Fig. 2- 5 below summarizes the applications of cellulose-based materials as antibacterial agents.

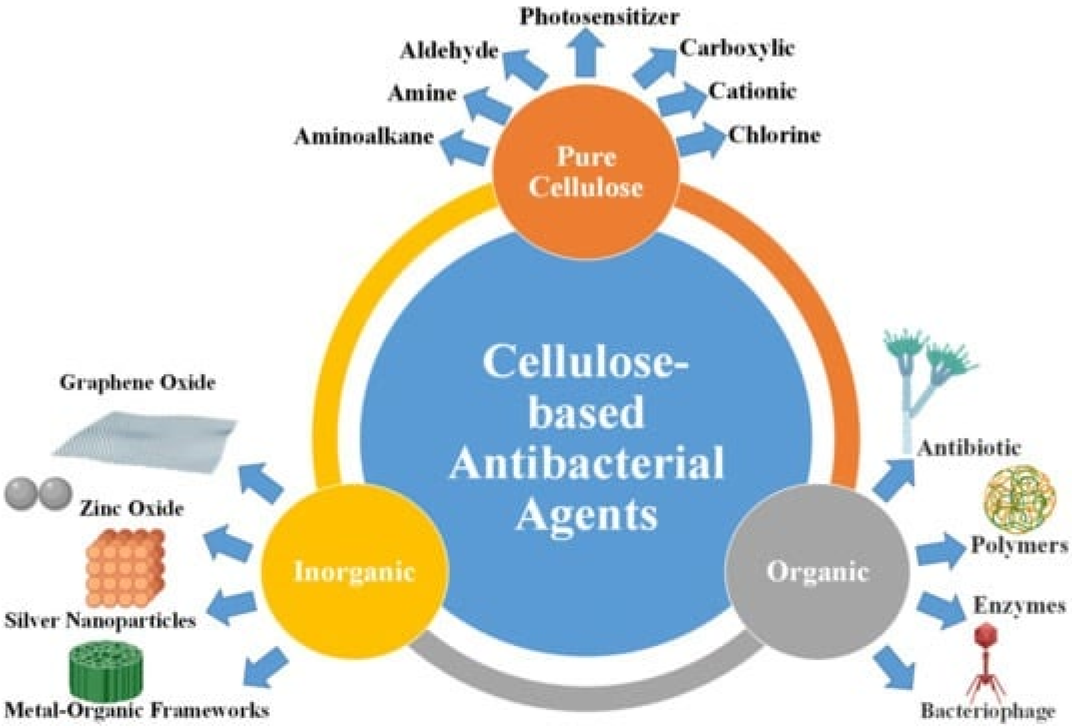

Fig. 2- 5. Cellulose based materials as antibacterial agents[202]

Surface modification with functional groups such as carboxylic groups[203], aldehyde[204], amine[67], alkylamine[205], and quaternary ammonium groups[206] can improve the antibacterial properties of pure cellulose. Cellulose can also be modified with photoactive compounds that can trigger photodynamic inactivation (PDI) of bacteria by converting light radiation to thermal energy or generate reactive oxygen species[207, 208]. Chemical modification of cellulose with organic bioactive molecules such as antibiotics[200, 209, 210], antimicrobial peptides[211, 212], N-halamines[213], aminoalkyl groups[214], bacteriophages[215], and polymers[216] can improve its antibacterial activity. Table 2- 4 provides a summary of several antibacterial agents that have been synthesised utilising cellulose-based materials.

Table 2- 4. Antibacterial applications for cellulose-based materials (Reprinted from ref[202])

Materials	**Preparation Methods**	**Form**	**Microorganism**	**Methods**	**Time**	**Efficiency**	**Mechanism**	**Ref.**
DANFC	1. Mechanical grinding 2. Enzyme treatment 3. $NaIO_4$ oxidation 4. Dialysis 5. Freeze-drying	Mat	*S. aureus* *MERSA*	Zone inhibition Plate counting method	24 h	100%	Drop-in pH value	204
TOCNF	1. TEMPO oxidation 2. Oxygenation	Suspension	*P. aeruginosa* *S. aureus*	Plate counting method	24 h	71%	The formation of a network surrounding the bacteria	217

	1. TEMPO oxidation 2. Autoclaving (121 °C, 20 min)	Gels			24 h	71%	Increase in aldehydes, drop in pH value	218
CNC-Porphyrin	1. HBr acid hydrolysis of Whatman filter paper 2. Cu(I)-catalyzed Huisgen–Meldal–Sharpless 1,3-dipolar cycloaddition	Suspension	*Mycobacterium smegmatis*, *S. aureus*, *E. coli*		60 min	>99%	Generation of ROS, photodynamic	208

Porphyrin-cellulose paper	Cu(I)-catalyzed Huisgen–Meldal–Sharpless cycloaddition	Paper	*S. aureus*, *VER*, *Enterococcus faecium*, *Acinetobacter baumannii*, *P. aeruginosa*, *Klebsiella pneumoniae*		30 min	>99.9 %		219
NFC-Porphyrin	Cyanuric chloride coupling	Paper	MRSA, VER, *E. faecium*, *A. baumannii* *K. pneumoniae*		30 min	99.999%		220

CHPTAC-Cellulose triacetate	1. Immersion precipitation technique 2. Alkaline hydrolysis 3. Esterification	Membrane	*S. aureus* *E. coli*		24 h	78.7–89.0% 64.7–76.6%	Cationic charge	221
BC-aminoalkyl	Stirring for 5 h at 25 °C			Dynamic shake flask method	24 h	>99.9%	Increase in lipophilicity	222
DAC/CTS	1. $NaIO_4$ oxidation 2. Stirring 3. Filtration	Fibers		Plate counting method	24 h	95.1% 90.2%	Drop in pH, cationic CTS	223

T7 phage-Cellulose acetate	Electrospinning of cellulose acetate	Membrane	*E. coli*	Plaque-forming units (PFU)	24 h	6 log(PFU/mL)	Release of phage and hydrolysis	224
Am-CNC-HEWL Am-CNC-T4L	1. Ammonium persulfate oxidation 2. Modification 3. Coupling	Suspension	*M. lysodeikticus*, *Corynebacterium* sp., *E. coli*, *P. smendocina*	Time–kill study with Alamar Blue assay	24 h	100%	Lytic activity	225
CNC-Lysozyme	1. Sulfuric acid hydrolysis 2. Evaporation-induced self-assembly	Thin film	*E. coli* *S. aureus*	Diffusion assays	24 h	0%		226

ZnO-BC	In situ synthesis	Sheets		Inhibition zone	24 h	5.7 ± 0.29 mm 2.9 ± 0.75 mm	Formation of ROS	227
	Ex situ synthesis	Film	*E. coli*	Inhibition zone	24 h	34–41 mm		228
TiO$_2$-BC	Ex situ synthesis	Pieces		Optical density (OD$_{600}$)	12 h	60%		229
Faujasite-cellulose	Hydrothermal	Membrane	*E. coli*, *Enterococci* *Clostridium*	Standard FS ISO9308 and ISO17025		80%		230
SSD/BC	Impregnation and ultrasonication	Commercial membrane	*P. aeruginosa*, *E. coli* *S. aureus*	Zone inhibition	24 h	6.5 mm		231

In this thesis, we focused on investigating the antibacterial activity of cationic cellulose compounds, specifically ANCC. Therefore, we will delve into a more comprehensive analysis of the antibacterial properties exhibited by these compounds. Similar to chitosan, cationic cellulose compounds show inherent antibacterial characteristics. This is attributed to the negative charge present in the cell walls of both Gram-positive (G+) and Gram-negative (G-) bacteria. The negative charge is primarily due to the presence of phosphate groups in the peptidoglycan of G+ bacteria and phospholipids in the outer membranes of G- bacteria. To effectively combat bacterial cells, it is necessary to develop materials that can efficiently adsorb and strongly bind to them. Cationic cellulose materials are capable of electrostatically binding and interacting with the bacterial cell membrane, causing disruptions in membrane integrity. This interaction ultimately leads to the release of cytoplasmic content and, consequently, cell lysis[197, 232]. By compromising the integrity of bacterial cells, cationic cellulose compounds offer a promising approach for antibacterial applications.

2.8. Characterization methods

These are the characterization methods that were used in Chapters 3-5. These methods were X-ray Photoelectron Spectroscopy (XPS), Fourier Transform-infrared (FT-IR) and conductometric titration. Atomic Force Microscopy (AFM) was used to investigate the morphology of the materials. Since these techniques may be unfamiliar to the reader, we provide a concise explanation of the FT-IR, XPS, DLS and conductometric titration in the following paragraphs.

Fourier transform infrared (FT-IR) spectroscopy.

The Fourier transform infrared spectroscopy (FTIR) technique is extensively utilized for the identification of distinct functional groups in a compound. FTIR is a rapid and non-destructive method employed for the qualitative and quantitative analysis of biomass constituents in the mid-infrared spectral range[233]. With its ability to provide insights into molecular fragments and the presence or absence of specific functional groups, FTIR spectroscopy offers a comprehensive understanding of fiber structure. When coupled with an Attenuated Total Reflectance (ATR) unit, FTIR enables the reduction of incident light and allows for the acquisition of infrared spectra without the interference of aqueous background absorbance[234].

This thesis uses FT-IR to confirm the modifications performed on cellulose. The difference in the functional groups of cellulose (starting material), dialdehyde cellulose (intermediate) and diaminocellulose (product) can be confirmed by this method. For cellulose, the broad peak around 3330 cm^{-1} is characteristic for stretching vibration of the hydroxyl group in polysaccharides and also includes also inter- and intra-molecular hydrogen bond vibrations in cellulose [235]. The band around 2890 cm^{-1} is attributed to CH stretching vibration of all hydrocarbon constituents in polysaccharides. Other typical bands assigned to cellulose are observed in the region of 1630 - 900 cm^{-1}. The peaks located at 1630 cm^{-1} correspond to vibration of water molecules absorbed in cellulose[236, 237]. In dialdehyde cellulose, a band around 1730 cm^{-1}, which is characteristic of the carbonyl group, typically appears[238]. This band disappears in diaminocellulose, but we do not observe the characteristic N-H bands in the 3330 cm^{-1} region, most likely because it merged with the OH band. The amine groups are confirmed by XPS and conductometric titration.

X-ray photoelectron spectroscopy (XPS)

The surface chemical characterization technique known as XPS provides information about the surface properties, elemental makeup, and electronic state of the elements that are present inside a substance. By exposing the sample to an X-ray beam and instantly counting the number of electrons and their kinetic energy, the XPS spectrum is created. In conjunction with IR spectroscopy, XPS has typically been used to evaluate the elemental composition and chemical bonding present in materials. XPS is a widely used characterization method for identifying the functional groups and elemental composition as it provides information on the individual atomic units present in a given compound, such as nitrogen-, oxygen-, and carbon-bonded units present on the surface, in addition to illuminating the functional groups present on the external surface[239]. It can also be used to detect and measure metallic elements such as Pb, Na, Cu, etc[240].

In this thesis, XPS was used to verify the introduction of amine groups to cellulose structure and confirm attachment of Pb ion (in chapter 4). We were also able to determine the amine content of DAmC using its chemical composition percentage.

2.8.1. Dynamic light scattering (DLS)

DLS (Dynamic Light Scattering) is a widely used non-destructive technique for measuring particle size[241]. It has been commonly employed to measure the size of CNCs and HNCs in various studies[242, 243]. However, it is important to adopt a critical approach when using DLS for HNCs dimensions. The hydrodynamic diameter obtained from DLS represents the effective size of the particles in solution, including any adsorbed or surrounding molecules. Therefore, the hydrodynamic diameter reported by DLS instruments should not be confused with their actual size, length, or mean diameter. In chapter 5, we use DLS to confirm the presence of hairs in ANCC using the same protocol by Yang, et al. [64, 68]. The change in the hydrodynamic diameter is measured with the change in ionic strength of the solution. Since the hair is electrosterically stable, HNCs are very stable in water due to steric stabilization. When salt is added to a charged HNC like ENCC, the ions partially screen the charges and “folds” the hairs of these particles thereby decreasing their effective diameter. After full charge screening, the measured hydrodynamic radius increases as ENCC starts to aggregate at a specific salt concentration (~2 M)[64].

2.8.2. Conductometric titration

Charge density represents the electric charge per unit mass and serves as a quantitative indicator of charged groups within the molecular structure of biomacromolecules. These groups can be positively or negatively charged. Various methods are utilized to determine charge density, with electrophoretic and light scattering techniques, colloidal titration, and pH titration being the most commonly employed techniques. These methods offer valuable insights into the distribution and extent of charged groups, aiding in the characterization of biomacromolecules. Conductometric titration is an analytical technique that relies on the difference in mobility of ions. It offers several advantages over acid-base or potentiometric titrations, especially when studying specific systems. These systems are characterized by the formation of highly soluble products or hydrolysis products at the equivalence point[244]. Conductometric titration also maintains its accuracy in both dilute and concentrated solutions. Additionally, it can be used to analyze both colorless and colored solutions. One important aspect of conductometric titration is the use of measurement electrodes. Unlike indicators in acid-base titrations, these electrodes do not interact with the system or introduce contamination[245, 246]. They play a crucial role in monitoring the changes in electrical conductivity during the titration process. On the other hand, conductometric titration does have a disadvantage related to the system under study. It is not suitable for systems with high concentrations of foreign electrolytes, as these can interfere with the reaction and reduce the precision of the results[245]. The amine content of a cellulose based material and chitosan have been measured using this method as was done by Tavakolian, et al. and Farris, et al. respectively[239, 247].

2.9. Concluding remark

In this chapter, we reviewed cellulose on four different scales. macro, micro, nano, dissolved. On the macroscale, we looked at the properties of cellulose fibers, on the microscale, we discussed cellulose microfibrils (CMF), and, on the nanoscale, we studied a variety of nanocellulose. We also discussed different modifications that can be performed on cellulose and some of its applications. In this thesis, we studied on the macroscale - diaminocellulose fibers (DAmF), nanoscale - aminated nanocrystalline cellulose (ANCC) and on the dissolved cellulose - diaminocellulose (DAmC). In addition, we discussed the techniques used to characterize these materials.

2.10. References

1. Eyley, S.; Thielemans, W., Surface modification of cellulose nanocrystals. *Nanoscale* **2014,** *6* (14), 7764-7779.

2. Kamide, K., Cellulose and Cellulose Derivatives. *Cellulose and Cellulose Derivatives* **2005**.

3. Yeasmin, F.; Masud, R. A.; Chisty, A. H.; Hossain, M. A.; Mallik, A. K.; Mizanur Rahman, M., 14 - Lignin-metal oxide composite for photocatalysis and photovoltaics. In *Renewable Polymers and Polymer-Metal Oxide Composites*, Haider, S.; Haider, A., Eds. Elsevier: 2022; pp 447-476.

4. Chen, W. C. Functionalization of carbohydrates on the macro-, nano-, and molecular scale. McGill university, Montreal, 2016.

5. Zhang, X.; Li, L.; Xu, F., Chemical Characteristics of Wood Cell Wall with an Emphasis on Ultrastructure: A Mini-Review. *Forests* **2022,** *13* (3), 439.

6. Sjöström, E., Wood chemistry : fundamentals and applications. Academic Press, Inc.: San Diego, California, 1993.

7. Sim, G. Carboxylated Cellulose Pulp Fibers: from Fundamentals to Applications. McGill university, Montreal, QC, 2015.

8. Habibi, Y.; Lucia, L. A.; Rojas, O. J., Cellulose Nanocrystals: Chemistry, Self-Assembly, and Applications. *Chemical Reviews* **2010,** *110* (6), 3479-3500.

9. Fernandes, A. N.; Thomas, L. H.; Altaner, C. M.; Callow, P.; Forsyth, V. T.; Apperley, D. C.; Kennedy, C. J.; Jarvis, M. C., Nanostructure of cellulose microfibrils in spruce wood. *Proceedings of the National Academy of Sciences* **2011,** *108* (47), E1195-E1203.

10. Fratzl, P.; Weinkamer, R., Nature's hierarchical materials. *Progress in materials Science* **2007,** *52* (8), 1263-1334.

11. Mautner, A.; Hakalahti, M.; Rissanen, V.; Tammelin, T., Crucial interfacial features of nanocellulose materials. In *Nanocellulose and Sustainability*, CRC Press: 2018; pp 87-128.

12. Phanthong, P.; Reubroycharoen, P.; Hao, X.; Xu, G.; Abudula, A.; Guan, G., Nanocellulose: Extraction and application. *Carbon Resources Conversion* **2018,** *1* (1), 32-43.

13. Zhuo, X.; Liu, C.; Pan, R.; Dong, X.; Li, Y., Nanocellulose Mechanically Isolated from Amorpha fruticosa Linn. *ACS Sustainable Chemistry & Engineering* **2017,** *5* (5), 4414-4420.

14. Münch, A. S.; Wölk, M.; Malanin, M.; Eichhorn, K.-J.; Simon, F.; Uhlmann, P., Smart functional polymer coatings for paper with anti-fouling properties. *Journal of Materials Chemistry B* **2018,** *6* (5), 830-843.

15. Khalil, H. A.; Bhat, A.; Yusra, A. I., Green composites from sustainable cellulose nanofibrils: A review. *Carbohydrate polymers* **2012,** *87* (2), 963-979.

16. Koshani, R.; van de Ven, T. G. M., Carboxylated Cellulose Nanocrystals Developed by Cu-Assisted H2O2 Oxidation as Green Nanocarriers for Efficient Lysozyme Immobilization. *Journal of Agricultural and Food Chemistry* **2020,** *68* (21), 5938-5950.

17. Vasconcelos, N. F.; Feitosa, J. P. A.; da Gama, F. M. P.; Morais, J. P. S.; Andrade, F. K.; de Souza Filho, M. d. S. M.; Rosa, M. d. F., Bacterial cellulose nanocrystals produced under different hydrolysis conditions: Properties and morphological features. *Carbohydrate Polymers* **2017,** *155*, 425-431.

18. Sheikhi, A.; Yang, H.; Alam, M. N.; van de Ven, T. G. M., Highly stable, functional hairy nanoparticles and biopolymers from wood fibers: towards sustainable nanotechnology. *JoVE (Journal of Visualized Experiments)* **2016,** (113), e54133.

19. Lee, K. Y.; Tammelin, T.; Schulfter, K.; Kiiskinen, H.; Samela, J.; Bismarck, A., High performance cellulose nanocomposites: comparing the reinforcing ability of bacterial cellulose and nanofibrillated cellulose. *ACS Appl Mater Interfaces* **2012,** *4* (8), 4078-86.

20. Isogai, A.; Saito, T.; Fukuzumi, H., TEMPO-oxidized cellulose nanofibers. *Nanoscale* **2011,** *3* (1), 71-85.

21. Dufresne, A., Nanocellulose: a new ageless bionanomaterial. *Materials today* **2013,** *16* (6), 220-227.

22. Kumar, V.; Elfving, A.; Koivula, H.; Bousfield, D.; Toivakka, M., Roll-to-roll processed cellulose nanofiber coatings. *Industrial & Engineering Chemistry Research* **2016,** *55* (12), 3603-3613.

23. De France, K. J.; Hoare, T.; Cranston, E. D., Review of hydrogels and aerogels containing nanocellulose. *Chemistry of Materials* **2017,** *29* (11), 4609-4631.

24. Aaen, R.; Simon, S.; Wernersson Brodin, F.; Syverud, K., The potential of TEMPO-oxidized cellulose nanofibrils as rheology modifiers in food systems. *Cellulose* **2019,** *26*, 5483-5496.

25. Turbak, A. F.; Snyder, F. W.; Sandberg, K. R. In *Microfibrillated cellulose, a new cellulose product: properties, uses, and commercial potential*, J Appl Polym Sci Appl Polym Symp, 1983; pp 815-827.

26. Herrick, F. W.; Casebier, R. L.; Hamilton, J. K.; Sandberg, K. R. In *Microfibrillated cellulose: morphology and accessibility*, J. Appl. Polym. Sci.: Appl. Polym. Symp.;(United States), ITT Rayonier Inc., Shelton, WA: 1983.

27. Taniguchi, T.; Okamura, K., New films produced from microfibrillated natural fibres. *Polymer International* **1998,** *47* (3), 291-294.

28. Carrasco, F.; Mutjé, P.; Pelach, M., Refining of bleached cellulosic pulps: characterization by application of the colloidal titration technique. *Wood science and technology* **1996,** *30*, 227-236.

29. Ho, T. T. T.; Abe, K.; Zimmermann, T.; Yano, H., Nanofibrillation of pulp fibers by twin-screw extrusion. *Cellulose* **2015,** *22*, 421-433.

30. Uetani, K.; Yano, H., Nanofibrillation of wood pulp using a high-speed blender. *Biomacromolecules* **2011,** *12* (2), 348-353.

31. Wang, S.; Cheng, Q., A novel process to isolate fibrils from cellulose fibers by high-intensity ultrasonication, Part 1: Process optimization. *Journal of applied polymer science* **2009,** *113* (2), 1270-1275.

32. Dufresne, A.; Cavaillé, J. Y.; Vignon, M. R., Mechanical behavior of sheets prepared from sugar beet cellulose microfibrils. *Journal of applied polymer science* **1997,** *64* (6), 1185-1194.

33. Zhang, L.; Tsuzuki, T.; Wang, X., Preparation of cellulose nanofiber from softwood pulp by ball milling. *Cellulose* **2015,** *22*, 1729-1741.

34. Kose, R.; Mitani, I.; Kasai, W.; Kondo, T., "Nanocellulose" as a single nanofiber prepared from pellicle secreted by Gluconacetobacter xylinus using aqueous counter collision. *Biomacromolecules* **2011,** *12* (3), 716-720.

35. Kondo, T., Cellulose Nanofibrils Pulverized from Biomass Resources: Past, Present, and Future Perspectives. *KONA Powder and Particle Journal* **2023,** *40*, 109-123.

36. Isogai, A.; Zhou, Y., Diverse nanocelluloses prepared from TEMPO-oxidized wood cellulose fibers: Nanonetworks, nanofibers, and nanocrystals. *Current Opinion in Solid State and Materials Science* **2019,** *23* (2), 101-106.

37. Liao, J.; Pham, K. A.; Breedveld, V., TEMPO-CNF suspensions in the viscoelastic regime: capturing the effect of morphology and surface charge with a rheological parameter. *Cellulose* **2021,** *28* (2), 813-827.

38. Wågberg, L.; Decher, G.; Norgren, M.; Lindström, T.; Ankerfors, M.; Axnäs, K., The build-up of polyelectrolyte multilayers of microfibrillated cellulose and cationic polyelectrolytes. *Langmuir* **2008,** *24* (3), 784-795.

39. Tejado, A.; Alam, M. N.; Antal, M.; Yang, H.; van de Ven, T. G., Energy requirements for the disintegration of cellulose fibers into cellulose nanofibers. *Cellulose* **2012,** *19*, 831-842.

40. Liimatainen, H.; Visanko, M.; Sirviö, J.; Hormi, O.; Niinimäki, J., Sulfonated cellulose nanofibrils obtained from wood pulp through regioselective oxidative bisulfite pre-treatment. *Cellulose* **2013,** *20*, 741-749.

41. Liimatainen, H.; Suopajärvi, T.; Sirviö, J.; Hormi, O.; Niinimäki, J., Fabrication of cationic cellulosic nanofibrils through aqueous quaternization pretreatment and their use in colloid aggregation. *Carbohydrate polymers* **2014,** *103*, 187-192.

42. Hassan, M. L.; Hassan, E. A.; Oksman, K. N., Effect of pretreatment of bagasse fibers on the properties of chitosan/microfibrillated cellulose nanocomposites. *Journal of Materials Science* **2011,** *46*, 1732-1740.

43. Carrillo, C. A.; Laine, J.; Rojas, O. J., Microemulsion systems for fiber deconstruction into cellulose nanofibrils. *ACS Applied Materials & Interfaces* **2014,** *6* (24), 22622-22627.

44. Sirviö, J. A.; Visanko, M.; Liimatainen, H., Deep eutectic solvent system based on choline chloride-urea as a pre-treatment for nanofibrillation of wood cellulose. *Green Chemistry* **2015,** *17* (6), 3401-3406.

45. Beck-Candanedo, S.; Roman, M.; Gray, D. G., Effect of reaction conditions on the properties and behavior of wood cellulose nanocrystal suspensions. *Biomacromolecules* **2005,** *6* (2), 1048-1054.

46. George, J.; N, S., Cellulose nanocrystals: Synthesis, functional properties, and applications. *Nanotechnology, Science and Applications* **2015,** *8*, 45.

47. Mukherjee, S.; Woods, H., X-ray and electron microscope studies of the degradation of cellulose by sulphuric acid. *Biochimica et biophysica acta* **1953,** *10*, 499-511.

48. Liu, B.; Li, Y.; Yuan, Y.; Zheng, B.; Liu, C.; Zhou, L.; Zhang, J., Controllable self-assembly of cellulose nanospheres through phosphoric acid triggered dissolution-regeneration and degradation. *International Journal of Biological Macromolecules* **2023,** *243*, 125119.

49. Sucaldito, M. R.; Camacho, D. H., Characteristics of unique HBr-hydrolyzed cellulose nanocrystals from freshwater green algae (Cladophora rupestris) and its reinforcement in starch-based film. *Carbohydrate Polymers* **2017,** *169*, 315-323.

50. Hastuti, N.; Kanomata, K.; Kitaoka, T., Hydrochloric Acid Hydrolysis of Pulps from Oil Palm Empty Fruit Bunches to Produce Cellulose Nanocrystals. *Journal of Polymers and the Environment* **2018,** *26* (9), 3698-3709.

51. Filson, P. B.; Dawson-Andoh, B. E., Sono-chemical preparation of cellulose nanocrystals from lignocellulose derived materials. *Bioresource Technology* **2009,** *100* (7), 2259-2264.

52. Andrews P. Mark, M. T. Method for producing functionalized nanocrystalline cellulose and functionalized nanocrystalline cellulose thereby produced. 2021.

53. Mcalpine S., N. J. Production of crystalline cellulose. 2017.

54. Lam, E.; Hemraz, U. D., Preparation and surface functionalization of carboxylated cellulose nanocrystals. *Nanomaterials* **2021,** *11* (7), 1641.

55. Fraschini, C.; Chauve, G.; Bouchard, J., TEMPO-mediated surface oxidation of cellulose nanocrystals (CNCs). *Cellulose* **2017,** *24* (7), 2775-2790.

56. Liu, Y.; Liu, L.; Wang, K.; Zhang, H.; Yuan, Y.; Wei, H.; Wang, X.; Duan, Y.; Zhou, L.; Zhang, J., Modified ammonium persulfate oxidations for efficient preparation of carboxylated cellulose nanocrystals. *Carbohydrate Polymers* **2020,** *229*, 115572.

57. Man, Z.; Muhammad, N.; Sarwono, A.; Bustam, M. A.; Vignesh Kumar, M.; Rafiq, S., Preparation of Cellulose Nanocrystals Using an Ionic Liquid. *Journal of Polymers and the Environment* **2011,** *19* (3), 726-731.

58. Montes, S.; Azcune, I.; Cabañero, G.; Grande, H.-J.; Odriozola, I.; Labidi, J., Functionalization of Cellulose Nanocrystals in Choline Lactate Ionic Liquid. *Materials* **2016,** *9* (7), 499.

59. Lazko, J.; Sénéchal, T.; Landercy, N.; Dangreau, L.; Raquez, J.-M.; Dubois, P., Well defined thermostable cellulose nanocrystals via two-step ionic liquid swelling-hydrolysis extraction. *Cellulose* **2014,** *21* (6), 4195-4207.

60. Peponi, L.; Barrera-Rivera, K. A.; Kenny, J. M.; Marcos-Fernandez, Á.; Martinez-Richa, A.; López, D. Bio-Catalysis for the Functionalization of Cellulose Nanocrystals *Nanomaterials* [Online], 2022.

61. Wang, H.; Li, J.; Zeng, X.; Tang, X.; Sun, Y.; Lei, T.; Lin, L., Extraction of cellulose nanocrystals using a recyclable deep eutectic solvent. *Cellulose* **2020,** *27* (3), 1301-1314.

62. Conley, K.; Whitehead, M.; van de Ven, T., Chemically peeling layers of cellulose nanocrystals by periodate and chlorite oxidation. *Cellulose* **2016,** *23*.

63. Yang, H.; Tejado, A.; Alam, N.; Antal, M.; van de Ven, T. G. M., Films prepared from electrosterically stabilized nanocrystalline cellulose. *Langmuir* **2012,** *28* (20), 7834-42.

64. Yang, H.; Alam, M. N.; van de Ven, T. G. M., Highly charged nanocrystalline cellulose and dicarboxylated cellulose from periodate and chlorite oxidized cellulose fibers. *Cellulose* **2013,** *20* (4), 1865-1875.

65. Yang, H.; Chen, D.; van de Ven, T. G. M., Preparation and characterization of sterically stabilized nanocrystalline cellulose obtained by periodate oxidation of cellulose fibers. *Cellulose* **2015,** *22* (3), 1743-1752.

66. Yang, H.; Sheikhi, A.; van de Ven, T. G. M., Reusable green aerogels from cross-linked hairy nanocrystalline cellulose and modified chitosan for dye removal. *Langmuir* **2016,** *32* (45), 11771-11779.

67. Koshani, R.; Eiyegbenin, J. E.; Wang, Y.; van de Ven, T. G. M., Synthesis and characterization of hairy aminated nanocrystalline cellulose. *J Colloid Interface Sci* **2022,** *607* (Pt 1), 134-144.

68. Yang, H.; van de Ven, T. G. M., Preparation of hairy cationic nanocrystalline cellulose. *Cellulose* **2016,** *23* (3), 1791-1801.

69. van de Ven, T. G. M.; Sheikhi, A., Hairy cellulose nanocrystalloids: a novel class of nanocellulose. *Nanoscale* **2016,** *8* (33), 15101-15114.

70. Lenfant, G.; Heuzey, M.-C.; van de Ven, T. G. M.; Carreau, P. J., A comparative study of ECNC and CNC suspensions: effect of salt on rheological properties. *Rheologica Acta* **2017,** *56* (1), 51-62.

71. Yang, H.; van de Ven, T. G., A Bottom-up Route to a Chemically End-to-End Assembly of Nanocellulose Fibers. *Biomacromolecules* **2016,** *17* (6), 2240-7.

72. Tavakolian, M.; Lerner, J.; Medina Tovar, F.; Frances, J.; van de Ven, T. G. M.; Kakkar, A., Dendrimer directed assembly of dicarboxylated hairy nanocellulose. *J Colloid Interface Sci* **2019,** *541*, 444-453.

73. Sannino, A.; Demitri, C.; Madaghiele, M., Biodegradable cellulose-based hydrogels: design and applications. *Materials* **2009,** *2* (2), 353-373.

74. Chen, K.; Lv, W.; Chen, W.; Wang, Y.; Zhang, Y.; Zhang, X.; Yao, J., 2,3,6-Tricarboxylate Cellulose as a Fully Biodegradable Flocculant: Efficient Synthesis and Flocculation Performance. *BioResources* **2016,** *11*.

75. Schulz, M. B.; Daniels, R., Hydroxypropylmethylcellulose (HPMC) as emulsifier for submicron emulsions: influence of molecular weight and substitution type on the droplet size after high-pressure homogenization. *European Journal of Pharmaceutics and Biopharmaceutics* **2000,** *49* (3), 231-236.

76. Khare, V. P.; Greenberg, A. R.; Kelley, S. S.; Pilath, H.; Juhn Roh, I.; Tyber, J., Synthesis and characterization of dense and porous cellulose films. *Journal of applied polymer science* **2007,** *105* (3), 1228-1236.

77. Swatloski, R. P.; Spear, S. K.; Holbrey, J. D.; Rogers, R. D., Dissolution of cellose with ionic liquids. *Journal of the American chemical society* **2002,** *124* (18), 4974-4975.

78. Chen, D.; van de Ven, T. G. M., Flocculation kinetics of precipitated calcium carbonate induced by electrosterically stabilized nanocrystalline cellulose. *Colloids and Surfaces A: Physicochemical and Engineering Aspects* **2016,** *504*, 11-17.

79. GORDY, S. T.; TRUMPER, M., CARBON DISULFIDE POISONING: WITH A REPORT OF SIX CASES. *Journal of the American Medical Association* **1938,** *110* (19), 1543-1549.

80. Partanen, T.; Hernberg, S.; Nordman, C. H.; Sumari, P., Coronary heart disease among workers exposed to carbon disulphide. *Br J Ind Med* **1970,** *27* (4), 313-25.

81. Liss, G. M.; Finkelstein, M. M., Mortality among workers exposed to carbon disulfide. *Arch Environ Health* **1996,** *51* (3), 193-200.

82. Nurminen, M.; Hernberg, S., Cancer mortality among carbon disulfide-exposed workers. *J Occup Med* **1984,** *26* (5), 341.

83. Hurley, N., Dirty fashion: How H and M, Zara and Marks and Spencer are buying viscose from highly polluting factories in Asia. *Guardian (Sydney)* **2017,** (1786), 12.

84. Almeida, R. O.; Maloney, T. C.; Gamelas, J. A. F., Production of functionalized nanocelluloses from different sources using deep eutectic solvents and their applications. *Industrial Crops and Products* **2023,** *199*, 116583.

85. Matheus, P.; Vinícios, P.; Ademir, J. Z., Structural Characteristics and Thermal Properties of Native Cellulose. In *Cellulose*, Theo van de, V.; Louis, G., Eds. IntechOpen: Rijeka, 2013; p Ch. 2.

86. Pinkert, A.; Marsh, K. N.; Pang, S.; Staiger, M. P., Ionic Liquids and Their Interaction with Cellulose. *Chemical Reviews* **2009,** *109* (12), 6712-6728.

87. Nechyporchuk, O.; Belgacem, M. N.; Bras, J., Production of cellulose nanofibrils: A review of recent advances. *Industrial Crops and Products* **2016,** *93*, 2-25.

88. Sichinga, M. C.; Kline, T.; Whitehead, M. A.; van de Ven, T. G. M., One-pot eco-friendly oxidative synthesis of imine carboxymethyl dialdehyde cellulosic fibers. *Cellulose* **2022,** *29* (2), 799-815.

89. Sichinga, M. C.; Koshani, R.; van de Ven, T. G. J. C.; Physicochemical, S. A.; Aspects, E., Chemisorption of basic fuchsine in packed beds of dialdehyde cellulose fibres. **2022,** *632*, 127726.

90. Conley, K.; Whitehead, M.; van de Ven, T., Probing the structural chirality of crystalline cellulose with induced circular dichroism. *Cellulose* **2017,** *24*.

91. Dufresne, A., *Nanocellulose: from nature to high performance tailored materials*. Walter de Gruyter GmbH & Co KG: 2017.

92. Klemm, D.; Heublein, B.; Fink, H. P.; Bohn, A., Cellulose: fascinating biopolymer and sustainable raw material. *Angewandte chemie international edition* **2005,** *44* (22), 3358-3393.

93. O'sullivan, A. C. J. C., Cellulose: the structure slowly unravels. **1997,** *4* (3), 173-207.

94. Moon, R. J.; Martini, A.; Nairn, J.; Simonsen, J.; Youngblood, J., Cellulose nanomaterials review: structure, properties and nanocomposites. *Chem Soc Rev* **2011,** *40* (7), 3941-94.

95. Kamide, K., Characterization of Molecular Structure of Cellulose Derivatives. 2005; pp 25-188.

96. Saracino, G. A.; Improta, R.; Barone, V., Absolute pKa determination for carboxylic acids using density functional theory and the polarizable continuum model. *Chemical physics letters* **2003,** *373* (3-4), 411-415.

97. Juranić, I., Simple method for the estimation of pKa of amines. *Croatica Chemica Acta* **2014,** *87* (4), 343-347.

98. Chen, X.; Zheng, N.; Wang, Q.; Liu, L.; Men, Y., Side-chain crystallization in alkyl-substituted cellulose esters and hydroxypropyl cellulose esters. *Carbohydrate polymers* **2017,** *162*, 28-34.

99. Wang, Q.; Espert, M.; Larrea, V.; Quiles, A.; Salvador, A.; Sanz, T., Comparison of different indirect approaches to design edible oleogels based on cellulose ethers. *Food Hydrocolloids* **2023,** *134*, 108007.

100. Nunes, S.; Ramacciotti, F.; Neves, A.; Angelin, E. M.; Ramos, A. M.; Roldão, É.; Wallaszkovits, N.; Armijo, A. A.; Melo, M. J., A diagnostic tool for assessing the conservation condition of cellulose nitrate and acetate in heritage collections: quantifying the degree of substitution by infrared spectroscopy. *Heritage Science* **2020,** *8*, 1-14.

101. Chantereau, G.; Brown, N.; Dourges, M.-A.; Freire, C. S.; Silvestre, A. J.; Sebe, G.; Coma, V., Silylation of bacterial cellulose to design membranes with intrinsic anti-bacterial properties. *Carbohydrate polymers* **2019,** *220*, 71-78.

102. Kumar, R.; Sharma, R. K.; Singh, A. P., Grafted cellulose: a bio-based polymer for durable applications. *Polymer Bulletin* **2018,** *75*, 2213-2242.

103. Rol, F.; Sillard, C.; Bardet, M.; Yarava, J. R.; Emsley, L.; Gablin, C.; Léonard, D.; Belgacem, N.; Bras, J., Cellulose phosphorylation comparison and analysis of phosphorate position on cellulose fibers. *Carbohydrate polymers* **2020,** *229*, 115294.

104. Choi, H. Y.; Bae, J. H.; Hasegawa, Y.; An, S.; Kim, I. S.; Lee, H.; Kim, M., Thiol-functionalized cellulose nanofiber membranes for the effective adsorption of heavy metal ions in water. *Carbohydrate Polymers* **2020,** *234*, 115881.

105. Dryhurst, G., *Periodate oxidation of diol and other functional groups: analytical and structural applications*. Elsevier: 2015; Vol. 2.

106. Pfeifer, V.; Sohns, V.; Conway, H.; Lancaster, E.; Dabic, S.; Griffin, E., Two stage process for dialdehyde starch using electrolytic regeneration of periodic acid. *Industrial & Engineering Chemistry* **1960,** *52* (3), 201-206.

107. Liimatainen, H.; Sirviö, J.; Pajari, H.; Hormi, O.; Niinimäki, J., Regeneration and Recycling of Aqueous Periodate Solution in Dialdehyde Cellulose Production. *Journal of Wood Chemistry and Technology* **2013,** *33* (4), 258-266.

108. Koprivica, S.; Siller, M.; Hosoya, T.; Roggenstein, W.; Rosenau, T.; Potthast, A., Regeneration of Aqueous Periodate Solutions by Ozone Treatment: A Sustainable Approach for Dialdehyde Cellulose Production. *ChemSusChem* **2016,** *9* (8), 825-833.

109. Lin, L.; Jiang, T.; Liang, Y.; Zhu, W.; Inamdar, U. Y.; Pervez, M. N.; Navik, R.; Yang, X.; Cai, Y.; Naddeo, V., Combination of Pre- and Post-Mercerization Processes for Cotton Fabric. *Materials* **2022,** *15* (6), 2092.

110. Painter, T. J., Control of depolymerisation during the preparation of reduced dialdehyde cellulose. *Carbohydrate Research* **1988,** *179*, 259-268.

111. Siller, M.; Amer, H.; Bacher, M.; Roggenstein, W.; Rosenau, T.; Potthast, A., Effects of periodate oxidation on cellulose polymorphs. *Cellulose* **2015,** *22*.

112. Sichinga, M. C.; Koshani, R.; van de Ven, T. G. M., Chemisorption of basic fuchsine in packed beds of dialdehyde cellulose fibres. *Colloids and Surfaces A: Physicochemical and Engineering Aspects* **2022,** *632*, 127726.

113. Tavakolian, M.; Okshevsky, M.; van de Ven, T. G. M.; Tufenkji, N., Developing Antibacterial Nanocrystalline Cellulose Using Natural Antibacterial Agents. *ACS Applied Materials & Interfaces* **2018,** *10* (40), 33827-33838.

114. Sabzalian, Z.; Alam, M.; van de Ven, T., Hydrophobization and characterization of internally crosslink-reinforced cellulose fibers. *Cellulose* **2014,** *21*.

115. Zhang, H.; Liu, P.; Musa, S. M.; Mai, C.; Zhang, K., Dialdehyde Cellulose as a Bio-Based Robust Adhesive for Wood Bonding. *ACS Sustainable Chemistry & Engineering* **2019,** *7* (12), 10452-10459.

116. Sirviö, J. A.; Kolehmainen, A.; Visanko, M.; Liimatainen, H.; Niinimäki, J.; Hormi, O. E. O., Strong, Self-Standing Oxygen Barrier Films from Nanocelluloses Modified with Regioselective Oxidative Treatments. *ACS Applied Materials & Interfaces* **2014,** *6* (16), 14384-14390.

117. Denissen, W.; Winne, J. M.; Du Prez, F. E., Vitrimers: permanent organic networks with glass-like fluidity. *Chemical Science* **2016,** *7* (1), 30-38.

118. Tian, X.; Yang, R.; Xiong, C.; Deng, H.; Ni, Y.; Jiang, X., Dialdehyde cellulose nanocrystal cross-linked chitosan foam with high adsorption capacity for removal of acid red 134. *Frontiers of Chemical Science and Engineering* **2023**.

119. Zou, Y. C.; Zhang, A. P.; Lin, L.; El-Sohaimy, S. A.; Li, Y.; Wu, L. R.; Zhang, H., Schiff base cross-linked dialdehyde cellulose/gelatin composite aerogels as porous structure templates for oleogels preparation. *International Journal of Biological Macromolecules* **2023,** *224*, 667-675.

120. Safari, S.; Sheikhi, A.; van de Ven, T. G. M., Electroacoustic characterization of conventional and electrosterically stabilized nanocrystalline celluloses. *Journal of Colloid and Interface Science* **2014,** *432*, 151-157.

121. Varma, A. J.; Chavan, V. B., A study of crystallinity changes in oxidised celluloses. *Polymer Degradation and Stability* **1995,** *49* (2), 245-250.

122. A.J.Varma, Proceedings of International Symposium on Bioplastic Materials,. *Bonn, Germany,* **1999,** *June 23-24*.

123. Zhang, X.; Duan, C.; Jia, X.; Dai, B., Carboxylation kapok fiber as a low-cost, environmentally friendly adsorbent with remarkably enhanced adsorption capacity for cationic dyes. *Research on Chemical Intermediates* **2016,** *42* (5), 5069-5085.

124. Zulu, B.; Oyewo, O. A.; Sithole, B.; Leswifi, T. Y.; Onyango, M. S., Functionalized Sawdust-Derived Cellulose Nanocrystalline Adsorbent for Efficient Removal of Vanadium From Aqueous Solution. *Frontiers in Environmental Science* **2020,** *8*.

125. Campano, C.; Lopez-Exposito, P.; Blanco, A.; Negro, C.; van de Ven, T. G. M., Hairy cationic nanocrystalline cellulose as a novel flocculant of clay. *Journal of Colloid and Interface Science* **2019,** *545*, 153-161.

126. Campano, C.; Lopez-Exposito, P.; Blanco, A.; Negro, C.; van de Ven, T. G. M., Hairy cationic nanocrystalline cellulose as retention additive in recycled paper. *Cellulose* **2019,** *26* (10), 6275-6289.

127. Hamed, O.; Radad, R.; Jodeh, S.; Deghles, A.; Qrareya, H.; Dagdag, O.; Azzaoui, K.; Al-Kerm, R.; Al-Kerm, R.; Adwan, G., Design, synthesis and antimicrobial properties of cellulose-based amine film. *Polymer Bulletin* **2021**.

128. Jin, L.; Li, W.; Xu, Q.; Sun, Q., Amino-functionalized nanocrystalline cellulose as an adsorbent for anionic dyes. *Cellulose* **2015,** *22* (4), 2443-2456.

129. Zeifman, L.; Hertog, S.; Kantorova, V.; Wilmoth, J., A world of 8 billion. **2022**.

130. Rahman, N. S. A.; Yhaya, M. F.; Azahari, B.; Ismail, W. R., Utilisation of natural cellulose fibres in wastewater treatment. *Cellulose* **2018,** *25* (9), 4887-4903.

131. Mao, G.; Han, Y.; Liu, X.; Crittenden, J.; Huang, N.; Ahmad, U. M., Technology status and trends of industrial wastewater treatment: A patent analysis. *Chemosphere* **2022,** *288*, 132483.

132. Demirbas, A., Heavy metal adsorption onto agro-based waste materials: a review. *J Hazard Mater* **2008,** *157* (2-3), 220-9.

133. Chandramohan, D.; Marimuthu, K., A review on natural fibers. *International Journal of Research and Reviews in Applied Sciences* **2011,** *8* (2), 194-206.

134. Ticoalu, A.; Aravinthan, T.; Cardona, F., A Review of Current Development in Natural Fiber Composites for Structural and Infrastructure Applications. **2010**.

135. Gupta, V.; Carrott, P.; Singh, R.; Chaudhary, M.; Kushwaha, S., Cellulose: a review as natural, modified and activated carbon adsorbent. *Bioresource technology* **2016,** *216*, 1066-1076.

136. Chequer, F. M. D.; Angeli, J. P. F.; Ferraz, E. R. A.; Tsuboy, M. S.; Marcarini, J. C.; Mantovani, M. S.; de Oliveira, D. P., The azo dyes Disperse Red 1 and Disperse Orange 1 increase the micronuclei frequencies in human lymphocytes and in HepG2 cells. *Mutation Research/Genetic Toxicology and Environmental Mutagenesis* **2009,** *676* (1-2), 83-86.

137. Kausar, A.; Zohra, S. T.; Ijaz, S.; Iqbal, M.; Iqbal, J.; Bibi, I.; Nouren, S.; El Messaoudi, N.; Nazir, A., Cellulose-based materials and their adsorptive removal efficiency for dyes: A review. *International Journal of Biological Macromolecules* **2023,** *224*, 1337-1355.

138. Gupta, V., Application of low-cost adsorbents for dye removal–a review. *Journal of environmental management* **2009,** *90* (8), 2313-2342.

139. Wang, X. S.; Zhou, Y.; Jiang, Y.; Sun, C., The removal of basic dyes from aqueous solutions using agricultural by-products. *Journal of Hazardous Materials* **2008,** *157* (2-3), 374-385.

140. Sun, Q.; Yang, L., The adsorption of basic dyes from aqueous solution on modified peat–resin particle. *Water research* **2003,** *37* (7), 1535-1544.

141. Shahid, M.; Mohammad, F., Recent advancements in natural dye applications: a review. *Journal of cleaner production* **2013,** *53*, 310-331.

142. Laissaoui, M.; Elbatal, Y.; Vioque, I.; Manjon, G., Adsorption of methylene blue on bituminous schists from Tarfaya-Boujdour. *Chem Int* **2017,** *3* (4), 343-352.

143. Yagub, M. T.; Sen, T. K.; Afroze, S.; Ang, H. M., Dye and its removal from aqueous solution by adsorption: a review. *Advances in colloid and interface science* **2014,** *209*, 172-184.

144. Minas, F.; Chandravanshi, B. S.; Leta, S., Chemical precipitation method for chromium removal and its recovery from tannery wastewater in Ethiopia. *Chem. Int* **2017,** *3* (4), 291-305.

145. Iqbal, M.; Khera, R. A., Adsorption of copper and lead in single and binary metal system onto Fumaria indica biomass. *Chem. Int* **2015,** *1* (3), 157b-163b.

146. Salleh, M. A. M.; Mahmoud, D. K.; Karim, W. A. W. A.; Idris, A., Cationic and anionic dye adsorption by agricultural solid wastes: a comprehensive review. *Desalination* **2011,** *280* (1-3), 1-13.

147. Alkherraz, A. M.; Ali, A. K.; Elsherif, K. M., Removal of Pb (II), Zn (II), Cu (II) and Cd (II) from aqueous solutions by adsorption onto olive branches activated carbon: equilibrium and thermodynamic studies. *Chem. Int* **2020,** *6* (1), 11-20.

148. Dutta, S.; Gupta, B.; Srivastava, S. K.; Gupta, A. K., Recent advances on the removal of dyes from wastewater using various adsorbents: A critical review. *Materials Advances* **2021,** *2* (14), 4497-4531.

149. Abdelhamid, H. N.; Mathew, A. P., Cellulose-based materials for water remediation: adsorption, catalysis, and antifouling. *Frontiers in Chemical Engineering* **2021,** *3*, 790314.

150. Belhalfaoui, B.; Aziz, A.; Elandaloussi, E. H.; Ouali, M. S.; De Ménorval, L. C., Succinate-bonded cellulose: A regenerable and powerful sorbent for cadmium-removal from spiked high-hardness groundwater. *Journal of hazardous materials* **2009,** *169* (1-3), 831-837.

151. Tashiro, T.; Shimura, Y., Removal of mercuric ions by systems based on cellulose derivatives. *Journal of applied polymer science* **1982,** *27* (2), 747-756.

152. Saito, T.; Isogai, A., Ion-exchange behavior of carboxylate groups in fibrous cellulose oxidized by the TEMPO-mediated system. *Carbohydrate Polymers* **2005,** *61* (2), 183-190.

153. Liu, P.; Borrell, P. F.; Božič, M.; Kokol, V.; Oksman, K.; Mathew, A. P., Nanocelluloses and their phosphorylated derivatives for selective adsorption of Ag+, Cu2+ and Fe3+ from industrial effluents. *Journal of hazardous materials* **2015,** *294*, 177-185.

154. Fomina, M.; Gadd, G. M., Biosorption: current perspectives on concept, definition and application. *Bioresource technology* **2014,** *160*, 3-14.

155. Rocky, M. M. H.; Rahman, I. M. M.; Biswas, F. B.; Rahman, S.; Endo, M.; Wong, K. H.; Mashio, A. S.; Hasegawa, H., Cellulose-based materials for scavenging toxic and precious metals from water and wastewater: A review. *Chemical Engineering Journal* **2023,** *472*, 144677.

156. Pearson, R. G., Hard and soft acids and bases. *Journal of the American Chemical society* **1963,** *85* (22), 3533-3539.

157. Tsezos, M.; Remoudaki, E.; Angelatou, V., A study of the effects of competing ions on the biosorption of metals. *International Biodeterioration & Biodegradation* **1996,** *38* (1), 19-29.

158. Olivera, S.; Muralidhara, H. B.; Venkatesh, K.; Guna, V. K.; Gopalakrishna, K.; Kumar, Y., Potential applications of cellulose and chitosan nanoparticles/composites in wastewater treatment: a review. *Carbohydrate polymers* **2016,** *153*, 600-618.

159. Sud, D.; Mahajan, G.; Kaur, M., Agricultural waste material as potential adsorbent for sequestering heavy metal ions from aqueous solutions–A review. *Bioresource technology* **2008,** *99* (14), 6017-6027.

160. Miretzky, P.; Cirelli, A. F., Cr (VI) and Cr (III) removal from aqueous solution by raw and modified lignocellulosic materials: a review. *Journal of hazardous materials* **2010,** *180* (1-3), 1-19.

161. Wang, L.; Peng, H.; Liu, S.; Yu, H.; Li, P.; Xing, R., Adsorption properties of gold onto a chitosan derivative. *International journal of biological macromolecules* **2012,** *51* (5), 701-704.

162. Velazquez-Jimenez, L. H.; Pavlick, A.; Rangel-Mendez, J. R., Chemical characterization of raw and treated agave bagasse and its potential as adsorbent of metal cations from water. *Industrial Crops and Products* **2013,** *43*, 200-206.

163. Ho, Y.-S.; McKay, G., Pseudo-second order model for sorption processes. *Process biochemistry* **1999,** *34* (5), 451-465.

164. Sutradhar, T.; Misra, A., Role of Electron-Donating and Electron-Withdrawing Groups in Tuning the Optoelectronic Properties of Difluoroboron–Napthyridine Analogues. *The Journal of Physical Chemistry A* **2018,** *122* (16), 4111-4120.

165. Das, R.; Lindström, T.; Sharma, P. R.; Chi, K.; Hsiao, B. S., Nanocellulose for Sustainable Water Purification. *Chemical Reviews* **2022,** *122* (9), 8936-9031.

166. Kaur, J.; Sengupta, P.; Mukhopadhyay, S., Critical Review of Bioadsorption on Modified Cellulose and Removal of Divalent Heavy Metals (Cd, Pb, and Cu). *Industrial & Engineering Chemistry Research* **2022,** *61* (5), 1921-1954.

167. Zheng, L.; Zhu, C.; Dang, Z.; Zhang, H.; Yi, X.; Liu, C., Preparation of cellulose derived from corn stalk and its application for cadmium ion adsorption from aqueous solution. *Carbohydrate Polymers* **2012,** *90* (2), 1008-1015.

168. Daochalermwong, A.; Chanka, N.; Songsrirote, K.; Dittanet, P.; Niamnuy, C.; Seubsai, A., Removal of Heavy Metal Ions Using Modified Celluloses Prepared from Pineapple Leaf Fiber. *ACS Omega* **2020,** *5* (10), 5285-5296.

169. Saravanan, R.; Ravikumar, L., Renewable Modified Cellulose Bearing Chelating Schiff Base for Adsorptive Removal of Heavy Metal Ions and Antibacterial Action. *Water Environment Research* **2017,** *89* (7), 629-640.

170. Kenawy, I. M.; Hafez, M. A. H.; Ismail, M. A.; Hashem, M. A., Adsorption of Cu(II), Cd(II), Hg(II), Pb(II) and Zn(II) from aqueous single metal solutions by guanyl-modified cellulose. *International Journal of Biological Macromolecules* **2018,** *107*, 1538-1549.

171. Nguyen, T. A.; Tran, D. B.; Le, H. D. C.; Nguyen, Q. L.; Pham, V., Thiosemicarbazone-Modified Cellulose: Synthesis, Characterization, and Adsorption Studies on Cu(II) Removal. *ACS Omega* **2020,** *5* (24), 14481-14493.

172. Jiao, C.; Zhang, Z.; Tao, J.; Zhang, D.; Chen, Y.; Lin, H., Synthesis of a poly (amidoxime-hydroxamic acid) cellulose derivative and its application in heavy metal ion removal. *RSC advances* **2017,** *7* (44), 27787-27795.

173. Zhou, Y.; Hu, X.; Zhang, M.; Zhuo, X.; Niu, J., Preparation and characterization of modified cellulose for adsorption of Cd (II), Hg (II), and acid fuchsin from aqueous solutions. *Industrial & Engineering Chemistry Research* **2013,** *52* (2), 876-884.

174. Zhang, C.; Su, J.; Zhu, H.; Xiong, J.; Liu, X.; Li, D.; Chen, Y.; Li, Y., The removal of heavy metal ions from aqueous solutions by amine functionalized cellulose pretreated with microwave-H 2 O 2. *RSC advances* **2017,** *7* (54), 34182-34191.

175. Zhan, W.; Xu, C.; Qian, G.; Huang, G.; Tang, X.; Lin, B., Adsorption of Cu (ii), Zn (ii), and Pb (ii) from aqueous single and binary metal solutions by regenerated cellulose and sodium alginate chemically modified with polyethyleneimine. *RSC advances* **2018,** *8* (33), 18723-18733.

176. Manzoor, K.; Ahmad, M.; Ahmad, S.; Ikram, S., Synthesis, characterization, kinetics, and thermodynamics of EDTA-modified chitosan-carboxymethyl cellulose as Cu (II) ion adsorbent. *ACS omega* **2019,** *4* (17), 17425-17437.

177. Chen, Q.; Zheng, J.; Wen, L.; Yang, C.; Zhang, L., A multi-functional-group modified cellulose for enhanced heavy metal cadmium adsorption: Performance and quantum chemical mechanism. *Chemosphere* **2019,** *224*, 509-518.

178. Zheng, L.; Yang, Y.; Meng, P.; Peng, D., Absorption of cadmium (II) via sulfur-chelating based cellulose: characterization, isotherm models and their error analysis. *Carbohydrate Polymers* **2019,** *209*, 38-50.

179. Meng, Q.; Wu, S.; Shen, C., Polyethylenimine-grafted-corncob as a multifunctional biomaterial for removing heavy metal ions and killing bacteria from water. *Industrial & Engineering Chemistry Research* **2020,** *59* (39), 17476-17482.

180. d'Halluin, M.; Rull-Barrull, J.; Bretel, G.; Labrugère, C.; Le Grognec, E.; Felpin, F.-X., Chemically modified cellulose filter paper for heavy metal remediation in water. *ACS Sustainable Chemistry & Engineering* **2017,** *5* (2), 1965-1973.

181. Hashem, A.; Fletcher, A.; Younis, H.; Mauof, H.; Abou-Okeil, A., Adsorption of Pb (II) ions from contaminated water by 1, 2, 3, 4-butanetetracarboxylic acid-modified microcrystalline

cellulose: Isotherms, kinetics, and thermodynamic studies. *International journal of biological macromolecules* **2020,** *164*, 3193-3203.

182. Wang, J.; Dang, M.; Duan, C.; Zhao, W.; Wang, K., Carboxymethylated cellulose fibers as low-cost and renewable adsorbent materials. *Industrial & Engineering Chemistry Research* **2017,** *56* (51), 14940-14948.

183. Qu, W.; He, D.; Guo, Y.; Tang, Y.; Shang, J.; Zhou, L.; Zhu, R.; Song, R.-J., Modified water hyacinth functionalized with citric acid as an effective and inexpensive adsorbent for heavy metal-ion removal. *Industrial & Engineering Chemistry Research* **2019,** *58* (40), 18508-18518.

184. Bérdy, J., Thoughts and facts about antibiotics: where we are now and where we are heading. *The Journal of antibiotics* **2012,** *65* (8), 385-395.

185. Khattak, S.; Wahid, F.; Liu, L.-P.; Jia, S.-R.; Chu, L.-Q.; Xie, Y.-Y.; Li, Z.-X.; Zhong, C., Applications of cellulose and chitin/chitosan derivatives and composites as antibacterial materials: current state and perspectives. *Applied Microbiology and Biotechnology* **2019,** *103* (5), 1989-2006.

186. Wahid, F.; Zhong, C.; Wang, H.-S.; Hu, X.-H.; Chu, L.-Q., Recent advances in antimicrobial hydrogels containing metal ions and metals/metal oxide nanoparticles. *Polymers* **2017,** *9* (12), 636.

187. Jung, S.-M.; Yoon, G. H.; Lee, H. C.; Shin, H. S., Chitosan nanoparticle/PCL nanofiber composite for wound dressing and drug delivery. *Journal of Biomaterials Science, Polymer Edition* **2015,** *26* (4), 252-263.

188. Le Ouay, B.; Stellacci, F., Antibacterial activity of silver nanoparticles: A surface science insight. *Nano today* **2015,** *10* (3), 339-354.

189. Li, C.; Zhu, C.; Ren, B.; Yin, X.; Shim, S. H.; Gao, Y.; Zhu, J.; Zhao, P.; Liu, C.; Yu, R., Two optimized antimicrobial peptides with therapeutic potential for clinical antibiotic-resistant Staphylococcus aureus. *European Journal of Medicinal Chemistry* **2019,** *183*, 111686.

190. Carmona-Ribeiro, A. M.; de Melo Carrasco, L. D., Cationic antimicrobial polymers and their assemblies. *Int J Mol Sci* **2013,** *14* (5), 9906-46.

191. Ng, V. W.; Chan, J. M.; Sardon, H.; Ono, R. J.; García, J. M.; Yang, Y. Y.; Hedrick, J. L., Antimicrobial hydrogels: A new weapon in the arsenal against multidrug-resistant infections. *Advanced drug delivery reviews* **2014,** *78*, 46-62.

192. Asare, N.; Instanes, C.; Sandberg, W. J.; Refsnes, M.; Schwarze, P.; Kruszewski, M.; Brunborg, G., Cytotoxic and genotoxic effects of silver nanoparticles in testicular cells. *Toxicology* **2012,** *291* (1-3), 65-72.

193. Iyer, P. V.; Ananthanarayan, L., Enzyme stability and stabilization—aqueous and non-aqueous environment. *Process biochemistry* **2008,** *43* (10), 1019-1032.

194. Roy, D.; Knapp, J. S.; Guthrie, J. T.; Perrier, S., Antibacterial cellulose fiber via RAFT surface graft polymerization. *Biomacromolecules* **2008,** *9* (1), 91-99.

195. Kenawy, E.-R.; Worley, S.; Broughton, R., The chemistry and applications of antimicrobial polymers: a state-of-the-art review. *Biomacromolecules* **2007,** *8* (5), 1359-1384.

196. Dash, M.; Chiellini, F.; Ottenbrite, R. M.; Chiellini, E., Chitosan—A versatile semi-synthetic polymer in biomedical applications. *Progress in polymer science* **2011,** *36* (8), 981-1014.

197. Tavakolian, M.; Jafari, S. M.; van de Ven, T. G. M., A Review on Surface-Functionalized Cellulosic Nanostructures as Biocompatible Antibacterial Materials. *Nano-Micro Letters* **2020,** *12* (1), 73.

198. Rieger, K. A.; Cho, H. J.; Yeung, H. F.; Fan, W.; Schiffman, J. D., Antimicrobial activity of silver ions released from zeolites immobilized on cellulose nanofiber mats. *ACS applied materials & interfaces* **2016,** *8* (5), 3032-3040.

199. Fu, F.; Li, L.; Liu, L.; Cai, J.; Zhang, Y.; Zhou, J.; Zhang, L., Construction of cellulose based ZnO nanocomposite films with antibacterial properties through one-step coagulation. *ACS applied materials & interfaces* **2015,** *7* (4), 2597-2606.

200. Saini, S.; Belgacem, N.; Mendes, J.; Elegir, G.; Bras, J., Contact antimicrobial surface obtained by chemical grafting of microfibrillated cellulose in aqueous solution limiting antibiotic release. *ACS Applied Materials & Interfaces* **2015,** *7* (32), 18076-18085.

201. Li, W.; Li, X.; Wang, Q.; Pan, Y.; Wang, T.; Wang, H.; Song, R.; Deng, H., Antibacterial activity of nanofibrous mats coated with lysozyme-layered silicate composites via electrospraying. *Carbohydrate polymers* **2014,** *99*, 218-225.

202. Abdelhamid, H. N.; Mathew, A. P., Cellulose-Based Nanomaterials Advance Biomedicine: A Review. *International Journal of Molecular Sciences* **2022,** *23* (10), 5405.

203. Chinga-Carrasco, G.; Johansson, J.; Heggset, E. B.; Leirset, I.; Björn, C.; Agrenius, K.; Stevanic, J. S.; Håkansson, J., Characterization and Antibacterial Properties of Autoclaved Carboxylated Wood Nanocellulose. *Biomacromolecules* **2021,** *22* (7), 2779-2789.

204. Mou, K.; Li, J.; Wang, Y.; Cha, R.; Jiang, X., 2, 3-Dialdehyde nanofibrillated cellulose as a potential material for the treatment of MRSA infection. *Journal of Materials Chemistry B* **2017,** *5* (38), 7876-7884.

205. Fernandes, S. C. M.; Sadocco, P.; Alonso-Varona, A.; Palomares, T.; Eceiza, A.; Silvestre, A. J. D.; Mondragon, I.; Freire, C. S. R., Bioinspired Antimicrobial and Biocompatible

Bacterial Cellulose Membranes Obtained by Surface Functionalization with Aminoalkyl Groups. *ACS Applied Materials & Interfaces* **2013,** *5* (8), 3290-3297.

206. Vyhnalkova, R.; Mansur-Azzam, N.; Eisenberg, A.; van de Ven, T. G., Ten million fold reduction of live bacteria by bactericidal filter paper. *Advanced Functional Materials* **2012,** *22* (19), 4096-4100.

207. Koshani, R.; Zhang, J.; van de Ven, T. G.; Lu, X.; Wang, Y., Modified hairy nanocrystalline cellulose as photobactericidal nanofillers for food packaging application. *ACS Sustainable Chemistry & Engineering* **2021,** *9* (31), 10513-10523.

208. Feese, E.; Sadeghifar, H.; Gracz, H. S.; Argyropoulos, D. S.; Ghiladi, R. A., Photobactericidal porphyrin-cellulose nanocrystals: synthesis, characterization, and antimicrobial properties. *Biomacromolecules* **2011,** *12* (10), 3528-3539.

209. Shin, H.; Kim, S.; Kim, J.; Kong, S.; Lee, Y.; Lee, J. C., Preparation of 3-pentadecylphenol-modified cellulose nanocrystal and its application as a filler to polypropylene nanocomposites having improved antibacterial and mechanical properties. *Journal of Applied Polymer Science* **2022,** *139* (13), 51848.

210. Jebali, A.; Hekmatimoghaddam, S.; Behzadi, A.; Rezapor, I.; Mohammadi, B. H.; Jasemizad, T.; Yasini, S. A.; Javadzadeh, M.; Amiri, A.; Soltani, M., Antimicrobial activity of nanocellulose conjugated with allicin and lysozyme. *Cellulose* **2013,** *20*, 2897-2907.

211. Rouabhia, M.; Asselin, J.; Tazi, N.; Messaddeq, Y.; Levinson, D.; Zhang, Z., Production of biocompatible and antimicrobial bacterial cellulose polymers functionalized by RGDC grafting groups and gentamicin. *ACS Applied Materials & Interfaces* **2014,** *6* (3), 1439-1446.

212. Basmaji, P.; de Olyveira, G. M.; dos Santos, M. L.; Guastaldi, A. C., Novel antimicrobial peptides bacterial cellulose obtained by symbioses culture between polyhexanide biguanide (PHMB) and green tea. *Journal of Biomaterials and Tissue Engineering* **2014,** *4* (1), 59-64.

213. Jiang, Z.; Qiao, M.; Ren, X.; Zhu, P.; Huang, T.-S., Preparation of antibacterial cellulose with s-triazine-based quaternarized N-halamine. *Journal of Applied Polymer Science* **2017,** *134* (26).

214. He, W.; Zhang, Z.; Zheng, Y.; Qiao, S.; Xie, Y.; Sun, Y.; Qiao, K.; Feng, Z.; Wang, X.; Wang, J., Preparation of aminoalkyl-grafted bacterial cellulose membranes with improved antimicrobial properties for biomedical applications. *Journal of Biomedical Materials Research Part A* **2020,** *108* (5), 1086-1098.

215. Lone, A.; Anany, H.; Hakeem, M.; Aguis, L.; Avdjian, A.-C.; Bouget, M.; Atashi, A.; Brovko, L.; Rochefort, D.; Griffiths, M. W., Development of prototypes of bioactive packaging materials based on immobilized bacteriophages for control of growth of bacterial pathogens in foods. *International journal of food microbiology* **2016,** *217*, 49-58.

216. Rong, L.; Yang, D.; Wang, B.; Xiao, D.; Lu, M.; Mao, Z.; Xu, H.; Gu, Y.; Feng, X.; Sui, X., Durable and effective antibacterial cotton fabric collaborated with polypropylene tissue mesh for abdominal wall defect repair. *ACS Biomaterials Science & Engineering* **2020,** *6* (7), 3868-3877.

217. Knutsen, M. F.; Agrenius, K.; Ugland, H.; Petronis, S.; Haglerod, C.; Håkansson, J.; Chinga-Carrasco, G., Oxygenated Nanocellulose—A Material Platform for Antibacterial Wound Dressing Devices. *ACS Applied Bio Materials* **2021,** *4* (10), 7554-7562.

218. Chinga-Carrasco, G.; Johansson, J.; Heggset, E. B.; Leirset, I.; Bjorn, C.; Agrenius, K.; Stevanic, J. S.; Hakansson, J., Characterization and antibacterial properties of autoclaved carboxylated wood nanocellulose. *Biomacromolecules* **2021,** *22* (7), 2779-2789.

219. Pham, T. C.; Nguyen, V.-N.; Choi, Y.; Lee, S.; Yoon, J., Recent strategies to develop innovative photosensitizers for enhanced photodynamic therapy. *Chemical Reviews* **2021,** *121* (21), 13454-13619.

220. Alvarado, D. R.; Argyropoulos, D. S.; Scholle, F.; Peddinti, B. S.; Ghiladi, R. A., A facile strategy for photoactive nanocellulose-based antimicrobial materials. *Green Chemistry* **2019,** *21* (12), 3424-3435.

221. Fei, P.; Liao, L.; Meng, J.; Cheng, B.; Hu, X.; Song, J., Non-leaching antibacterial cellulose triacetate reverse osmosis membrane via covalent immobilization of quaternary ammonium cations. *Carbohydrate polymers* **2018,** *181*, 1102-1111.

222. Fernandes, S. C.; Sadocco, P.; Alonso-Varona, A.; Palomares, T.; Eceiza, A.; Silvestre, A. J.; Mondragon, I.; Freire, C. S., Bioinspired antimicrobial and biocompatible bacterial cellulose membranes obtained by surface functionalization with aminoalkyl groups. *ACS applied materials & interfaces* **2013,** *5* (8), 3290-3297.

223. Hou, Q.; Liu, W.; Liu, Z.; Duan, B.; Bai, L., Characteristics of antimicrobial fibers prepared with wood periodate oxycellulose. *Carbohydrate polymers* **2008,** *74* (2), 235-240.

224. Abdelhamid, H. N.; Georgouvelas, D.; Edlund, U.; Mathew, A. P., CelloZIFPaper: Cellulose-ZIF hybrid paper for heavy metal removal and electrochemical sensing. *Chemical Engineering Journal* **2022,** *446*, 136614.

225. Abouhmad, A.; Dishisha, T.; Amin, M. A.; Hatti-Kaul, R., Immobilization to positively charged cellulose nanocrystals enhances the antibacterial activity and stability of hen egg white and T4 lysozyme. *Biomacromolecules* **2017,** *18* (5), 1600-1608.

226. De France, K. J.; Kummer, N.; Ren, Q.; Campioni, S.; Nyström, G., Assembly of cellulose nanocrystal–lysozyme composite films with varied lysozyme morphology. *Biomacromolecules* **2020,** *21* (12), 5139-5147.

227. Katepetch, C.; Rujiravanit, R.; Tamura, H., Formation of nanocrystalline ZnO particles into bacterial cellulose pellicle by ultrasonic-assisted in situ synthesis. *Cellulose* **2013,** *20*, 1275-1292.

228. Ul-Islam, M.; Khattak, W. A.; Ullah, M. W.; Khan, S.; Park, J. K., Synthesis of regenerated bacterial cellulose-zinc oxide nanocomposite films for biomedical applications. *Cellulose* **2014,** *21*, 433-447.

229. Khan, S.; Ul-Islam, M.; Khattak, W. A.; Ullah, M. W.; Park, J. K., Bacterial cellulose-titanium dioxide nanocomposites: nanostructural characteristics, antibacterial mechanism, and biocompatibility. *Cellulose* **2015,** *22*, 565-579.

230. Baghdad, K.; Hasnaoui, A. M., Zeolite–cellulose composite membranes: Synthesis and applications in metals and bacteria removal. *Journal of Environmental Chemical Engineering* **2020,** *8* (4), 104047.

231. Luan, J.; Wu, J.; Zheng, Y.; Song, W.; Wang, G.; Guo, J.; Ding, X., Impregnation of silver sulfadiazine into bacterial cellulose for antimicrobial and biocompatible wound dressing. *Biomedical Materials* **2012,** *7* (6), 065006.

232. Timofeeva, L.; Kleshcheva, N., Antimicrobial polymers: mechanism of action, factors of activity, and applications. *Applied Microbiology and Biotechnology* **2011,** *89* (3), 475-492.

233. Xu, F.; Yu, J.; Tesso, T.; Dowell, F.; Wang, D., Qualitative and quantitative analysis of lignocellulosic biomass using infrared techniques: A mini-review. *Applied Energy* **2013,** *104*, 801-809.

234. Ahmad, Z.; Iis, S.; Halim, Z.; Sarifuddin, N., EFFECT OF FIBER LENGTH VARIATIONS ON PROPERTIES OF COIR FIBER REINFORCED CEMENT-ALBUMEN COMPOSITE (CFRCC). *IIUM Engineering Journal* **2011,** *12* (1), 63-76.

235. Poletto, M.; Pistor, V.; Zeni, M.; Zattera, A. J., Crystalline properties and decomposition kinetics of cellulose fibers in wood pulp obtained by two pulping processes. *Polymer Degradation and Stability* **2011,** *96* (4), 679-685.

236. Rosa, M. F.; Medeiros, E. S.; Malmonge, J. A.; Gregorski, K. S.; Wood, D. F.; Mattoso, L. H. C.; Glenn, G.; Orts, W. J.; Imam, S. H., Cellulose nanowhiskers from coconut husk fibers: Effect of preparation conditions on their thermal and morphological behavior. *Carbohydrate Polymers* **2010,** *81* (1), 83-92.

237. Hospodarova, V.; Singovszka, E.; Stevulova, N., Characterization of Cellulosic Fibers by FTIR Spectroscopy for Their Further Implementation to Building Materials. *American Journal of Analytical Chemistry* **2018,** *09* (06), 303-310.

238. Dang, X.; Liu, P.; Yang, M.; Deng, H.; Shan, Z.; Zhen, W., Production and characterization of dialdehyde cellulose through green and sustainable approach. *Cellulose* **2019,** *26* (18), 9503-9515.

239. Tavakolian, M.; Munguia-Lopez, J. G.; Valiei, A.; Islam, M. S.; Kinsella, J. M.; Tufenkji, N.; van de Ven, T. G. M., Highly Absorbent Antibacterial and Biofilm-Disrupting Hydrogels from Cellulose for Wound Dressing Applications. *ACS Applied Materials & Interfaces* **2020,** *12* (36), 39991-40001.

240. Daniel, S., Chapter 4 - Characterization of carbon dots. In *Carbon Dots in Analytical Chemistry*, Kailasa, S. K.; Hussain, C. M., Eds. Elsevier: 2023; pp 43-58.

241. Zakharov, P.; Scheffold, F., Advances in Dynamic Light Scattering Techniques BT—Light Scattering Reviews 4: Single Light Scattering and Radiative Transfer; Kokhanovsky, AA, Ed. Springer Berlin Heidelberg: Berlin/Heidelberg, Germany: 2009.

242. Gallardo-Sánchez, M. A.; Diaz-Vidal, T.; Navarro-Hermosillo, A. B.; Figueroa-Ochoa, E. B.; Ramirez Casillas, R.; Anzaldo Hernández, J.; Rosales-Rivera, L. C.; Soltero Martínez, J. F. A.; García Enríquez, S.; Macías-Balleza, E. R., Optimization of the obtaining of cellulose nanocrystals from agave Tequilana weber var. Azul Bagasse by acid hydrolysis. *Nanomaterials* **2021,** *11* (2), 520.

243. Young, S. A. E.; Muthami, J.; Pitcher, M.; Antovski, P.; Wamea, P.; Murphy, R. D.; Haghniaz, R.; Schmidt, A.; Clark, S.; Khademhosseini, A.; Sheikhi, A., Engineering hairy cellulose nanocrystals for chemotherapy drug capture. *Mater Today Chem* **2022,** *23*.

244. Lavorante, M. J.; Franco, J. I., Conductometric titration as a technique to determine variation in conductivity in perfluorosulfonic acid materials for fuel cells and electrolyzers. *International Journal of Energy and Environmental Engineering* **2017,** *8* (2), 123-134.

245. Mendham, J.; Denney, R.; Barnes, J., *Textbook of Quantit A Tive Chemical Analysis*. Pearson: 2016.

246. Bochek, A.; Zabivalova, N.; Petropavlovskii, G., Determination of the esterification degree of polygalacturonic acid. *Russian Journal of Applied Chemistry* **2001,** *74*, 796-799.

247. Farris, S.; Mora, L.; Capretti, G.; Piergiovanni, L., Charge Density Quantification of Polyelectrolyte Polysaccharides by Conductometric Titration: An Analytical Chemistry Experiment. *Journal of Chemical Education* **2012,** *89* (1), 121-124.

Chapter 3

THE REMOVAL OF ANIONIC DYE IN WASTEWATER TREATMENT BY ADSORPTION ON DIAMINOCELLULOSE

Preface

The water treatment industry has a critical requirement for the development of adsorbents that are renewable, biodegradable, easily-regenerable, and possess a high capacity. The majority of the existing commercial adsorbents are non-renewable and, in certain instances, pose a threat to the environment and human well-being due to their toxicity. This chapter introduces the utilization of aminated cellulose fibers as a highly promising alternative to address the limitations associated with existing commercial adsorbents. This chapter has been published in the *Journal of Colloid and Interface Science*.

3.1. Abstract

Diaminocellulose fiber (DAmF) was synthesized by periodate oxidation of Kraft pulp, followed by a reductive amination reaction. DAmF was dissolved in water at 60 ^{0}C and pH 3 to produce diaminocellulose (DAmC). At room temperature, both DAmF and DAmC are present in water. The presence of amine was confirmed by FT-IR, ζ-potential measurements and XPS. Amine content of diaminocellulose was determined by conductometric titration and was found to be 9.5 mmol g^{-1} which is double the amine content in chitosan, another cationic biopolymer. DAmC and DAmF were investigated for their ability to remove an anionic dye, Procion Red mx-5B (PR), from wastewater. DAmC and DAmF showed good adsorption capacity for the anionic dye, PR. The Langmuir model was used for describing the adsorption isotherm of PR on DAmF, with the maximum adsorption capacity for PR being 3.72 g g^{-1}. NaOH was used to desorb the adsorbed dye and regenerate the biosorbent. The adsorption-desorption test demonstrated the good reusability of this fiber.

3.2. Introduction

Synthetic dyes are vital in the manufacturing of cosmetics, drugs, textiles, food, leather, and paper. They are more advantageous than natural dyes because of their simple synthesis, lower cost, higher colour fastness, broader spectrum of colour availability, and ability to dye synthetic fibres[1]. Yearly, 800,000 tons of dyes are produced annually, of which 10-15% are lost during utilization; therefore, pollution of surrounding water bodies is inevitable. There are over 100,000 types of dye with about 70% of them being azo dyes that have complex structures which are non-biodegradable[2-5]. Azo dyes are characterized by having one or more azo groups (-N=N-) and substituted aromatic groups in their chemical structure. Pollution caused by these dyes in the environment includes aesthetic damage to water bodies, decrease in the rate of aquatic plants' photosynthesis due to reduced sunlight penetration, and diminished vitality of aquatic life from reduced dissolved oxygen levels[6, 7]. Many azo dyes undergo cleavage reactions to form aromatic amines which have been linked to various forms of cancers, specifically bladder and liver cancer[8]. Since azo dyes do not biodegrade naturally and are resistant to conventional wastewater treatments such as aerobic biodegradation, the need for treatment of wastewater containing synthetic dyes is imperative[9]. Different methods have been employed in treating dyed wastewater, including biodegradation[10, 11], advanced oxidation processes (AOPs)[12, 13], adsorption, chemical coagulation and flocculation with sedimentation[14]. Flocculation and adsorption are most attractive because of their low cost of operation, non-selectivity of pollutants, simplicity in design and operation, and with an added advantage of reusability to the later. Both methods have been successfully employed for the removal of dyes from wastewater[15-17].

Wastewater treatment often uses precipitation to remove contaminants by process of coagulation/ flocculation due to its low capital cost. This process typically removes heavy metals, dyes, and other pollutants that can harm the environment or human health. Chemicals added during precipitation react with wastewater contaminants to form solid particles that can be sedimented or filtered out. The effectiveness of this process depends on the type of contaminants in wastewater, their concentration, and the type and dosage of chemicals used. Flocculation followed by sedimentation is a process of separating colloids and suspended particles from aqueous suspension. Organic flocculants are polymers which can absorb and bridge particles and are economic as well as efficient in water/wastewater purification, especially for removing low molecular weight and hydrophilic substances[18, 19]. Polymers are advantageous over inorganic coagulants like salts because they are large enough to screen electrostatic forces and can strongly adsorb onto several particles, causing flocculation by polymer bridging, and lower dosages are required and in addition, they are effective over a wider pH range[20]. Common organic anionic and cationic flocculants employed are anionic polyacrylamide (aPAM) and cationic polyethylene imine (PEI)[21]. But these synthetic polymers are non-biodegradable, environmentally unfriendly and toxic, therefore, there is a need for new "green" flocculants.

Adsorption is a surface phenomenon where adsorbates (atoms, molecules, or ions) are attracted to the surface of an adsorbent material through chemical, physical or electrostatic interactions. The key parameters of a promising adsorbent include high surface area, high selectivity, good regeneration capacity, and low cost[17, 22]. Exploration of adsorbents that meet industrial water treatment standards while also being cost-effective, environmentally friendly, highly efficient, and widely available is essential[23-27]. Dye adsorption on the adsorbent surface occurs via various mechanisms such as hydrogen bonding, π-π interactions, electrostatic attraction, and hydrophobic interaction[28-30].

The process of desorption involves the liberation of molecules that have been adsorbed onto an adsorbent material[31]. By understanding the desorption process, researchers can develop methods to release the dye from the adsorbent, allowing for the reuse of the material. Desorption and regeneration of the adsorbent are beneficial as they decrease processing costs by eliminating the need for frequent replacement of the adsorbent material. The desorption process often involves the use of solvents, both organic and inorganic, to break the interactions between the adsorbent and the dye molecules. Common solvents used in desorption include methanol, ethanol, isopropanol, acid and base solutions, sodium chloride (NaCl), nitric acid (HNO_3), and hydrogen peroxide (H_2O_2)[32-34]. The choice of desorption solvent depends on the specific adsorbate and adsorbent being used. This has significant implications for cost savings, environmental sustainability, and resource efficiency in various applications such as water treatment, air purification, and gas separation processes[34]. Cellulose and its derivatives in various forms have extensively been used in the treatment of wastewater including for the removal of dyes[35-37]. Nanocellulose provides a high surface area per mass (surface-to-volume ratio), and unique mechanical, thermal, and optical properties that are different from cellulose fibers, which can result in a higher adsorption capacity[38]. Still, these benefits often come with higher production costs and handling challenges. Cellulose fibers offer the convenience of being easier to handle and separated from a medium after adsorption, due to their larger size compared to nanocellulose, which may require additional processes for complete separation[39]. Cellulose fibers offer low-cost adsorbent for dyes because of its very large internal and external (200-300 $m^2\ g^{-1}$) surface area, ease of separation after adsorption, and reusability[39-41]. Macromolecular (dissolved) cellulose offers the advantages of low capital cost, being able to capture fine particles, large enough to screen charges and flexible to strongly absorb unto several particles[18]. Cationic cellulose, an important cellulose derivative, finds wide applications in various fields such as papermaking, cosmetics, adsorbents, and antibacterial agents[42, 43]. The three common methods of preparing cationic modified fibers involve direct cationization of the fiber, coupling of cationic oligomers (short chain polymers) to the fiber surface, and graft copolymerization of cationic polymers to the fiber surface[44]. These methods result in different links between the cationic groups and the fibers, which ultimately impact the fiber morphology and performance[45]. The choice of method depends on the desired properties of the modified fibers and their specific application requirements. Direct cationization is usually done through the introduction of quaternary amine groups on cellulose[46-48]. These materials were synthesized by attaching quaternary amines to the surface of cellulose and used for the adsorption of anionic dyes, but quaternary amines are permanently charged, unlike primary amines. This implies that although they are good adsorbents at all pHs, the desorption of anionic dyes during the recovery process would be difficult due to electrostatic interaction. Materials with primary amines that can be easily tuned by pH (they are protonated at low pH and deprotonated in alkaline solution) would serve as better reusable biosorbents.

In this study, we aim at synthesizing a new cationic modified cellulose fibre (DAmF) by a sequential periodate oxidation and reductive amination reaction of cellulose pulp. Dissolution of DAmF (which are still in fiber form after these reactions) coupled with heat in acidic media leads to a water-soluble polymer, DAmC. DAmF and DAmC each contain a high amount of primary amine groups which are very reactive and easily protonated/deprotonated. To be more specific, DAmC is the solubilized version of DAmF, as both compounds share the same chemical structure. DAmC is diaminocellulose that has been solubilized using heat and pH 3, whereas DAmF is diaminocellulose that has not been broken down and is in the form of fibres. Characterization of these adsorbents was done by FTIR spectroscopy, conductometric titration and XPS. The target molecule for dye adsorption used in this study was procion Red mx-5B dye (PR) also known as reactive red 2, shown in Fig. 3- 1. This dye is a highly soluble anionic dye that is utilized in the textile industry for dyeing cellulose, nylon, silk, and wool. It offers excellent colorfastness and has a wide range of applications due to its vibrant and long-lasting red color[49]. The dye was selected due to its complex chemical structure ($C_{19}H_{10}Cl_2N_6Na_2O_7S_2$), high molecular weight (615.33 g/mol), high solubility in water and its persistence once it is discharged into natural environment[50, 51]. We have also used this dye in an adsorption study published by our research group[52]. We aim to utilize DAmF as a reusable biosorbent to remove this dye and investigate the adsorption mechanism by its adsorption on the macromolecular counterpart (DAmC). The effect of pH, ionic strength and fibre reusability were investigated in this work. To our best knowledge, no studies have been conducted on the direct cationization of cellulose by our method and the removal of procion red MX-5b dye from aqueous solutions by the produced diaminocellulose fiber.

3.3. Materials and methods

3.3.1. Reagents and Materials.

Cellulose softwood kraft pulp (Domtar, Canada) was used as the starting material to synthesize DAmF. Sodium periodate (NaIO4), ethylene glycol (≥ 99%), ammonium acetate (NH_4OAc), ammonium in ethanol (2M), sodium borohydride ($NaBH_4$), and hydroxylamine hydrochloride ($NH_2OH \cdot HCl$) were purchased from Sigma-Aldrich. Sodium chloride (NaCl) was purchased from ACP. Sodium hydroxide (NaOH) and hydrochloric acid (HCl) solutions of various concentrations were purchased from Merck. Anhydrous ethanol (EtOH) was purchased from Greenfield Global. Deionized (DI) water (resistivity ~ 10 MΩ cm) was used in all experiments, unless otherwise specified. The adsorbate, procion Red MX-5B (PR) was procured from Sigma–Aldrich. The dye structure is given in Fig. 3- 1. Molecular formula: $C_{19}H_{10}Cl_2N_6Na_2O_7S_2$; molecular weight: 615.33 g mol^{-1}; CAS number: 17804-49-8; λ_{max} 538 nm (wavelength at maximum light absorption); Dye purity of 40%. This low purity is because the contained impurities are similar in structure to the dye and difficult to separate. In industrial applications, the same unpurified dye is used. The same unpurified dye was used in a several publications[51, 53-56]. Because of the difficulty in purifying the dye, we used it as supplied. We assume that the impurities are structurally similar to that of PR, therefore the calculations were based on 100% PR.

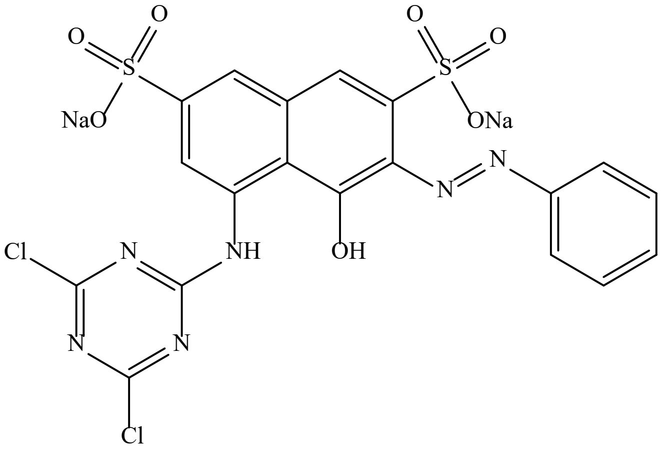

Fig. 3- 1. Chemical structure of procion red MX-5B (PR) dye[57]

3.3.2. Periodate oxidation of cellulose pulp

Dialdehyde cellulose (DAC) was synthesized with the protocol developed in our lab with minor alterations[58]. DAC was prepared under the following reaction conditions: Pre-soaked kraft pulp (10.0 g) was added to a solution containing 26.4 g of $NaIO_4$ (12.3 mmol based on 2 mol per 1mol glucose unit), 29.3 g NaCl and 500 mL DI water. The reaction mixture was stirred at room temperature in the dark for 6 days. Ethylene glycol was added to the reaction mixture to quench the residual periodate. DAC fibres were rinsed thoroughly with DI water 5 times and filtered through a 4 µm pore nylon cloth. DAC was dried in the oven at 50 °C and a small amount of DAC was set aside for aldehyde content determination.

3.3.3. Reductive amination of DAC fibres to produce DAmF and DAmC

Dangerfield, et al. developed the methodology for protecting-group-free synthesis of primary amines[59]. In their study, they converted methyl iodo-glycosides to primary amines in a single step using ammonia and a nitrogen source. To the best of our knowledge, this is the first time that this protocol has been applied in modifying cellulose. 10g of DAC, 4.2 g NH_4OAc (3 mol per 1 mol -CHO), 625 mL 2M NH_3 (10 mol per mol -CHO) was added to 100 mL of dry methanol (methanol was dried with 4 Å activated molecular sieves). The mixture was stirred at 80ºC under reflux for 18 hrs, then cooled in an ice bath and sodium borohydride (1 g) was added and stirred at room temperature for one hour. 20 mL 0.1 M NaOH solution was used to quench the reaction and the aminated fibres were washed with DI water 5 times and dried at room temperature. A small amount of DAmF was taken for amine content determination.

To prepare DAmC, 4 g of DAmF was stirred in water at pH 3 at 60 ºC for 1 hour after which all DAmF dissolved resulting in the water-soluble polymer.

3.3.4. Characterization of DAC and DAmF

3.3.4.1. Determination of aldehyde content.

The aldehyde content before and after amination was determined by the hydroxylamine hydrochloride method[60]. A known amount of DAC was dissolved in water (2%) at 80°C for 6 hrs. After solubilization, the pH was adjusted to 3.5 by HCl. The pH of a solution of $NH_2OH{\cdot}HCl$ (5% w/w) was also adjusted to 3.5 before adding it to the sample solution. The pH of the reaction was maintained at 3.5 with the addition of 10 mM NaOH. NaOH was added until the pH remained constant at 3.5, indicating the complete conversion of aldehydes to oximes. The aldehyde content was determined by equation 1

$$\text{Aldehyde content (mmol g}^{-1}) = \frac{N_{NaOH} * V_{NaOH}}{W} \qquad 1$$

Here, N_{NaOH} is the normality of base (mmol L^{-1}), V_{NaOH} is the volume of base used and W is the weight of the sample used for titration.

3.3.4.2. Determination of charge content.

Conductometric titration with a standardized HCl solution on an 836 Titrando titrator (Metrohm, Switzerland) was used to determine the amine content of DAmF. A known amount of DAmF was distributed in 100 mL milli-Q water (ion content), and the pH was adjusted to 11.5 with 0.1 M NaOH. The addition HCl and data collection were controlled by a computer system. 45mL of standardized 10 mM HCl solution to the solution at a rate of 0.1 mL min^{-1} until the pH reached 3.5. The amine (charge) content in mmol per gram of DAmF was estimated using the middle portion of the titration curve, which represented the volume of HCl solution used to neutralize the weak base[61].

3.3.4.3. Fourier Transform Infrared (FTIR) Spectroscopy.

To confirm the change in functional groups, Fourier transform infrared spectra were measured from dried fibres (pulp, DAC and DAmF) using ATR method in a Bruker ALPHA FTIR spectrometer (Bruker Optics Inc., Billerica, USA) with single bounce diamond crystal and standard room-temperature LiTaO3 MIR detector in the spectral region of 400 cm-1 to 4000 cm-1 using 32 scans at the best resolution of 4 cm^{-1}. Peak fitting was done using *OriginPro 2018b* software (OriginLab, Northampton, USA).

3.3.4.4. X-ray photoelectron spectroscopy (XPS).

XPS was used to quantitatively determine the formation of primary amine groups onto the DAmC. Fibers were characterized by K-Alpha™ XPS instrument (Thermo Scientific, USA) using monochromatic Al Kα radiation under a 10^{-8} mbar vacuum. DAC and DAmF fibers were dried under vacuum before XPS measurement. All measurements were made on copper strips. The X-ray Photoelectron Spectroscopy (XPS) analysis was performed with the flood gun on, meaning that the surface charge of the insulating samples was neutralized. This is important to ensure accurate measurements of the sample's electronic structure. The X-ray emission angle used in the analysis was 90 degrees with respect to the specimen surface. Spectra were recorded from at least three points on each sample, with the diameter of the analyzed area being 400 μm. Single survey scans with a pass energy of 200 eV were conducted to measure the elemental composition. High-resolution scans with a pass energy of 50 eV for N 1s peaks were recorded. The obtained spectra were deconvoluted using the Avantage Data System software[62]. The software utilized a combination of Gaussian and Lorentzian functions to deconvolute the spectra. Before deconvolution, the spectra underwent background subtraction using the Shirley method. After deconvolution and background subtraction, the resulting curves were attributed to different types of bonds based on their binding energy values. Binding energy values were calculated relative to the C (1s) photoelectron peak at 285.0 eV. Integration of the obtained curves allowed for the determination of the percent nitrogen content.

3.3.4.5. Particle size analysis by dynamic light scattering (DLS)

The effective diameter of DAmC polymer was determined by a Brookhaven dynamic light scattering (DLS) instrument BI9000 AT with a digital correlator. The concentration of DAmC was kept at 0.1 wt. %. The effect of pHs of 2, 4, 5.5, 7.5 and 10.5 on the size of DAmC polymer was studied. All experiments were carried out by monitoring the scattered light intensity at 90° scattering angle at 25 °C. DAmC was observed to be soluble in solution at all pH with the exception of pH 7.5, where it precipitated out of solution.

3.3.4.6. Electrophoretic mobility (μ) by electrophoretic light scattering (ELS)

To study the effect of pH changes, the average electrophoretic mobility of a 0.1 wt. % polymer solution of DAmC was measured using Zeta-sizer Nano ZS (Malvern Instruments Ltd., U.K.). DAmC was observed to be soluble in solution at all pH except for pH 7.5, where it precipitated out of solution. The electrophoretic mobility results were not converted to ζ-potentials, as no theory for weak base cationic polyelectrolytes as a function of pH and heterogeneity in charge group contents is available.

3.3.4.7. Study of irreversible partitioning between DAmF and DAmC in the absence of Dye.

It was observed that depending on the pH of solution, DAmF dissolves to form DAmC. This is likely due to the dissolution of a fraction of diaminocellulose polymers with high charge content and low molecular weight, as diaminocellulose was obtained in a heterogenous reaction, which causes a non-uniform distribution of diamino groups. This dissolution is irreversible as DAmC in the supernatant does not convert back to DAmF (unless at pH 7.7, sec section 3.4.). Partitioning between DAmF and DAmC was studied at different pH at room temperature. All 20 mL glass vials used for this experiment contained 20 mg DAmF and 5 mL water. The pH was adjusted with 0.1 M HCl or 0.1M NaOH as needed. The suspensions were shaken at 175 rpm in a Thermo Scientific Precision TSSWB15 Shaking Water Bath at 25°C for 12 hours. At different time intervals, fibres were allowed to sediment for 5 mins, and the absorbance of the supernatant was determined with ultraviolet−visible spectrophotometry (UV−vis) at a wavelength of 271 nm with a quartz cuvette (see Fig. 3- 6b below).

3.3.5. Removal of Procion MX red (PR) from water

3.3.5.1. Dye adsorption on DAmF.

All adsorption experiments were carried out as batch studies. Typically, 20 mg of dry DAmF (unless stated otherwise) and 20 mL of Procion Red MX-5B (PR) test solutions (1 g L^{-1}) were placed in 40 mL glass vials. The initial pH of the solutions was controlled by adding 0.1 M HCl or NaOH to achieve the desired pH. The mixtures were shaken at 175 rpm in a Thermo Scientific Precision TSSWB15 Shaking Water Bath at 25°C for 10 hours. The equilibrium was determined experimentally as there was no change in adsorption when experiments were run for longer periods of time. Afterwards, separation of the adsorbent from the solution was done by centrifugation at 1000 rpm for 5 min and the supernatant was taken for UV-Vis measurement at 536 nm (the experimental absorption maximum wavelength of the PR, close to value reported in literature[57]).

The amount of dye removed by DAmF at equilibrium, q_e (g g^{-1}) was calculated by the equation 2 below.

$$\text{Dye removed } q_e = \frac{(C_0 - C_e) * V}{m} \tag{2}$$

Here C_0 is the initial dye concentration (g L^{-1}), C_e is the dye concentration in solution at equilibrium (g L^{-1}), V is the volume of dye solution used (L) and m is the initial mass of DAmC in solution (g).

The percentage of dye removal was calculated using equation 3 below.

$$\text{Percent Dye removal } (\%) = \frac{(C_0 - C_e)}{C_0} * 100 \tag{3}$$

The effect of initial dye concentrations was studied by adding 20 mg of DAmF into PR solutions with different initial concentrations at 298 K and at optimum pH (pH 2) and measuring the concentration of PR solutions before and after adsorption by UV−vis at a wavelength of 536 nm. After adsorption, we did not observe any dissolution of diaminocellulose fibers, therefore, λ_{max} did not change.

The effect of salt was also studied by performing adsorption experiments in the presence of 0.5 M and 1 M NaCl at different PR concentrations (0.25 – 10 g g^{-1}). Due to the hypochromic effects of PR in NaCl, new calibration curves were employed for each salt concentration to compute q_e.

3.3.5.2. Adsorption isotherm

Adsorption isotherms offer valuable information about the characteristics of adsorption active sites and are interconnected with the thermodynamic properties of the adsorption process. We investigated dye adsorption on DAmF using Langmuir kinetics, which assumes that adsorption occurs at uniformly distributed sites on a solid surface, with the adsorbent surface being homogeneous. It also assumes that adsorbed molecules do not interact, and that all adsorption follows the same mechanism[63]. The linearized form of the Langmuir isotherm is given in equation 4 below.

$$\frac{1}{q_e} = \frac{1}{q_m} + \frac{K}{C_e} \qquad 4$$

Here q_e is the amount of PR adsorbed per g of DAmF (mg g^{-1}), q_m is the maximum adsorption capacity (mg g^{-1}), C_e is the concentration of PR in solution at equilibrium expressed in mg of dye per g DAmF, K is the equilibrium constant that relates to the affinity of the dye to the binding sites and equals $\frac{k_{des}}{k_{ads}}$, with k_{des} and k_{ads} being the desorption and adsorption rate constants respectively. K and q_m were determined from the slope and intercept respectively, from the plot of $\frac{1}{q_e}$ vs. $\frac{1}{C_e}$.

3.3.5.3. Dye desorption and DAmF regeneration.

For regeneration tests, 50 mg of DAmF was used with 20 mL of 0.5 g L^{-1} PR solution at pH 2. After adsorption, desorption experiments were carried out by stirring dyed DAmF in 20 mL of water at pH 10. The mixture was stirred for 30 mins, after which the fibres sediment, and the absorbance of the supernatant measured by UV-Vis. Results were expressed as equation 5.

$$\text{Percent dye desorbed} = \frac{C_d}{C_0} * 100 \qquad 5$$

where c_d is the concentration of dye desorbed, c_0 is the initial concentration used during the adsorption experiments.

DAmF was rinsed three more times with pH 10 DI water until there was no more color observed in the rinse water. DAmF was dried in the oven overnight at 50 °C and reused for dye adsorption experiments. There was a ~5 % fiber loss after every desorption cycle as we rinsed the fibres with pH 10 DI water.

3.3.5.4. Dye adsorption by DAmC.

All adsorption experiments were carried out in batch studies. 1% DAmC solution was produced by dissolving 200 mg DAmF in 20 mL distilled water at pH 3 and stirred at 60 °C for 1 hour. The solution was stable when cooled to room temperature and was used in all adsorption experiments.

To determine the effect of pH on adsorption, 200 µL of 1% DAmC solution was added to 5 mL of Procion Red MX-5B (PR) test solutions (0.5 g L^{-1}) in 15 mL centrifuge vials (pH ranged from 2 -

12). The pH of the solutions was decreased or increased by adding 0.1 M HCl or NaOH respectively. The solutions were shaken at 175 rpm in a Thermo Scientific Precision TSSWB15 Shaking Water Bath at 25°C (large flocs formed almost immediately when the two solutions were mixed). Afterwards, the solution was centrifuged at 1000 rpm for 5 min. The flocs collected at the bottom of the centrifuge vail, while the supernatant was taken for UV-Vis measurement at 536 nm.

After centrifugation, the sediment contains precipitated DAmC with adsorbed dye. The supernatant contains both non-precipitated DAmC with dye attached and non-adsorbed dye. We observed a shift of λ_{max} of PR, when both DAmC and dye were present in solution due to their interaction. Therefore, we only plotted the raw data (e.g., abs. vs. pH) since all measurements were taken at 536 nm.

The effect of initial dye concentrations was studied by adding 200 µL of 1% DAmC solution into different initial concentrations of 5 mL PR solution ranging from 0.1 to 4 mg L^{-1} at 298 K and at optimum pH (pH 2).

Dosage of flocculant was studied by adding various volumes (0.1 – 3 mL) of 1% DAmC solution to 5 mL of 1 g L^{-1} PR solutions.

The effect of salt was also studied by performing adsorption experiments in the presence of 0.5 M and 1 M NaCl.

3.4. Result and discussion

3.4.1. Synthesis of DAmF.

The protocol for oxidation of cellulose pulp to dialdehyde cellulose by periodate oxidation has been developed in earlier works[58, 64, 65]. Hydroxyl groups on the C_2 and C_3 positions on the glucose ring are converted to aldehyde groups and the C-C bond is broken resulting in a flexible dialdehyde cellulose polymer (Scheme 3- 1a). The process employed to convert aldehyde groups to primary amine groups was first reported by Dangerfield, et al.[59] In this protocol (Scheme 3- 1b), a Schiff base reaction occurs between the aldehyde group of DAC (dialdehyde cellulose fiber) and ammonia resulting in the formation of an imine. Excess NH_3OAc and NH_3 are used to prevent over-alkylation reaction and maintain the pH of the reaction to 12[59]. This helps in the selectivity of primary amines over secondary and tertiary. Also, the reaction must be devoid of moisture to prevent the neutralization of nucleophilic ammonia, hence the solvent exchange with methanol. $NaBH_4$ is added to reduce the resulting imine (C=NH) from the Schiff base reaction to amines ($C\text{-}NH_2$, Scheme 3- 1c).

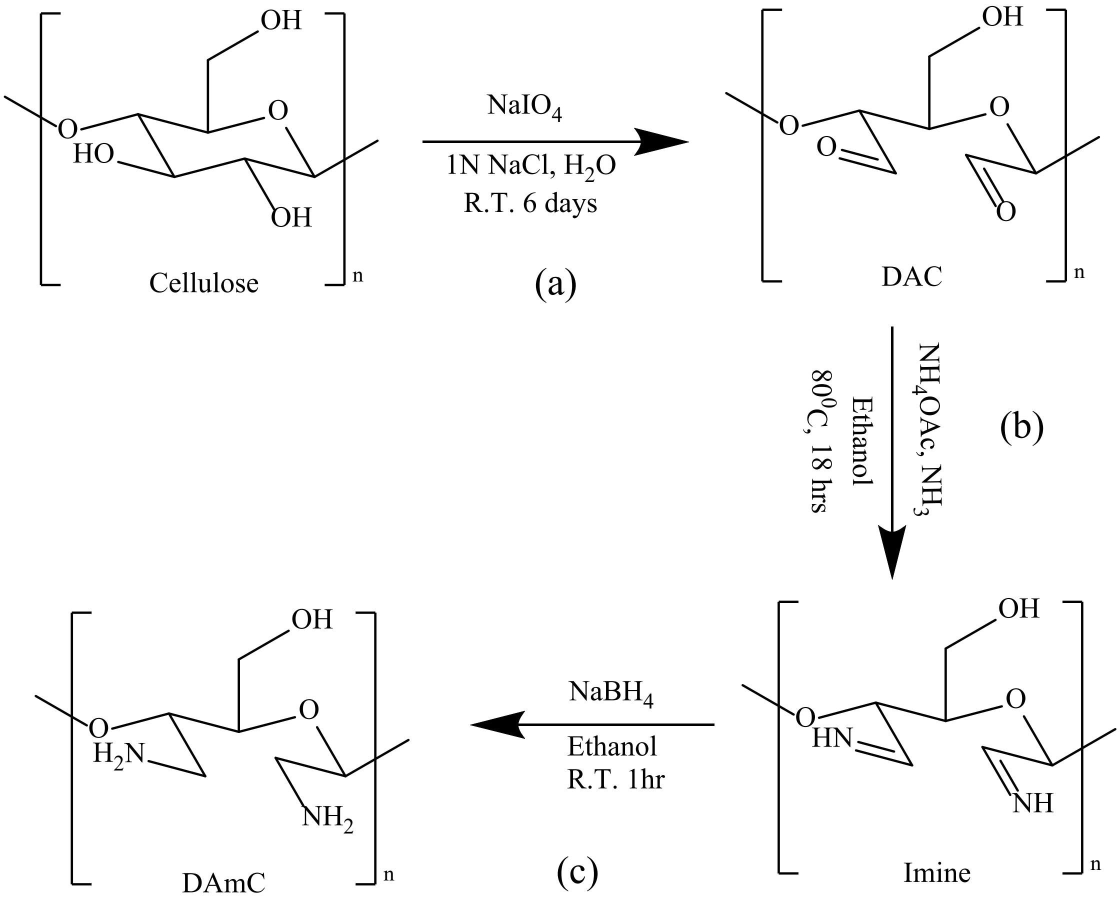

Scheme 3- 1. Reaction schematic of (a) oxidation of cellulose to DAC, (b) amination reaction of DAC to imine and (c) subsequent reduction of imine to DAmF

The image in Fig. 3- 2b shows the physical state of the DAmF after reductive amination. The colour of the fibres changes from white (DAC) (Fig. 3- 2a) to dark brown (DAmF). This colour change strongly indicates that the fibres have undergone chemical modification with the addition of the amine groups.

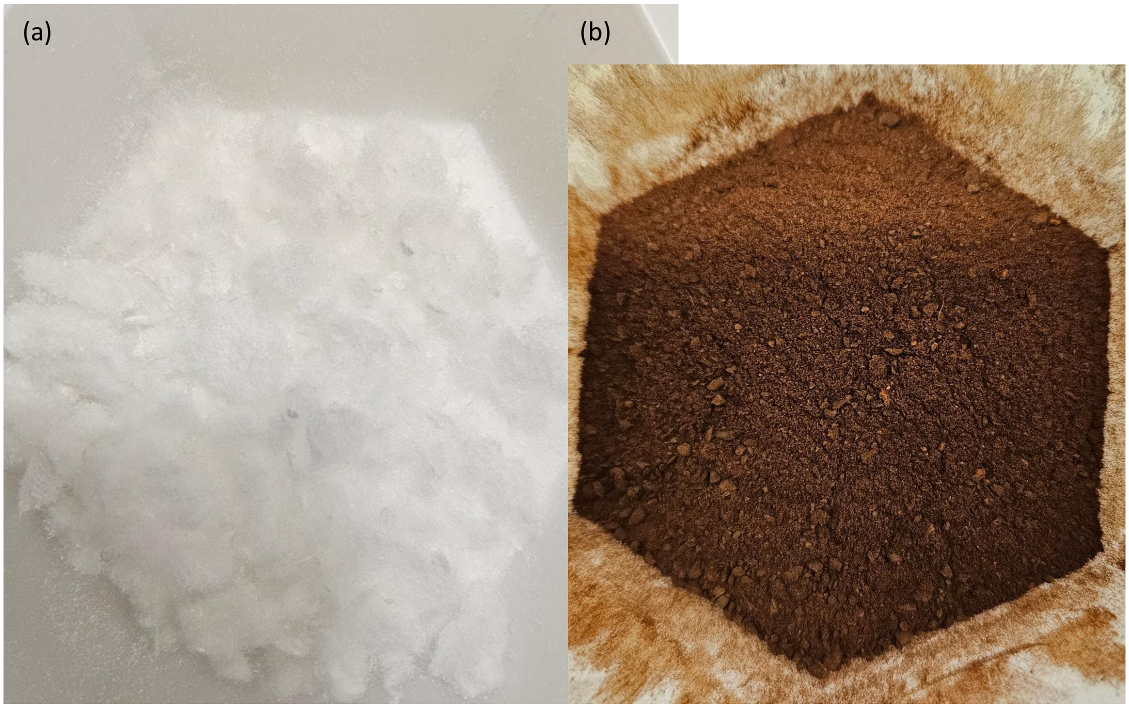

Fig. 3- 2. Photographs of (a) DAC fiber and (b) DAmF

To produce DAmC, DAmF was mixed in water and heated to 60 °C and stirred for 1 hour after which all DAmF fully dissolved. The DAmF fully dissolves at pH 3 because the presence of positive charges on the fiber and heat increases solubility. After the solution of DAmC is cooled to room temperature, DAmC is stable in solution and does not precipitate because it is kinetically stable due to its positive charges leading to a high energy barrier which prevents DAmC from reverting back to DAmF.

3.4.2. Characterization of DAC and DAmC

3.4.2.1 Aldehyde and Amine content.

The aldehyde content of DAC was 10.9 ± 0.3 mmol g^{-1}. This equates to a degree of oxidation (DO) of 1.74 (max DO = 2). The amine content was determined by the curve produced by a conductometric titration (Fig. 3- 3a). Prior to titration, a strong base (NaOH) is used to fully deprotonate the amine groups by raising the pH of the fibre suspension to ~11.5. This is followed by titration with a strong acid (HCl) (Scheme 3- 2).

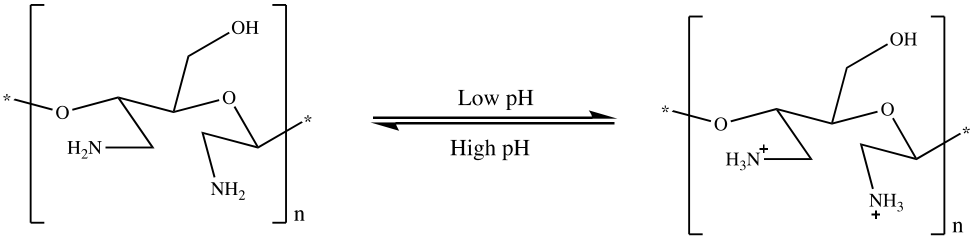

Scheme 3- 2. Schematic of protonation and deprotonation DAmC in acidic and alkaline media respectively.

The charge (amine) content of DAmF was determined by conductometric titration to be 9.5 ± 0.5 mmol g^{-1} (DO = 1.5). For comparison, the amine content of chitosan is 4.7 mmol g^{-1} (degree of deacetylation D.D. = 84 %)[61]. The pK_b values corresponds to the points of inflection on the pH curve and were determined by plotting the first derivative of pH vs. HCL added. From Fig. 3- 3b, the two maxima, corresponding to pK_b values of the amines located on the C_2 and C_3 positions of the polymeric chains of diaminocellulose, are found to be 5.7 and 8.5. These correspond to pK_a values of 5.5 and 8.3 for both amine groups. The reason for the two pK_a values is that the vicinity of a second amine group affects the pK_a of the first amine. The same is seen in compounds having two neighbouring carboxyl groups, such as hydrolyzed polystyrene maleic anhydride[66]. Also, from the aldehyde content of DAC, it can be concluded that the efficiency of reductive amination reaction is ≅ 87 %.

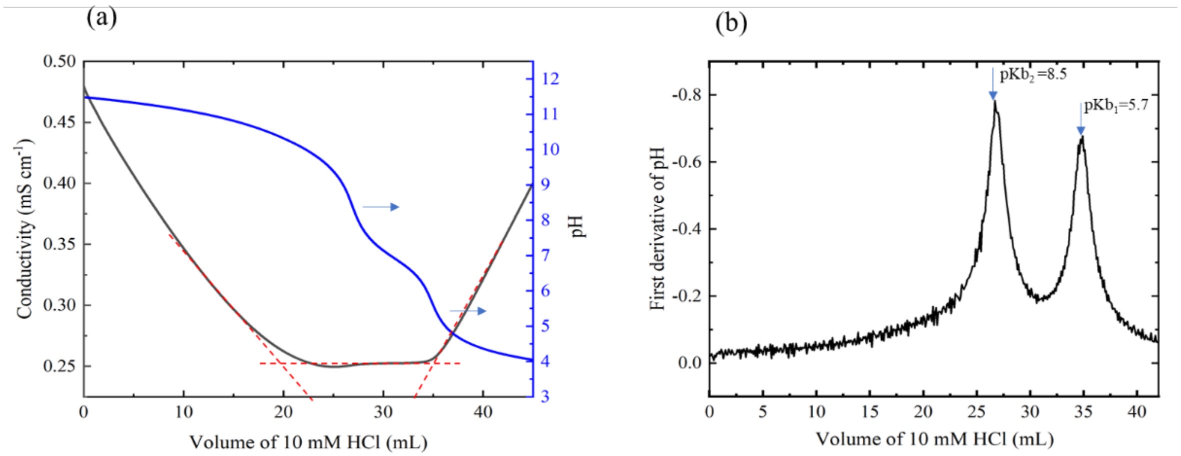

Fig. 3- 3. (a) Conductometric titration of DAmF using 10 mM HCl, indicating ~15 ± 1 mL of acid (shown by arrows) is needed to neutralize the weak base, implying a charge content of 9.5 mmol of -NH2 per gram of DAmF with two pK_b values shown by blue arrows. (b) first derivation of pH titration curve indicating the points of inflection and hence, the locations of pK_b.

3.4.2.2. Fourier Transform Infrared (FTIR) Spectroscopy.

To confirm the changes in functional groups, FTIR spectra of cellulose pulp, DAC fibre and DAmF were collected, and the data are presented in Fig. 3- 4. Characteristic peaks in cellulose are a broad peak at 3300 cm^{-1} (-O-H stretching vibration), and peaks at 2927 cm^{-1}(−C−H stretching vibration), 1630 cm^{-1} (vibration of water molecule absorbed by cellulose) and 1012 cm^{-1} (−C−O−C pyranose ring skeletal vibration)[67-70]. DAC spectrum shows a peak at 1725 cm^{-1} which is characteristic of an aldehyde carbonyl stretch. This band disappears in DAmF and the band at 1630 broadens due to the overlap of the N-H bending vibration and the absorbed H-O-H vibration band[71]. The usual two bands around 3300 cm^{-1} that are characteristics of primary amines do not show up on the spectrum due to its overlap with the broad -OH peak.

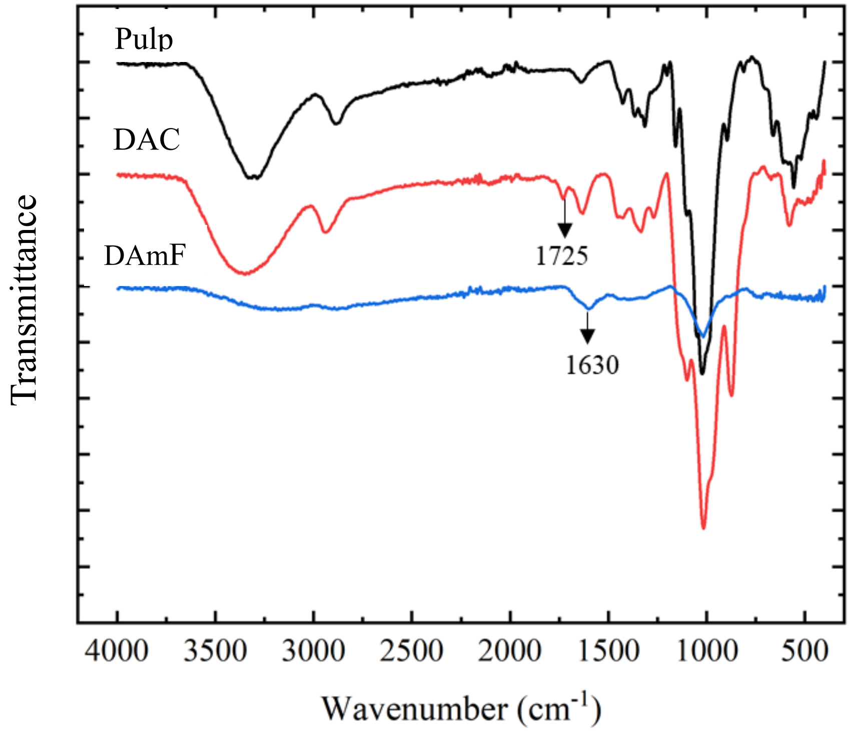

Fig. 3- 4. FTIR spectra of cellulose pulp, DAC fiber and DAmF.

3.4.2.3. XPS analysis.

To further confirm the addition of amine groups, XPS was employed to investigate the atomic chemical composition of DAmF (Fig. 3- 5). The peak at 400 eV represents nitrogen, which is due to amine groups in the fibre. C1s and N1s peaks were deconvoluted into their constituent sub-peaks to understand the nature of carbon and nitrogen bonds in DAmC. For C1s (Fig. 3- 5b), the peak at 286.0 ± 0.1 eV is deconvoluted into 284.4 ± 0.1 eV, 285.7 ± 0.1 eV and 287.9 ± 0.1 eV and they are assigned to C-C/C-H, amine (C-N)/ hydroxyl (C-O) and glycosidic bond (C-O-C) respectively. Pure cellulose does not contain any C-C bonds, (this component originates from carbon atoms that have no neighbouring oxygen), and consequently, DAmF should have no C-C bonds. Therefore, this bond at 284.4 eV can be assigned to either sp^3 C-H bond or, as Hua et al suggested, it may originate from the C-C-O contributions (C4 and C5 in the pyrose ring) which have a lower binding energy compared to hydroxylic carbon[72, 73]. The N1s peak at 399.1 ± 0.1 eV (Fig. 3- 5c) is deconvoluted into 398.1 ± 0.1 eV and 401.7 ± 0.1 eV and are assigned to residual imine groups that were not reduced by $NaBH_4$, and primary amine. These assignments are consistent with other studies reported in the literature[74, 75]. The peak area for both curves were 12.12 ± 4.1 and 87.9 ± 4.1 % respectively. From these data, the efficiency of the reduction reaction with $NaBH_4$ is about 88 %.

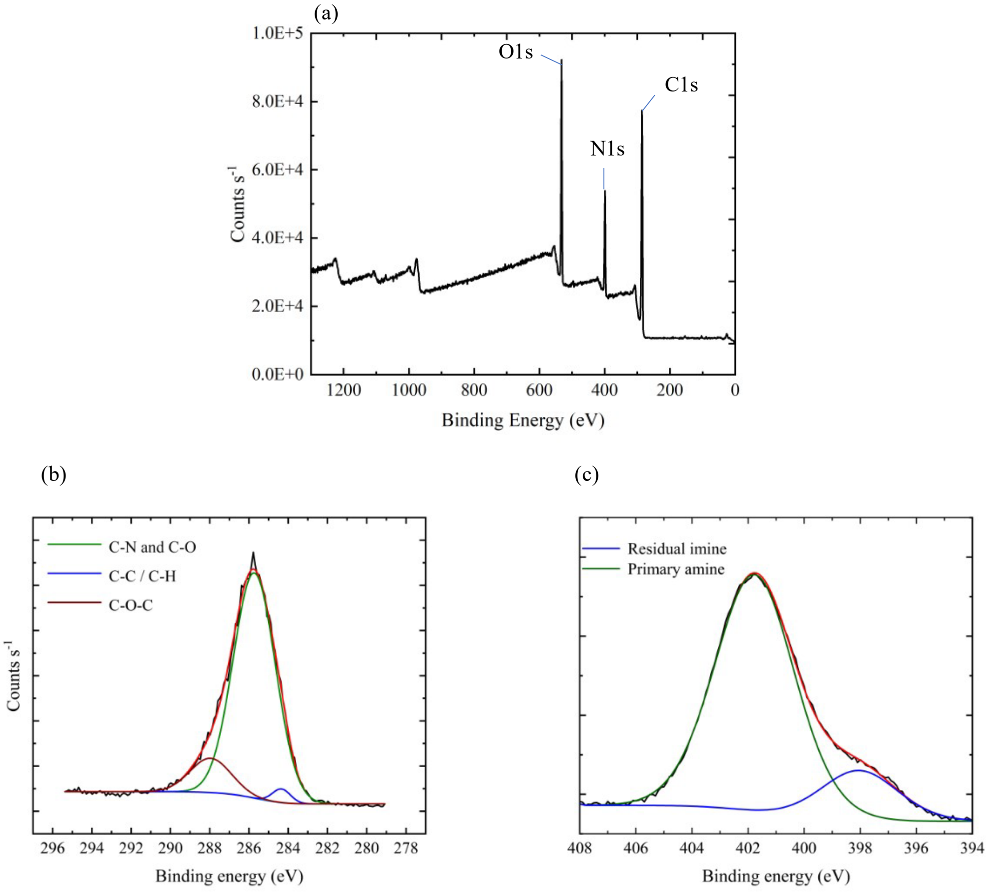

Fig. 3- 5. (a) XPS spectrum of DAmC (atomic composition- 63.3% C1, 21.3% O1s and 15.2% N1s); (b) C1s signal deconvoluted into C-O-C, C-O, C-C and C-N; (c) N1s signal deconvoluted into residual imine and primary amine groups

3.4.2.4. Stability of DAmC in solution.

To investigate the stability of DAmC in solution, 0.1 M HCl and 0.1 M NaOH were added to 0.1% DAmC solutions and visually inspected (pH 3, 5, 7.7 and 10). DAmC was stable in solution across all pH ranges except pH 7.7 (see Fig. 3- 6a) where it was converted back to DAmF and crashed out of solution. This is due to DAmC reaching the point of zero charge as confirmed by electrophoretic mobility measurements. The full scan UV-Vis spectra in Fig. 3- 6b show that there is a reduction in DAmC in solution at pH 7.7, as seen by the drop in intensity of the absorbance peak at 271 nm.

Fig. 3- 6c shows the effect of pH on the charge density and effective diameter of DAmC polymer in solution. At low pH, such as pH 2 and 4, the particle size of DAmC was ~6500 and ~2400 nm respectively. This large effective diameter is likely due to protonation of amines of the cellulose chains, leading to 'rigid rod' structure. Additionally, DAmC chains could associate with each other through H-bonding between adjacent polymers. As the pH increases the hydrodynamic radius of DAmC decreases due to the reduction in the density of positive charges on the polymer and the polymer conformation changes from a straight rod at high charge density to a random coil at low charge density. At pH 7.5, DAmC polymer is at the point of zero charge (PZC) at which the higher molecular weight DAmC polymers precipitate out of solution, leaving the lower molecular weight polymer in solution. This results in the lowest hydrodynamic radius of 103.2 nm at pH 7.7. After the PZC, the effective diameter increases due to the development of negative charge density on the polymer.

At pH 2, the amine groups on DAmF undergo complete protonation ($-NH_2 \rightarrow -NH_3^+$), leading to a high electrophoretic mobility. The electrophoretic mobility at pH 4 ($\mu \cong +3.5$) is higher than at pH 2 ($\mu \cong +2.5$) at which pH the ionic strength is higher, leading to more charge screening. The PZC of DAmC is determined to be at pH 7.5 ± 0.1, which is the pH at which we observed DAmC precipitate out of solution. For pHs above PZC, DAmC becomes negatively charged, possibly due to the deprotonation of hydroxyl groups and alkaline hydrolysis of the cellulose backbone. This result is consistent with electrophoretic mobility measurement of cotton treated with PEI and other amine functionalized cellulose systems[76, 77].

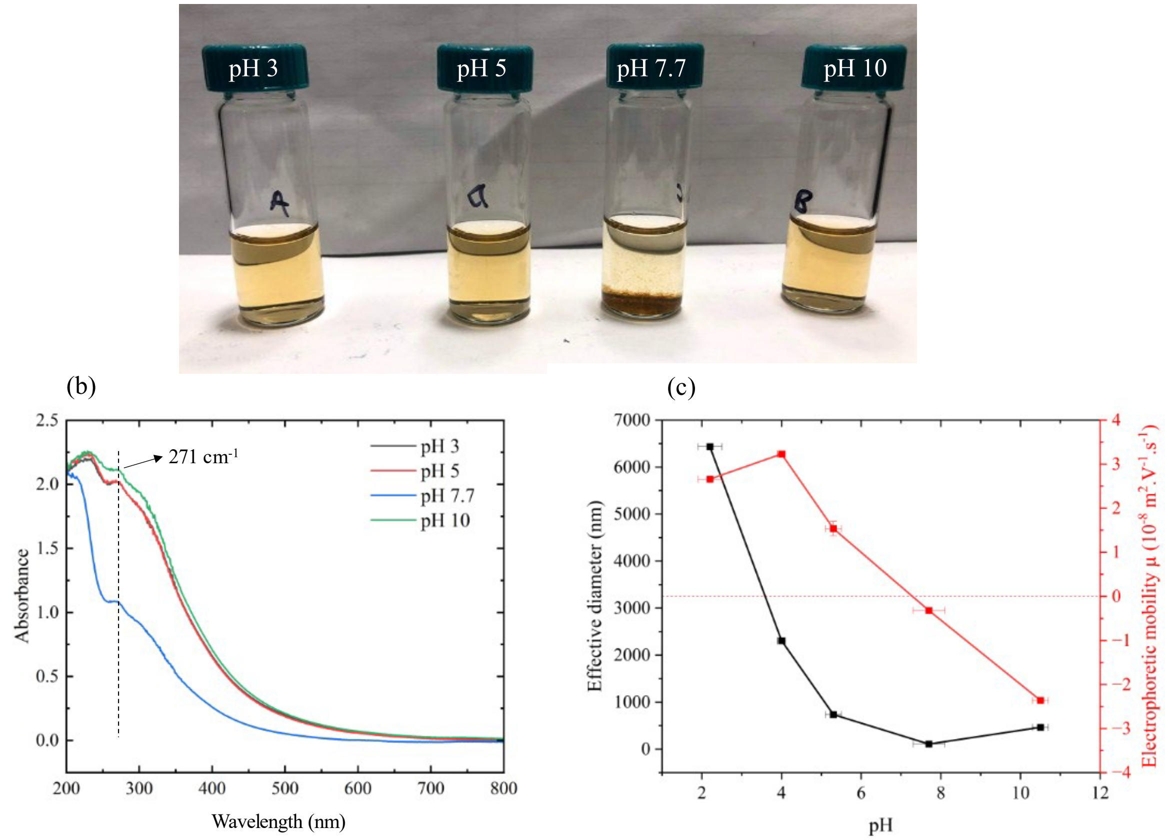

Fig. 3- 6. a) Photo showing 0.1 % DAmC solutions at pH 3, pH 5, pH 7.7 and pH 10. All solutions were stable for over 30 days, except for pH 7.7 at which a precipitate formed immediately after pH change, and the solution became clearer. The other solutions are brown because of the presence of DAmC (b) The corresponding UV-Vis spectra for the corresponding solutions. We observe a peak at 271 nm which was set at λmax for quantifying DAmC in solution. (c) equivalent spherical diameter and electrophoretic mobility of DAmC under different pH conditions, measured at T~25 °C by DLS and electrophoretic light scattering, respectively

3.4.2.5. Partitioning between DAmF and DAmC at room temperature in the absence of dye.

To understand the stability of DAmF in water over a range of pH, DAmF suspensions were studied to better understand the nature of the fibre. At room temperature, 20 mg of DAmF were placed in 5 mL of water at various pHs (1 -12) and the amount of fibre dissolved was measured over time. The graphs in Fig. 3- 7 represent the findings. In very acidic media, pH 1 and 2, dissolution of DAmF or conversion to DAmC is higher because of the complete protonation of amine groups as illustrated in Fig. 3- 7a. Like other amino-containing compounds such as chitosan, the primary amine groups on DAmF makes the fibers cationic in acidic media.[78, 79]. As protonation increases, electrostatic repulsion between the polymeric chains in the fibre intensifies, resulting in polymer separation and dissolution. The considerable difference in dissolution at pH 1 versus pH 2 is likely due to the extremely acidic media in pH 1, hydrolyzing the cellulose chain, causing the cellulose chains to shorten, resulting in a low average molecular weight thereby increasing the polymer's solubility.

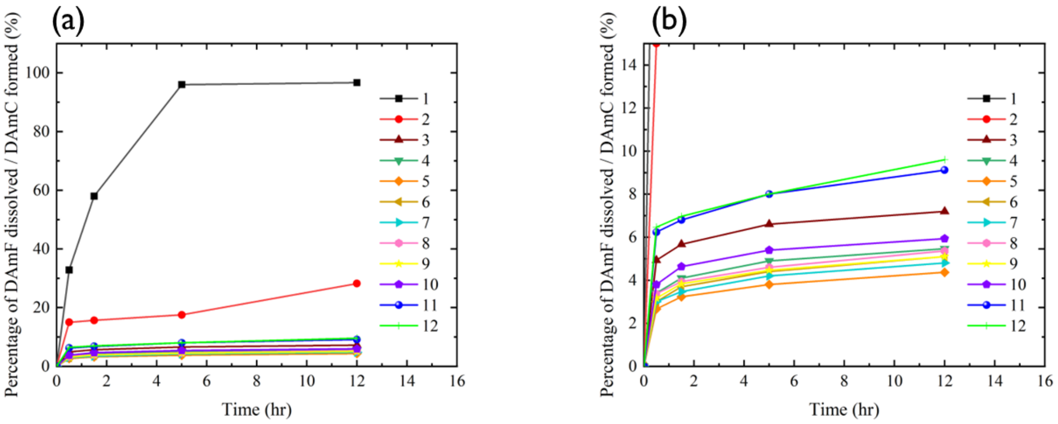

Fig. 3- 7. (a) Graph showing the dissolution of DAmF and partitioning between DAmF and DAmC in solution. DAmC is formed when DAmF dissolves. 20 mg of DAmF was added to 5 mL of water at pH 1-12 at room temperature and stirred over 12 hrs (b) graph a zoomed in at pH 3-12

As shown in Fig. 3- 7b, an increase in pH decreases DAmF solubility because the cellulose chains in DAmF become less charged as the amine groups are deprotonated. At pH >10, solubility slightly increases due to weakened intramolecular hydrogen bonds within its chains, that results from deprotonation of hydroxyl groups, therefore leading to its partial solubility in alkaline solutions[80].

3.4.3. Removal of PR from water by adsorption on DAmF

As was mentioned earlier, diaminocellulose fibre, DAmF, maintains its integrity in water at ambient temperature over a wide range of pH. Therefore, it can be employed as a reusable green adsorbent for the removal of PR from water.

3.4.3.1. Effect of pH.

In this study, the effect of pH was evaluated for pHs between 2 and 11 and the results are shown in Fig. 3- 8a. Dye adsorption on DAmF was shown to be optimum at pH 2 but decreases as the pH increases. This result is similar to chitosan, another known biopolymer with amine groups, for which the adsorption of anionic dyes is more pronounced at low pH[48]. DAmF have solid interfaces with many adsorption sites. The two main mechanisms for dye adsorption on pulp fibers are ion exchange and adsorption on specific sites of the external and internal fiber surface[81, 82]. Specific adsorption of negative PR ions on cationic protonated amine sites is the likely mechanism because a similar adsorption occurs on DAmC (see below), in which ion exchange with ions in pores is impossible. Adsorption is highest at pH 2, because at pH 2, PR is weakly charged, DAmF is highly charged, and more PR is needed to reach charge neutralization. Dye adsorption decreased from 0.8 g g^{-1} at pH 2 to less than 0.2 g g^{-1} at pH 5 because at higher pHs the charge of PR is higher, resulting in less PR required to reach charge neutralization. Furthermore, it was observed that DAmF, despite being slightly soluble in distilled water at a pH of 2 (refer to Fig. 3- 7a), exhibits remarkable stability in dyed water. The insolubility of the fibres is plausibly attributable to charge neutralisation by the dye and the rate of association with the dye surpasses that of DAmF dissolution at pH 2.

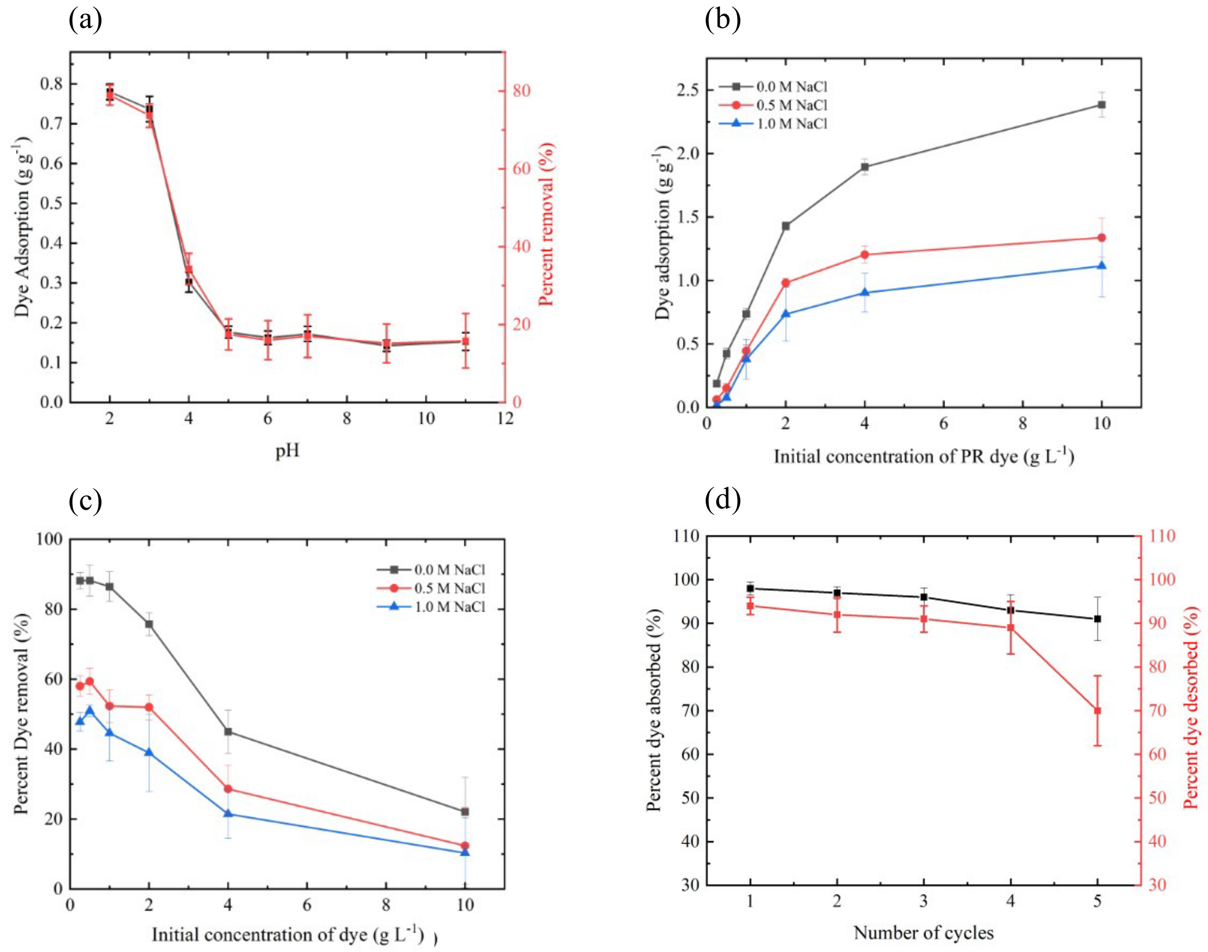

Fig. 3- 8. (a) Dye adsorption of PR on DAmF as a function of pH showing optimal adsorption at pH 2 (20 mg DAmF with 20 mL of 1g L^{-1} PR); (b) Adsorption of PR by DAmF as a function of initial concentration of dye in different concentration of NaCl(20 mg DAmF with 20 mL of 0.1 - 10 g L^{-1} PR at pH 2); (c) Percentage PR removed as a function of initial concentration of dye in different concentration of NaCl(20 mg DAmF with 20 mL of 0.1 - 10 g L^{-1} PR at pH 2); (d) Adsorption at pH 2 and desorption at pH 10 of PR from DAmF over 5 cycles. Error bars represent 2 standard errors of the mean (N=3)

3.4.3.2. Effect of ionic strength.

To understand the effect of ionic strength on the adsorption of PR-MX on DAmF, NaCl was added to PR solutions at various concentrations (0.1 – 10 g L^{-1}) at pH 2 before adding the fibres. We observed that the addition of salt led to a decrease in adsorption spectra (see Fig. S3- 1a). Therefore, different calibration curves were utilized for PR experiments done at 0.5 M and 1.0 M NaCl concentrations (see Fig. S3- 1b and Table S3- 1). As shown in Fig. 3- 8 b and c, the uptake of the dye decreases as the concentration of NaCl increases because salt screens the surface charge of the fibers, resulting in less PR molecules needed for charge neutralization on DAmF. Although high concentrations of NaCl results in the formation of microflocs (aggregates) of PR, as observed in the flocculation experiments (discussed in section 3.4.4.4.), these aggregates were probably too big to enter the pores of DAmF and thus did not end up on the fibers.

3.4.3.3. Adsorption isotherm

We investigated PR adsorption and compared the results with a Langmuir isotherm. Fig. 3- 9a shows that as the equilibrium concentration C_e increases, the amount of dye adsorbed q_e rapidly increases until Ce ~ 0.5 g L^{-1}. After this point, PR adsorption beings to reach the saturation point. The adsorption isotherm is an example of a finite affinity isotherm, implying a dynamic equilibrium between adsorption and desorption. The maximum adsorption capacity of DAmF at room temperature and pH 2 is 3.72 g g^{-1}, and K is 0.1966 and has no units, implying the adsorption rate constant is about 5 times the desorption rate constant. The maximum adsorbed amount q_m obtained from the Langmuir isotherm is not close to the theoretical value calculated by charge stoichiometry ($q_{m(c)}$). If we assume that at pH 2, 1 mol of SO_3^- on PR is required to neutralize 1 mol of NH_4^+ on DAmF, then, $q_{m(c)}$ is calculated as:

$$q_{m(c)} = \frac{1mol\ NH_4^+}{1mol\ SO_3^-} * 9.5\frac{mmol}{g} * 0.616\frac{g}{mmol} \cong 5.9\frac{g}{g}$$

The reason that the maximum amount of adsorbed dye is less than the theoretical maximum is likely due to that not all the amine groups in the pores of DAmF are accessible to PR.

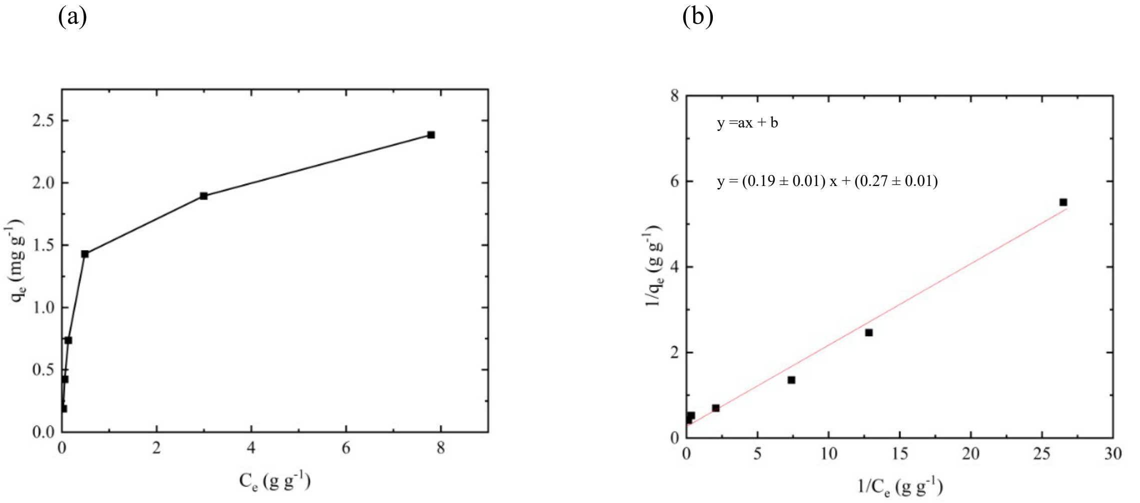

Fig. 3- 9. PR uptake isotherms and the Langmuir fit. (a) The relation between the amount of adsorbed PR per unit mass of DAmF and PR concentrations at equilibrium derived from experimental data for PR adsorption by DAmF in water. (b) Linear fit to the Langmuir isotherm. Ce is in mg of PR at equilibrium per unit mass of DAmF utilized.

Because the literature on the adsorption of procion Red mx 5B onto cellulosic materials is limited, Table S3- 2 contains a compilation of alternative biosorbents. Our material has a greater capacity for PR adsorption than the majority of the sorbents on this list. Comparatively, the max. adsorption capacity of our material inherently resembles that of the biosorbent Dendritic Fibrous Colloidal Silica Internally Cross-linked by Bivalent Organic Cations (DDS)[52]. Despite having a charge content of 4.5 mmol g^{-1}, which is half that of DAmF, DDS exhibited a maximum dye adsorption capacity of 3.19 g g^{-1}, which was comparable to ours. As explained, this might be due to some amines in DAmF not being accessible to PR molecules. Tertiary amine-containing DSS was an effective sorbent, but our material may have an advantage of reusability.

3.4.3.4. Regeneration test.

To study the recyclability of the adsorbent, dyed DAmF was stirred in a 20 mL aqueous solution at pH 10 for 30 mins after which the absorbance of the supernatant was measured. At pH 10, there is an abundance of OH^- ions that replace PR molecules on DAmF, thereby releasing the dye molecules. This can then be washed off and the adsorbent regenerated after drying. As shown in Fig. 3- 8d, the adsorbent is viable after 5 uses. 100% recovery of dye was not achieved probably due to dye molecules not having enough time to diffuse through the pores of DAmF.

3.4.4. Removal of PR from water by adsorption on DAmC

To understand the adsorption mechanism of PR on diaminocellulose, we also utilized the macromolecular (dissolved) form of DAmF, DAmC for the removal of PR from water. The adsorption of PR on DAmC led to the formation of precipitates that contained PR and DAmC. When the amount of PR adsorbed on DAmC was not enough to lead to precipitation, there was a red-shift in the absorption spectrum of PR as shown in Fig. S3- 2. The absorbance peak at 536 nm in PR solution alone is shifted to 550 nm in a PR-DAmC solution. Metachromasia is a phenomenon in which the absorption or emission properties of a substance is altered, leading to a change in the spectral band position of the molecule. The shift can either be bathochromic (redshift- move to longer wavelength/ lower energy) or hypochromic (blue shift- move to shorter wavelength/ higher energy). The strength of this interaction can be measured by the magnitude of metachromasia induced in its spectroscopic profile[83, 84]. Due to the bathochromic (red) shift of 14 nm observed in the spectra of DAmC-PR, we were not able to correctly estimate the amount of free PR molecules still left in solution after the adsorption experiments. This has led us to represent our data in adjusted absorbance. Adjusted absorbance is defined as the absorbance value at 536 nm, that has been corrected for the dilution that was done to the sample, before UV-vis measurements were taken.

Polyelectrolyte−dye complexation in solution has been extensively studied and reviewed.[83-85] Electrostatic forces between the polymer and the dye, the persistence length or conformational adaptability of the polymer, and the degree of cross-linking of the polymer are hypothesised to have a significant impact on these interactions. Here we study the effects of pH, ionic strength, polymer concentration and dye concentration on DAmC-PR complexation.

3.4.4.1. Effect of pH.

Dyes typically have a pH range in which adsorption onto a specific material is advantageous. The optimal pH value is determined by the adsorbent's properties and the interaction between the adsorbate and the solid surface. The pH effect was measured from 2 to 12 with 200 μL of 1% DAmC and 5 mL of 0.5 g L^{-1} PR. The graph in Fig. 3- 10a shows the effect of pH on the removal of dye by adsorption on DAmC. During this experiment, a precipitate of DAmC and PR was formed shortly after mixing both solutions together. This precipitate could be easily isolated from the solution by sedimentation or filtration. At 536 nm, the adjusted absorbance of a 0.5 g L^{-1} PR solution was 10.9. The highest amount of dye removed from the solution occurred at pH 2. Under these conditions all the dye is adsorbed on the modified cellulose chains in solution, and all the DAmC with the adsorbed dye precipitates out, evidently because the charge of the cellulose chains with adsorbed dye was much reduced and the chains were no longer water-soluble. We chose this pH as the optimal pH and the rest of the experiments were carried out at pH = 2. There is an upward trend from an adjusted absorbance of ~0 at pH ~3 to 1.05 g g^{-1} at pH 9 which further increases to ~6 at pH 12. This is because the anionic dye, PR displayed in Fig. 3- 1, has a pK_a of 2.5 and at a pH below the pK_a, PR is less negatively charged than at a pH above the pK_a, i.e., the charge of PR increases with pH. DAmC on the other hand is positively charged as the pK_a of the primary amines on the polymeric chains are 5.5 and 8.3. Precipitation occurs as a result of an electrostatic attraction between the opposite charges on DAmC and PR, resulting in charge neutralization thereby leading to destabilization. Precipitation, and thus dye removal from water, increases as pH decreases because the charge density of PR decreases and the charge density of DAmC increases. This leads to DAmC requiring a higher adsorption of PR to reach neutralization and thus precipitation. There is a decrease in dye removal as pH increases because the charge density on DAmC decreases with pH and requires lesser amounts of PR to precipitate. Significant dye removal is still observed when the pH of the solution is at or above the point of zero charge (PZC) of DAmC, where the polymer is either neutral or negatively charged. This suggests that the binding forces are not just based on electrostatic interaction, but also involve other mechanisms, particularly via hydrogen bonds formation and van der Waals forces.

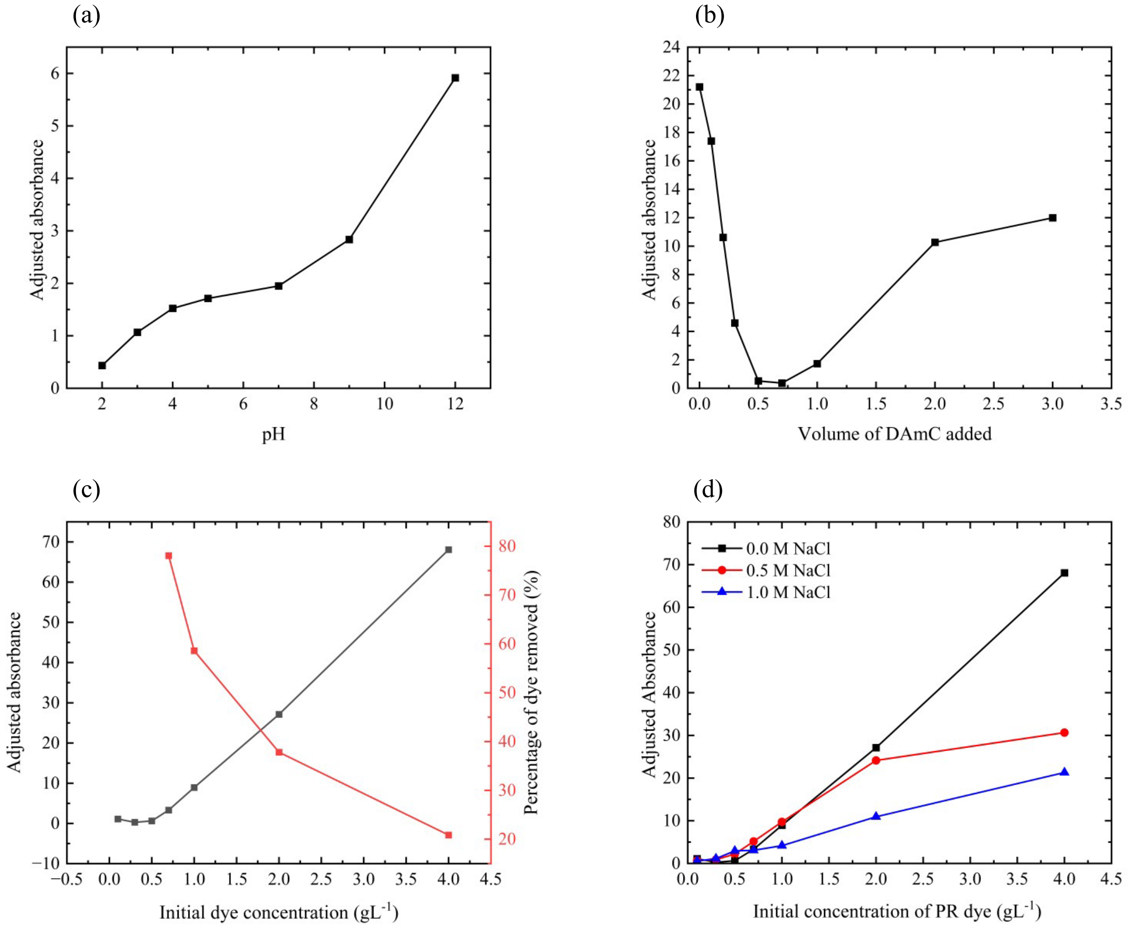

Fig. 3- 10. PR removal from water by adsorption on DAmC (a) as a function of pH showing optimal dye removal at pH 2 (200 μL of 1% DAmC with 5 mL of 0.5 g L-1 PR); (b) as a function of DAmC dose at pH 2(100 – 3000 μL of 1% DAmC with 5 mL of 1 g L-1 PR); (c) as a function of concentration of dye a pH 2 (200 μL of 1% DAmC with 5 mL of 0.1 -10 g L-1 PR); (d) In the presence of 0.5 - 1 M NaCl at pH 2 (200 μL of 1% DAmC with 5 mL of 0.1 - 4 g L-1 PR) solution.

3.4.4.2. Effect of flocculant dosage.

The graph in Fig. 3- 10b shows the effect of DAmC concentration. In these experiments, we varied the volume of 1% DAmC added (100 – 3000 μL) to a constant concentration and volume of PR (1 g L^{-1} and 5 mL respectively) at pH 2. At 536 nm, the adjusted absorbance of a 1.0 g L^{-1} PR solution was 21.8. According to the graph, 500 - 750 μL of 1% DAmC removed the most dye and was optimal for precipitation and produced a colourless solution, most likely due to sufficient cellulose chains present in solution to allow all the dye to adsorb. Hence, all dye was adsorbed on DAmC, which became water-insoluble and precipitated out. As the concentration of DAmC increased, the removal of dye decreased because there were not enough PR molecules adsorbed on the polymeric chains to precipitate out all the DAmC chains. It was also visually observed that at DAmC concentration of 2 and 3 mL, precipitation was significantly reduced because all PR dye was attached to DAmC chains, which remained in solution due to their remaining high charge content.

3.4.4.3. Effect of initial concentration of dye.

The graph in Fig. 3- 10c shows the effect of the initial concentration of dye on precipitation of DAmC, the case that 200 μL of 1% DAmC solution was added to various concentrations of dye, ranging from 0.1 g L^{-1} to 4 g L^{-1} at pH 2. We assumed that when the dye concentration was 0.75 g g^{-1} or higher, there were no longer DAmC-PR chains in solution, therefore λ_{max} did not change. For this case, we were able to determine the efficiency of dye removal, represented by the red curve on Fig. 3- 10c. As the dye concentration increases, the percentage of dye removed decreases from 80 % at 0.75 g g^{-1} to 20 % for 4 g g^{-1}, as the amount of PR molecules present in solution is significantly greater than that of DAmC.

3.4.4.4. Effect of ionic strength.

To understand the effect of ionic strength on the adsorption of PR by DAmC, NaCl was added to dye solutions to make 0.5 and 1 M solutions before adding DAmC. The results are shown in Fig. 3- 10d, and it was observed that adding salt increased precipitation. The persistence length of a polyelectrolyte (a stretched-out polymer is expected to complex small molecules less effectively than a coiled one), as well as the double-layer thickness of charged objects in solution (interactions between charges are believed to strongly influence complexation) can be affected by ionic strength[86]. Linford, et. al. observed that at low ionic strength and very high ionic strength, polyelectrolyte-dye binding was reduced in their system. This is due to polymer stiffness at low ionic strength, and polymer complexing the ions in solution instead of PR dye at very high ionic strength. They suggested that there was an optimum salt concentration or set of concentrations that facilitated the adsorption of dye[86]. We believe that 0.5 M and 1.0 M NaCl fall in that optimum range as the precipitation was higher in these systems in comparison to when no salt was added. At 0.5 M and 1.0 M, NaCl screens the charges on DAmC, leading to shorter persistent length and more flexible polymer, which is more effective in absorbing PR than the stiff DAmC polymeric chains (in the case of no salt).

Furthermore, NaCl ions screen the charges on the PR, resulting in less electrostatic repulsion between the PR molecules, ensuing in microflocs of dye which deposit on the DAmC chains, forming macroflocs by bridging the chains, that can be readily centrifuged. The evidence of aggregation is presented by the graph in Fig. S3- 1a. When the concentration of NaCl increases, the total absorbance of PR decreases, implying that there are fewer absorbing species in solution. Hamlin, et. al. also observed this hypochromic shift (decrease in absorption) when PR was in 60 g L^{-1} (~1.03 M) NaCl solution[87]. In the absence of DAmC no PR precipitation was observed, which implies that PR aggregates did not grow to very large sizes. These favourable conditions led to the higher adsorption (i.e., lower absorbance values at 536 nm) of PR molecules on DAmC.

3.5. Conclusions

Diaminocellulose fibre (DAmF), a new modified cellulose polymer with lots of primary amine groups, was synthesized from Kraft cellulose pulp by periodate oxidation and subsequent reductive amination. Diaminocellulose (DAmC) was produced by dissolution of DAmF in water at pH 3 and

60 ^{0}C. Both had an amine content of ~9.5 mmol g^{-1} (measured by conductometric titration) which is twice the amine content in chitosan. Successful functionalization of cellulose with primary amines was confirmed by electrophoretic mobility measurements, FTIR, XPS and conductometric titration by strong acid. DAmF and DAmC which are in form of fibres and solubilized polymer respectively were used for the removal of an anionic dye, Procion Red MX-5B (PR), from wastewater. DAmF showed good adsorption capacity of 3.72 g g^{-1} at the optimal pH of 2. At pH 10 desorption occurred, making DAmF a potential reusable sorbent for anionic dyes. In comparison to other biosorbents displayed in Table S3- 2, DAmF is a better alternative for adsorption. Diaminocellulose has potential applications in industrial and biomedical industries, such as in packaging and drug delivery, due to the accessibility of its primary amine groups to chemicals and because they can be further functionalized by Schiff base or bioconjugation reactions.

3.6. References

1. Mautner, A.; Hakalahti, M.; Rissanen, V.; Tammelin, T., Crucial interfacial features of nanocellulose materials. In *Nanocellulose and Sustainability*, CRC Press: 2018; pp 87-128.

2. Shah, K., Biodegradation of azo dye compounds. **2014,** *1*, 005-013.

3. Elliott, A.; Hanby, W. E.; Malcolm, B. R., The near infra-red absorption spectra of natural and synthetic fibres. *British Journal of Applied Physics* **1954,** *5* (11), 377-381.

4. Ananthashankar, R. Treatment of textile effluent containing reactive red 120 dye using advanced oxidation. Masters, Dalhousie University, Halifax, Nova Scotia, 2012.

5. Hassaan, M. A.; El Nemr, A.; Hassaan, A., Health and environmental impacts of dyes: mini review. *American Journal of Environmental Science and Engineering* **2017,** *1* (3), 64-67.

6. Hassan, M. M.; Carr, C. M., A critical review on recent advancements of the removal of reactive dyes from dyehouse effluent by ion-exchange adsorbents. *Chemosphere* **2018,** *209*, 201-219.

7. Imran, M.; Crowley, D. E.; Khalid, A.; Hussain, S.; Mumtaz, M. W.; Arshad, M., Microbial biotechnology for decolorization of textile wastewaters. *Reviews in Environmental Science and Bio/Technology* **2015,** *14* (1), 73-92.

8. BafanaAmit; Saravana, D.; ChakrabartiTapan, Azo dyes: past, present and the future. *Environmental Reviews* **2011,** *19* (NA), 350-371.

9. O'Neill, C.; Hawkes, F. R.; Hawkes, D. L.; Lourenço, N. D.; Pinheiro, H. M.; Delée, W., Colour in textile effluents – sources, measurement, discharge consents and simulation: a review. *Journal of Chemical Technology & Biotechnology* **1999,** *74* (11), 1009-1018.

10. Khan, R.; Bhawana, P.; Fulekar, M. H., Microbial decolorization and degradation of synthetic dyes: a review. *Reviews in Environmental Science and Bio/Technology* **2013,** *12* (1), 75-97.

11. van der Zee, F. P.; Villaverde, S., Combined anaerobic–aerobic treatment of azo dyes—A short review of bioreactor studies. *Water Research* **2005,** *39* (8), 1425-1440.

12. Oller, I.; Malato, S.; Sánchez-Pérez, J. A., Combination of Advanced Oxidation Processes and biological treatments for wastewater decontamination—A review. *Science of The Total Environment* **2011,** *409* (20), 4141-4166.

13. Adinew, B., Textile effluent treatment and decolorization techniques - A review. *Chemistry* **2012,** *21*, 434-456.

14. Naje, A. S.; Chelliapan, S.; Zakaria, Z.; Ajeel, M. A.; Alaba, P. A., A review of electrocoagulation technology for the treatment of textile wastewater. *Reviews in Chemical Engineering* **2017,** *33* (3), 263-292.

15. Nia, M. H.; Tavakolian, M.; Kiasat, A. R.; van de Ven, T. G. M., Hybrid aerogel nanocomposite of dendritic colloidal silica and hairy nanocellulose: an effective dye adsorbent. *Langmuir* **2020,** *36* (40), 11963-11974.

16. Yang, H.; Sheikhi, A.; van de Ven, T. G. M., Reusable green aerogels from cross-linked hairy nanocrystalline cellulose and modified chitosan for dye removal. *Langmuir* **2016,** *32* (45), 11771-11779.

17. Radoor, S.; Karayil, J.; Jayakumar, A.; Kandel, D. R.; Kim, J. T.; Siengchin, S.; Lee, J., Recent advances in cellulose- and alginate-based hydrogels for water and wastewater treatment: A review. *Carbohydrate Polymers* **2024,** *323*, 121339.

18. Koshani, R.; Tavakolian, M.; Van De Ven, T. G. M., Cellulose-based dispersants and flocculants. *Journal of Materials Chemistry B* **2020,** *8* (46), 10502-10526.

19. Sharma, B. R.; Dhuldhoya, N. C.; Merchant, U. C., Flocculants—an Ecofriendly Approach. *Journal of Polymers and the Environment* **2006,** *14* (2), 195-202.

20. Vajihinejad, V.; Gumfekar, S. P.; Bazoubandi, B.; Rostami Najafabadi, Z.; Soares, J. B. P., Water Soluble Polymer Flocculants: Synthesis, Characterization, and Performance Assessment. *Macromolecular Materials and Engineering* **2019,** *304* (2), 1800526.

21. Diab, M.; Curtil, D.; El-shinnawy, N.; Hassan, M. L.; Zeid, I. F.; Mauret, E., Biobased polymers and cationic microfibrillated cellulose as retention and drainage aids in papermaking: Comparison between softwood and bagasse pulps. *Industrial Crops and Products* **2015,** *72*, 34-45.

22. Al Naim, A. F.; El-Shamy, A. G., A new reusable adsorbent of polyvinyl alcohol/magnesium peroxide (PVA/MgO2) for highly selective adsorption and dye removal. *Materials Chemistry and Physics* **2021,** *270*, 124820.

23. Gupta, V. K.; Mittal, A.; Jain, R.; Mathur, M.; Sikarwar, S., Adsorption of Safranin-T from wastewater using waste materials— activated carbon and activated rice husks. *Journal of Colloid and Interface Science* **2006,** *303* (1), 80-86.

24. Ashraf, M. W.; Abulibdeh, N.; Salam, A., Adsorption Studies of Textile Dye (Chrysoidine) from Aqueous Solutions Using Activated Sawdust. *International Journal of Chemical Engineering* **2019,** *2019*, 9728156.

25. Ma, M.; Chen, Y.; Zhao, X.; Tan, F.; Wang, Y.; Cao, Y.; Cai, W., Effective removal of cation dyes from aqueous solution using robust cellulose sponge. *Journal of Saudi Chemical Society* **2020,** *24* (12), 915-924.

26. Hadi, A., Removal of Cationic Dye From Aqueous Solutions Using Chitosan. *Indian journal of Applied research* **2014,** *4*, 4-6.

27. Szymczyk, P.; Filipkowska, U.; Jóźwiak, T.; Kuczajowska-Zadrożna, M., The use of chitin and chitosan for the removal of reactive black 5 dye. *Progress on Chemistry and Application of Chitin and its Derivatives* **2015,** *XX*, 260-272.

28. Králik, M., Adsorption, chemisorption, and catalysis. *Chemical Papers* **2014,** *68* (12), 1625-1638.

29. Zhou, X.; Wei, J.; Liu, K.; Liu, N.; Zhou, B., Adsorption of Bisphenol A Based on Synergy between Hydrogen Bonding and Hydrophobic Interaction. *Langmuir* **2014,** *30* (46), 13861-13868.

30. Tran, H. N.; Wang, Y.-F.; You, S.-J.; Chao, H.-P., Insights into the mechanism of cationic dye adsorption on activated charcoal: The importance of π–π interactions. *Process Safety and Environmental Protection* **2017,** *107*, 168-180.

31. Alimohamadi, Z.; Younesi, H.; Bahramifar, N., Desorption of Reactive Red 198 from activated carbon prepared from walnut shells: effects of temperature, sodium carbonate concentration and organic solvent dose. *Advances in Environmental Technology* **2017,** *2* (3), 137-141.

32. Lu, P.-J.; Lin, H.-C.; Yu, W.-T.; Chern, J.-M., Chemical regeneration of activated carbon used for dye adsorption. *Journal of the Taiwan Institute of Chemical Engineers* **2011,** *42* (2), 305-311.

33. Chern, J. M.; Wu, C. Y., Desorption of dye from activated carbon beds: effects of temperature, pH, and alcohol. *Water Res* **2001,** *35* (17), 4159-65.

34. Fatma, F.; Hariani, P.; Riyanti, F.; Sepriani, W., Desorption and Re-Adsorption of Procion Red MX-5B Dye on Alumina-Activated Carbon Composite. *Indonesian Journal of Chemistry* **2018,** *18*, 222.

35. Paul, J.; Ahankari, S. S., Nanocellulose-based aerogels for water purification: A review. *Carbohydrate Polymers* **2023,** *309*, 120677.

36. Kausar, A.; Zohra, S. T.; Ijaz, S.; Iqbal, M.; Iqbal, J.; Bibi, I.; Nouren, S.; El Messaoudi, N.; Nazir, A., Cellulose-based materials and their adsorptive removal efficiency for dyes: A review. *International Journal of Biological Macromolecules* **2023,** *224*, 1337-1355.

37. Samuel, M. S.; John. J, A.; Ravikumar, M.; Raizada, P.; Wan Azelee, N. I.; Selvarajan, E.; Selvasembian, R., Recent progress on the remediation of dyes in wastewater using cellulose-based adsorbents. *Industrial Crops and Products* **2023,** *206*, 117590.

38. Almeida, R. O.; Maloney, T. C.; Gamelas, J. A. F., Production of functionalized nanocelluloses from different sources using deep eutectic solvents and their applications. *Industrial Crops and Products* **2023,** *199*, 116583.

39. Marques, B. S.; Frantz, T. S.; Sant'Anna Cadaval Junior, T. R.; de Almeida Pinto, L. A.; Dotto, G. L., Adsorption of a textile dye onto piaçava fibers: kinetic, equilibrium, thermodynamics, and application in simulated effluents. *Environmental Science and Pollution Research* **2019,** *26* (28), 28584-28592.

40. Ferrero, F.; Periolatto, M., *Dyes Adsorption on Functionalized Fibrous Materials*. 2011; Vol. 25, p 1037-1042.

41. Alince, B.; van de Ven, T., Porosity of swollen pulp fibers evaluated by polymer adsorption. *Fundamentals of Papermaking Materials* **1997,** *2*, 771-788.

42. Rodríguez, R. a.; Alvarez-Lorenzo, C.; Concheiro, A., Cationic cellulose hydrogels: kinetics of the cross-linking process and characterization as pH-/ion-sensitive drug delivery systems. *Journal of Controlled Release* **2003,** *86* (2-3), 253-265.

43. Chaker, A.; Boufi, S., Cationic nanofibrillar cellulose with high antibacterial properties. *Carbohydrate polymers* **2015,** *131*, 224-232.

44. Gao, Y.; Li, Q.; Shi, Y.; Cha, R., Preparation and Application of Cationic Modified Cellulose Fibrils as a Papermaking Additive. *International Journal of Polymer Science* **2016,** *2016*, 6978434.

45. GRUBER, E., Is there a future for chemically modified pulp? *Ipw. International paperworld* **2002,** (6), 73-85.

46. Yang, H.; van de Ven, T. T. G. M., Preparation of hairy cationic nanocrystalline cellulose. *Cellulose* **2016,** *23* (3), 1791-1801.

47. Zou, M.; Zhang, H.; Miyamoto, N.; Kano, N.; Okawa, H., Adsorption of an Anionic Surfactant (Sodium Dodecyl Sulfate) from an Aqueous Solution by Modified Cellulose with Quaternary Ammonium. *Polymers* **2022,** *14* (7), 1473.

48. Zhu, X.; Wen, Y.; Wang, L.; Li, C.; Cheng, D.; Zhang, H.; Ni, Y., Binding of Sodium Cholate In Vitro by Cationic Microfibrillated Cellulose. *Industrial & Engineering Chemistry Research* **2014,** *53* (48), 18508-18513.

49. Binupriya, A. R.; Sathishkumar, M.; Ku, C. S.; Yun, S. I., Biosorption of Procion Red MX 5B by Bacillus subtilis and Its Extracellular Polysaccharide: Effect of Immobilization. *CLEAN – Soil, Air, Water* **2010,** *38* (8), 775-780.

50. Pachhade, K.; Sandhya, S.; Swaminathan, K., Ozonation of reactive dye, Procion red MX-5B catalyzed by metal ions. *Journal of Hazardous Materials* **2009,** *167* (1), 313-318.

51. Nazifa, T. H.; Habba, N.; Salmiati; Aris, A.; Hadibarata, T., Adsorption of Procion Red MX-5B and Crystal Violet Dyes from Aqueous Solution onto Corncob Activated Carbon. *Journal of the Chinese Chemical Society* **2018,** *65* (2), 259-270.

52. Nia, M. H.; Kiasat, A. R.; van de Ven, T. G. M., Dendritic Fibrous Colloidal Silica Internally Cross-linked by Bivalent Organic Cations: An Efficient Support for Dye Removal and the Reduction of Nitrobenzene Derivatives. *Langmuir* **2021,** *37* (46), 13676-13688.

53. Taher, T.; Wulandari, A.; Mohadi, R.; Lesbani, A., TiO2/Kaolin composite as low-cost adsorbent for procion red removal from aqueous solution: kinetics, equilibrium, and thermodynamic studies. *Bulletin of the Chemical Society of Ethiopia* **2019,** *33* (3), 437.

54. Ribas, M. C.; de Franco, M. A. E.; Adebayo, M. A.; Lima, E. C.; Parkes, G. M. B.; Feris, L. A., Adsorption of Procion Red MX-5B dye from aqueous solution using homemade peach and commercial activated carbons. *Applied Water Science* **2020,** *10* (6), 154.

55. Tao, P.; Wang, Y., Enhanced photocatalytic performance of W-doped TiO2 nanoparticles for treatment of Procion Red MX-5B azo dye in textile wastewater. *International Journal of Electrochemical Science* **2023,** *18* (9), 100261.

56. Zhu, Q.; Song, J.; Liu, Z.; Wu, K.; Li, X.; Chen, Z.; Pang, H., Photothermal catalytic degradation of textile dyes by laccase immobilized on Fe3O4@SiO2 nanoparticles. *Journal of Colloid and Interface Science* **2022,** *623*, 992-1001.

57. Sigma, M. Procion® Red MX-5B. https://www.sigmaaldrich.com/CA/en/product/sial/404365.

58. Alam, M. N.; Van De Ven, T. G. M., AN AQUEOUS PROCESS FOR THE SEPARATION OF CELLULOSE FROM BIOMASS. *J-for-Journal of Science & Technology for Forest Products and Processes* **2014,** *4* (3), 22-26.

59. Dangerfield, E. M.; Plunkett, C. H.; Win-Mason, A. L.; Stocker, B. L.; Timmer, M. S. M., Protecting-Group-Free Synthesis of Amines: Synthesis of Primary Amines from Aldehydes via Reductive Amination. *The Journal of Organic Chemistry* **2010,** *75* (16), 5470-5477.

60. Kim, U.-J.; Wada, M.; Kuga, S., Solubilization of dialdehyde cellulose by hot water. *Carbohydrate polymers* **2004,** *56* (1), 7-10.

61. Farris, S.; Mora, L.; Capretti, G.; Piergiovanni, L., Charge Density Quantification of Polyelectrolyte Polysaccharides by Conductometric Titration: An Analytical Chemistry Experiment. *Journal of Chemical Education* **2012,** *89* (1), 121-124.

62. Wu J, L.-Z. A., Andrews M, Tuning the Physical Properties of Carboxylated Cellulose Nanocrystal (cCNC) Microspheres by Hybridizing with Silk Fibroin (SF). *ChemRxiv,* **2022**.

63. Azizian, S.; Eris, S., Chapter 6 - Adsorption isotherms and kinetics. In *Interface Science and Technology*, Ghaedi, M., Ed. Elsevier: 2021; Vol. 33, pp 445-509.

64. Maekawa, E.; Koshijima, T., Properties of 2, 3-dicarboxy cellulose combined with various metallic ions. *Journal of Applied Polymer Science* **1984,** *29* (7), 2289-2297.

65. Bruneel, D.; Schacht, E., Chemical modification of pullulan: 1. Periodate oxidation. *Polymer* **1993,** *34* (12), 2628-2632.

66. Malardier-Jugroot, C.; van de Ven, T. G. M.; Whitehead, M. A., Linear Conformation of Poly(styrene-alt-maleic anhydride) Capable of Self-Assembly: A Result of Chain Stiffening by Internal Hydrogen Bonds. *The Journal of Physical Chemistry B* **2005,** *109* (15), 7022-7032.

67. Zhou, S.; He, H.; Guo, W.; Zhu, H.; Xue, F.; Cheng, M.; Lin, J.; Wang, L.; Wang, S., Structural design of a high sensitivity biomass cellulose-based colorimetric sensor and its in situ visual recognition mechanism for Cu<sup>2</sup&gt. *Carbohydrate polymers* **2019,** *219*, 95-104.

68. Tan, J.; Song, Y.; Huang, X.; Zhou, L., Facile Functionalization of Natural Peach Gum Polysaccharide with Multiple Amine Groups for Highly Efficient Removal of Toxic Hexavalent Chromium (Cr(VI)) Ions from Water. *ACS Omega* **2018,** *3* (12), 17309-17318.

69. Xue, F.; He, H.; Zhu, H.; Huang, H.; Wu, Q.; Wang, S., Structural Design of a Cellulose-Based Solid Amine Adsorbent for the Complete Removal and Colorimetric Detection of Cr(VI). *Langmuir* **2019,** *35* (39), 12636-12646.

70. Hospodarova, V.; Singovszka, E.; Stevulova, N., Characterization of Cellulosic Fibers by FTIR Spectroscopy for Their Further Implementation to Building Materials. *American Journal of Analytical Chemistry* **2018,** *09* (06), 303-310.

71. Jin, L.; Li, W.; Xu, Q.; Sun, Q., Amino-functionalized nanocrystalline cellulose as an adsorbent for anionic dyes. *Cellulose* **2015,** *22* (4), 2443-2456.

72. Bastidas, J. C.; Venditti, R.; Pawlak, J.; Gilbert, R.; Zauscher, S.; Kadla, J. F., Chemical force microscopy of cellulosic fibers. *Carbohydrate Polymers* **2005,** *62* (4), 369-378.

73. Hua, Z. Q.; Sitaru, R.; Denes, F.; Young, R. A., Mechanisms of oxygen- and argon-RF-plasma-induced surface chemistry of cellulose. *Plasmas and Polymers* **1997,** *2* (3), 199-224.

74. Afshari, M.; Dinari, M.; Farrokhpour, H.; Zamora, F., Imine-Linked Covalent Organic Framework with a Naphthalene Moiety as a Sensitive Phosphate Ion Sensing. *ACS Appl Mater Interfaces* **2022,** *14* (19), 22398-22406.

75. Li, Y.; Ou, Z.; Liang, B.; Yang, J.; Chen, R.; Qi, H.; Kaiser, U.; Hong, W.; Chen, X.; Du, L.; Liu, W.; Zheng, Z., Cellulose Nanocrystals as Template for Improving the Crystallinity of Two-Dimensional Covalent Organic Framework Films. *Polymers (Basel)* **2021,** *13* (10).

76. Janhom, S., Kinetic and thermodynamic studies of cationic and anionic surfactants adsorption onto polyethyleneimine-modified cotton cloths. *Chiang Mai Journal of Science* **2018,** *45*, 2422-2437.

77. Akhlaghi, S. P.; Zaman, M.; Mohammed, N.; Brinatti, C.; Batmaz, R.; Berry, R.; Loh, W.; Tam, K. C., Synthesis of amine functionalized cellulose nanocrystals: optimization and characterization. *Carbohydrate Research* **2015,** *409*, 48-55.

78. Pillai, C.; Paul, W.; Sharma, C. P., Chitin and chitosan polymers: Chemistry, solubility and fiber formation. *Progress in polymer science* **2009,** *34* (7), 641-678.

79. Pardo-Castaño, C.; Bolaños, G., Solubility of chitosan in aqueous acetic acid and pressurized carbon dioxide-water: Experimental equilibrium and solubilization kinetics. *The Journal of Supercritical Fluids* **2019,** *151*, 63-74.

80. Kamida, K.; Okajima, K.; Matsui, T.; Kowsaka, K., Study on the Solubility of Cellulose in Aqueous Alkali Solution by Deuteration IR and 13C NMR. *Polymer Journal* **1984,** *16* (12), 857-866.

81. van de Ven, T. G. M.; Saint-Cyr, K.; Allix, M., Adsorption of toluidine blue on pulp fibers. *Colloids and Surfaces A: Physicochemical and Engineering Aspects* **2007,** *294* (1), 1-7.

82. Tavakolian, M.; Wiebe, H.; Sadeghi, M. A.; van de Ven, T. G. M., Dye Removal Using Hairy Nanocellulose: Experimental and Theoretical Investigations. *ACS Applied Materials & Interfaces* **2020,** *12* (4), 5040-5049.

83. Klotz, I. M.; Harris, J. U., Macromolecule-small molecule interactions. Strong binding by intramolecularly cross-linked polylysine. *Biochemistry* **1971,** *10* (6), 923-926.

84. Chakraborty, G.; Bhattarai, A.; De, R., Polyelectrolyte-Dye Interactions: An Overview. *Polymers (Basel)* **2022,** *14* (3).

85. Kim, Y. D.; Klotz, I. M., A cross-linked copolypeptide with increased affinity for cations. *Biopolymers: Original Research on Biomolecules* **1972,** *11* (2), 431-441.

86. Linford, M. R.; Auch, M.; Möhwald, H., Nonmonotonic Effect of Ionic Strength on Surface Dye Extraction during Dye−Polyelectrolyte Multilayer Formation. *Journal of the American Chemical Society* **1998,** *120* (1), 178-182.

87. Hamlin, J. D.; Phillips, D. A. S.; Whiting, A., UV/Visible spectroscopic studies of the effects of common salt and urea upon reactive dye solutions. *Dyes and Pigments* **1999,** *41* (1), 137-142.

88. Saputra, O. A.; Nauqinida, M.; Kurnia; Pujiasih, S.; Kusumaningsih, T.; Pramono, E., Improvement of anionic and cationic dyes removal in aqueous solution by Indonesian agro-waste oil palm empty fruit bunches through silylation approach. *Groundwater for Sustainable Development* **2021,** *13*, 100570.

89. Hariani, P. L.; Faizal, M.; Ridwan; Marsi; Setiabudidaya, D., Removal of Procion Red MX-5B from songket's industrial wastewater in South Sumatra Indonesia using activated carbon-Fe3O4 composite. *Sustainable Environment Research* **2018,** *28* (4), 158-164.

90. Handayani, D.; Kusumaningsih, T.; Hak, L., Utilization Chitosan- p-t- Butylcalix[4]Arene for Red MX 8B Adsorbent. *IOP Conference Series: Materials Science and Engineering* **2017,** *176*, 012016.

3.7. Supplementary Information

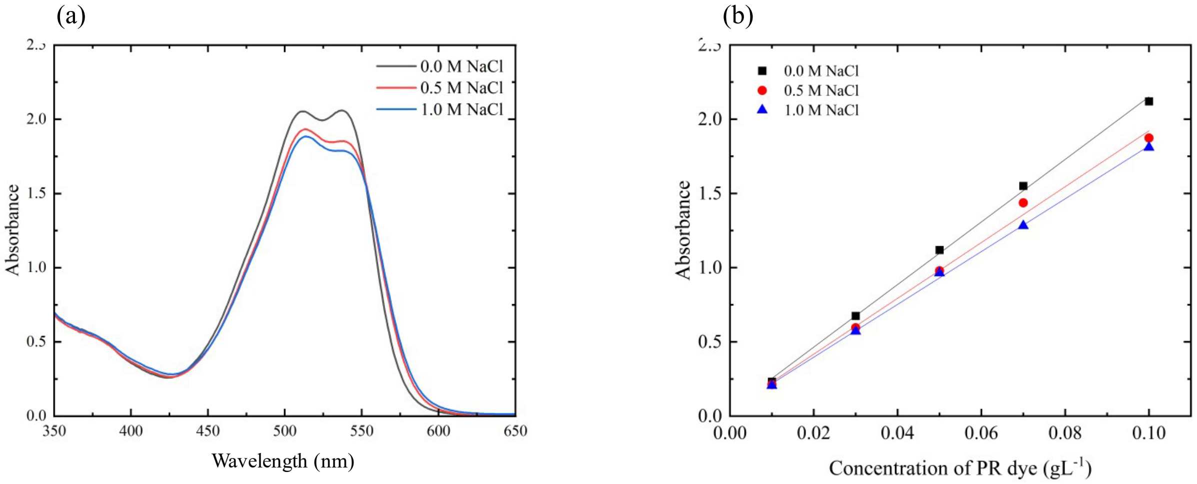

Fig. S3- 1. (a) UV-vis spectra of 0.1 gL-1 PR in no salt, 0.5 M NaCl and 1 M NaCl. (b) Calibration curve of PR at 536 nm

Table S3- 1. Trendline equation and R^2 values for the calibration curve in Fig. S3- 1b

Conc. of NaCl (M)	Trendline equation	R^2
0.0	y = 21.081x + 0.0432	0.9986
0.5	y = 18.815x + 0.0408	0.9948
1.0	y = 17.79x + 0.0413	0.9991

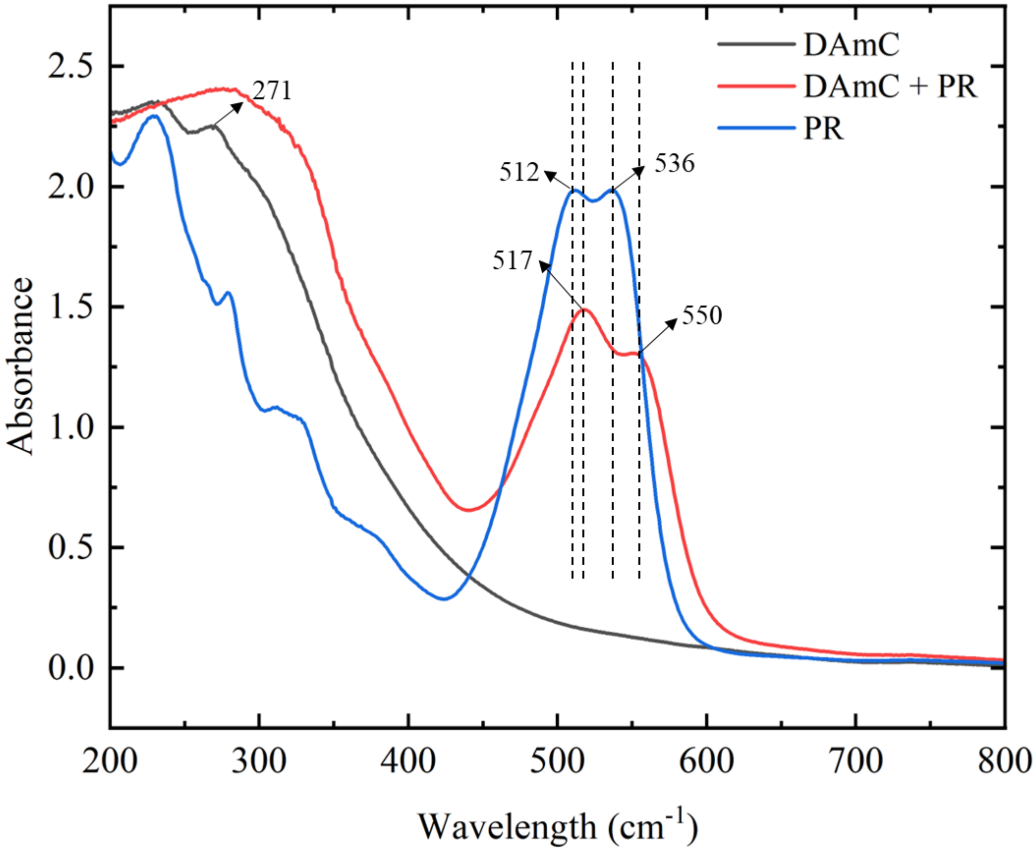

Fig. S3- 2. UV-vis spectra of 0.1% DAmC, 0.1gL PR and a mixture of DAmC and PR

Table S3- 2. Comparison of the maximum monolayer adsorption capacities of PR-MX (without purification) on various adsorbents

Adsorbent	Maximum adsorption capacity (mg/g)	Ref.
Diaminocellulose fibers (DAmF)	3720	This work
Dendritic Fibrous Colloidal Silica Internally Cross-linked by Bivalent Organic Cations (DDS)	3190	[52]

Activated peach carbon. Commercial activated carbon	297.2 174.0	[54]
Oil palm empty fruit bunch (OPEFB) Silylated-OPEFB	20.70 208.33	[88]
TiO_2/ kaolin	158	[53]
Activated carbon-Fe_3O_4 composite	278	[89]
Chitosan Chitosan-linked p-tbutylcalix[4]arene	136.1 147.4	[90]

Chapter 4

SORPTION OF LEAD USING DIIMINO- AND DIAMINOCELLULOSE

Preface

In Chapter 3, the main focus was on the process of animating cellulose directly to create diaminocellulose fiber (DAmF), which contains a substantial amount of primary amine groups. In order to further explore the potential applications of this fiber, DAmF, as well as its precursor diiminocellulose (DImF), were examined for their capacity to remove heavy metals from water. This is attributed to the substantial nitrogen and oxygen content present in the fibers.

4.1. Abstract

Cellulose pulp was functionalized with nitrogen to produce diiminocellulose fiber (DImF) and diaminocellulose fiber (DAmF). DImF and DAmF contain two imine and two amine groups respectively. Aldehyde content determination, conductometric titration, XPS and FT-IR were used to characterize the fibers. DImF and DAmF contain approximately 9.5 mmol g^{-1} imine content and 9.3 mmol g^{-1} amine content respectively. Imine content was determined by titration of the residual aldehyde groups before reduction of imine groups by $NaBH_4$, while the amine content was determined by conductometric titration. The fibers were employed for sorption of Pb^{2+} ions, with an investigation conducted on the effect of pH, initial concentration and sorbent dosage. Sorption was affected by pH with the highest sorption at pH 8 due to reduction of positive charges in and on the fibers. DAmF had slightly higher sorbed amounts (mg g^{-1}) than DImF at all pHs except 7 and 8 possibly due to ring closure in the polymeric chain. Kinetic studies showed that the sorption of the metal at pH 5.5 was slow due to establishment of a Donnan equilibrium, which causes much lower Pb^{2+} concentrations in the pores id the fibers than in the bulk. Depth profile analysis by XPS was used to confirm that amination and adsorption did not only occur on the surface of the fibers but also in the pores as well.

4.2. Introduction

The presence of heavy metals in the environment can have substantial consequences for both human health and the ecosystem, mostly because of their non-biodegradable properties and tendency to accumulate over time. The issue of water resource contamination caused by the discharge of contaminants, such as heavy metals, from industrial activities is a significant concern, particularly in developing nations[1, 2]. Anthropogenic sources of heavy metals encompass a range of activities, including mining, smelting, combustion of fossil fuels, incineration of solid waste, as well as the manufacturing processes involved in batteries, paints, electronics, ceramics, and glass industries. Natural events, including forest fires, volcanic activity, mineral weathering, and erosion, play a significant role in the presence of heavy metals[3, 4].

Lead (Pb) is a heavy, soft, and malleable metal that occurs naturally in the Earth's crust. It is typically found in the form of metal oxides. It has been used for a variety of purposes throughout history, primarily in car batteries, plumbing, pottery, etc.[5] Aside from its many applications, lead and its compounds are toxic to humans and other organisms. Lead is a potent neurotoxin that binds to various proteins (such as enzymes) in the human body and replaces calcium in life-sustaining processes, causing extensive damage. Lead poisoning has been reported since antiquity and scientifically established since the nineteenth century. Lead is now largely eliminated from applications involving human exposure in developed countries, such as lead paints, piping, and anti knocking agents in gasoline. Legislation varies in developing countries; despite a general tendency to limit lead exposure, lead poisoning cases still occur.[6] Lead is believed to be quickly sorbed in the blood stream and affects every organ of the body leading to devasting effects in both children and adults. Children are extremely sensitive to low levels of lead which may contribute to lower IQ, behavioral problems, and learning deficits[7]. In pregnant women, exposure may lead to miscarriage or premature birth and chronic exposure in men may lead to reduced male fertility[8]. Prolonged exposure to lead can also lead to anaemia, increase in blood pressure, severe damage to the brain and kidney, etc.

The maximum permissible limit (MPL) of lead in drinking water and wastewater, according to the World Health Organization (WHO) and Environmental Protection Agency (EPA) is 0.05 mg per liter[9]. Pb concentrations in industrial wastewaters can reach 200-500 mgL^{-1} and must be reduced to the EPA standard before being discharged into water bodies or sewage systems[10, 11]. As a result, finding a safe and effective way to remove lead from wastewater is critical. Precipitation[12], coagulation-flocculation[13], ion-exchange[14], electrodialysis[15], adsorption[16], and other approaches have all been investigated in the fight against lead water pollution. Among these approaches, sorption is thought to be the most cost-effective and efficient, with no drawbacks such as sludge development, low metal ion retention, high energy consumption, etc[4].

Cellulose is the most abundant biopolymer on earth that is also environmentally friendly, renewable, and biodegradable. Cellulosic materials like rice husk and sawdust have been used as green adsorbent for heavy metals due to the presence of hydroxyl groups on the cellulose chain[17]. However, cellulose has a low metal retention due to the inability of D-glucose units to form stable metal complexes. To improve the efficacy of cellulose in adsorbing heavy metals from wastewater, processes such as esterification, halogenation, etherification, grafting, oxidation, and others can be used to modify the biopolymer with "ligand" binding groups. Atoms such as S, N, and O serve as ligand atoms in chemical groups such as –SH, –S-S, $–NH_2$, =NH, –OH, $-OPO_3H$, and >C=O[18]. Numerous scholarly publications have explored the application of imino- and amino- modified cellulose for the purpose of adsorbing Pb^{2+} ions. A method of enhancing the adsorption of Pb^{2+} was observed through the functionalization of cellulose using diaminoguanidine[19]. Additionally, the adsorption of cellulose towards Pb^{2+} ions was improved through the complexation of cellulose with ethylene diaminetetraacetic dianhydride (EDTAD)[20]. Also, the adsorption of Pb^{2+} ions was further improved through the modification of cellulose using 1,2-pheneylnediamine[21]. Table 2-3 in Chapter 2 provides more examples of imine and amine modified cellulose-based Pb^{2+} sorbents.

The goal of this study is to modify cellulose fibres into a new type of heavy metal ion adsorbent by functionalizing them with amines and imines. To add these functional groups unto cellulose fibres, we use a periodate oxidation reaction followed by an amination and reductive amination reaction to synthesize diiminocellulose fiber (DImF) and diaminocellulose fiber (DAmF) respectively. The effects of pH, dosage amount, contact time, and initial concentration on the sorption of lead from water are investigated using these cellulose fibre derivatives. To the best of our knowledge, diimino- and diaminocellulose, have never been used to adsorb Pb^{2+} ions in wastewater treatment.

4.2. Materials and methods

4.2.1. Reagents and Materials.

Softwood kraft pulp (Domtar, Canada) was used as the starting material to synthesize DAmC. Sodium periodate ($NaIO_4$), ethylene glycol (≥99%), ammonium acetate (NH_4OAc), ammonium in ethanol (2M), sodium borohydride ($NaBH_4$), hydroxylamine hydrochloride ($NH_2OH \cdot HCl$), and lead nitrate ($Pb(NO_3)_2$) were purchased from Sigma-Aldrich. Sodium chloride (NaCl) was purchased from ACP. Sodium hydroxide (NaOH) and hydrochloric acid (HCl) solutions of various concentrations were purchased from Merck. Anhydrous ethanol (EtOH) was purchased from Greenfield Global. Deionized water (DI) was used in all experiments unless otherwise specified.

4.2.2. Preparation of adsorbents

4.2.2.1. Periodate oxidation of cellulose fibers

Dialdehyde cellulose (DAC) was synthesized with the protocol developed in our lab with minor alterations[22]. DAC was prepared under the following reaction conditions: Pre-soaked kraft pulp (10.0 g) was added to a solution containing 26.4 g of $NaIO_4$ (12.3 mmol based on 2 mol per 1mol glucose unit), 29.3 g NaCl and 500 mL DI water. The reaction mixture was stirred at room temperature in the dark for 6 days. Ethylene glycol was added to the reaction mixture to quench the residual periodate. DAC fibers were rinsed thoroughly with DI water 5 times and filtered through a 4 µm pore nylon cloth. To prepare DAC for the reductive amination reaction, wet DAC was placed in 200mL of methanol for solvent exchanges. Solvent exchange was carried out 5 times in methanol to ensure that there was no residual water to interfere with the amination reaction. A small amount of DAC was set aside for aldehyde content determination.

4.2.2.2. Synthesis of DImF and DAmF

To synthesize diiminocellulose fiber (DImF), 10.0 g of DAC fibers (dry weight) was added to a solution containing 4.2 g NH_4OAc (3 mol per 1 mol -CHO), 625 mL 2M NH_3 (10 mol per mol -CHO) and methanol. The mixture was stirred at 80^{o}C under reflux for 18 hrs and the product was washed with water three times with distilled water. After drying DImF, half of it was used to synthesize diaminocellulose (DAmC). 5.0 g DImF was dispersed in methanol and placed in an ice bath, then sodium borohydride (1 g) was added. After the addition, the mixture was stirred at room temperature for one hour. NaOH solution was used to quench the reaction and the DAmC fibers were washed with DI water 5 times and dried at room temperature. A small amount of DAmF was taken for amine content determination.

4.2.3. Characterization of adsorbents

4.2.3.1. Determination of aldehyde content.

A known amount of DAC sample was dissolved in water (2%) at 80 °C for 6 hrs. After solubilization, the pH was adjusted to 3.5 by HCl. The pH of a solution of $NH_2OH{\cdot}HCl$ (5% w/w) was also adjusted to 3.5 before adding it to the sample solution. The pH of the reaction was maintained at 3.5 with the addition of 10 mM NaOH. NaOH was added until the pH remained constant at 3.5, indicating the complete conversion of aldehydes to oximes. The aldehyde content was determined by the following equation 1.

$$\text{Aldehyde content (mmol g}^{-1}\text{)} = \frac{\mathrm{N_{NaOH}} * \mathrm{V_{NaOH}}}{\mathrm{W}} \quad 6$$

Here, N_{NaOH} is the normality of base, V_{NaOH} is the volume of base used and W is the weight of the sample used for titration.

This same procedure was followed for aldehyde determination in DImF, as the residual aldehydes in DAmF would undergo reduction to hydroxides after reaction with $NaBH_4$.

4.2.3.2. Potentiometric and conductometric titration.

Amine (charge) content of DAmF was measured by conductometric titration by a standardized HCl solution on an 836 Titrando titrator (Metrohm, Switzerland). A known amount of fiber was dispersed in 100 mL milli Q water and the pH was adjusted to ~11.5 with 0.1 M NaOH. The addition HCl and data collection were controlled by a computer system. 45mL of standardized 10 mM HCl solution to the solution at a rate of 0.1 mL min^{-1} until the pH reached ~3. The amine content in mmol per one gram of fibers was calculated from the middle part of the titration curve representing the volume of the HCl solution that neutralized the weak base. Potentiometric titration of DImF followed this same protocol. The pK_b values of DImF and DAmF were determined from the first derivative of the pH curve.

4.2.3.3. Fourier Transform Infrared (FTIR) Spectroscopy.

In order to verify the change in functional groups, Fourier transform infrared spectra were obtained from dried fibers (Pulp, DAC, DImF, and DAmF) using the attenuated total reflectance (ATR) technique on a Bruker ALPHA FTIR spectrometer (Bruker Optics Inc., Billerica, USA). The ATR method employed a single bounce diamond crystal and a standard room-temperature LiTaO3 mid-infrared (MIR) detector, covering the spectral range of 400 cm^{-1} to 4000 cm^{-1}. The spectra were acquired by performing 32 scans at a resolution of 4 cm^{-1}.

4.2.4.4. Electrophoretic mobility (µ) by electrophoretic light scattering (ELS)

In order to investigate the impact of pH variations on the charge density of DAmF and DImF, the electrophoretic mobility of a 0.1wt % polymer solution (DAmC and DImC) was determined using the Zeta-sizer Nano ZS instrument (Malvern Instruments Ltd., U.K). Prior to taking measurements, solutions of 1 wt. % DImC and DAmC were prepared by dissolving quantitative amounts of DImF and DAmF in water at a pH of 3 and a temperature of 60 °C. The solutions were further diluted to a concentration of 0.1 wt. % using distilled water. The pH of the solutions was then adjusted by adding either 0.5 N HCl or NaOH. DImC and DAmC were observed to be soluble in solution at all pH measured, with the exception of pH 7.5, where they precipitated out of solution. Prior to all measurements, the samples were ultrasonicated for 3 mins to ensure homogeneity in the solution. Each experimental point is a mean of three independent replicates.

4.2.4.5. X-ray photoelectron spectroscopy (XPS).

Pulp, DAC, DImF, DAmF were analyzed by X-ray photoelectron spectroscopy (XPS) to confirm modification done on the fibers. After Pb^{2+} adsorption, the DImF and DAmF were analyzed again to confirm binding with Pb^{2+} ions. The fibers were subjected to characterization using the K-Alpha™ XPS equipment (Thermo Scientific, USA). This instrument employed monochromatic Al Kα radiation and operated under a vacuum of 10^{-8} mbar. The DImF and DAmF fibers underwent a vacuum drying process prior to XPS analysis to stabilize the water content of the fibers. All measurements were conducted using copper strips. The X-ray Photoelectron Spectroscopy (XPS) study was conducted with the flood gun activated, so ensuring the neutralization of surface charge on the insulating samples. Ensuring precise measurements of the electronic structure of the sample is of paramount importance. The investigation employed an X-ray emission angle of 90 degrees relative to the surface of the material. Spectra were obtained from a minimum of three points on each sample, where the diameter of the investigated region measured 400 µm. The elemental composition was measured using single survey scans with a pass energy of 200 eV. The experimental procedure involved the acquisition of high-resolution scans for N 1s peaks, with a pass energy of 50 eV. The spectra acquired in this study were subjected to deconvolution using the Avantage Data System software. The software employed a hybrid approach, using Gaussian and Lorentzian functions, to perform spectral deconvolution. Prior to deconvolution, the spectra underwent background subtraction via the Shirley method. Following the processes of deconvolution and background subtraction, the resultant curves were assigned to distinct categories of bonds, determined by their respective binding energy levels. The binding energy estimates were computed with respect to the C (1s) photoelectron peak at 285.0 eV. The estimation of the percentage of nitrogen content was facilitated through the integration of the acquired curves.

Depth profile analysis by XPS was conducted on DAmF with adsorbed Pb^{2+}. An argon gun with an energy of 500 eV (monoatomic mode) and low current was used for surface etching. This was performed for a total etch time of ~1000 s with 33 observation cycles. XPS was performed on each etching level with the flood gun on, with a delay of 5 sec after each etch, before the spectrum was recorded. The etch rate was estimated as 0.03 nm s^{-1}.

4.2.4. Sorption studies

4.2.4.1. Preparation of metal ion solution

A stock solution of lead (II) ions concentration 1,000 ppm was prepared by dissolving a quantitative amount of 1.6 g $Pb(NO_3)_2$ in 1 L deionized water. Other concentrations prepared from stock solution by dilution varied between 50 and 500 mg/L and the pH of the working solutions was adjusted to desired values with 0.1 N HCl or 0.1 N NaOH.

4.2.4.2. Batch sorption studies.

In this study, a batch sorption approach was used; all experiments were carried out in (45 mL) centrifuge vials that were placed in a water bath with a shaker at 23 °C with no pH adjustment (~ pH 5.5) and contact time of 300 min except stated otherwise. To study the effects of metal ion concentration on sorption, the following conditions were used: 10 mL of 50 to 1000 ppm Pb^{2+} and 10 mg adsorbent. To investigate the effect of pH, pH was varied from 2.5 to 8 (10 mg adsorbent, 10 mL 1000 ppm Pb^{2+}). To investigate the effect of adsorbent dosage, the dosage was varied from 5 to 100 mg with 10 mL 1000 pm Pb^{2+} solution. The samples analyzed were filtered through a 0.45µm syringe filter and tested for residual metal ion concentration after each sorption experiment. To quantify residual Pb^{2+} ion concentration, a microwave plasma atomic emission spectrometer (MP-AES, Agilent) at the wavelength of 405 nm was used, characteristic of Pb peak in the spectrum[23]. All analysis investigations were done in triplicate, with the mean of the three runs given; standard deviation was ≤ 3.5 % in all runs. The amount of metal ions sorbed by the DImF and DAmF per gram of sorbent, q_e (mg/g) and the percentage of ions removed from solution were determined using equation 2 and 3 respectively:

$$q_e = \frac{(C_0 - C_e) * V}{m} \tag{7}$$

$$R\ (\%) = \frac{(C_0 - C_e) * V}{C_0} * 100 \tag{8}$$

C_0 and C_e are the initial and equilibrium Pb concentration (ppm) respectively, q_e is the equilibrium sorption capacity (mg g^{-1}), V is the volume of metal solution used (L) and m is the mass of fiber (g).

Sorption kinetics

Sorption kinetics were investigated by collecting and measuring multiple samples over time. The initial Pb^{2+} concentration was varied from 50 to 1000 ppm (40 mL), while the adsorbent dose was 50 mg (dry mass). Samples were taken from 15 to 300 minutes for each initial dye concentration and measured by MP-AES, q_t was calculated by equation 4.

$$q_t = \frac{(C_0 - C_t) * V}{m} \tag{9}$$

where q_t and C_t are the amount of Pb^{2+} sorbed and concentration of Pb^{2+} in solution at time t respectively.

4.3. Results and discussion

4.3.1. Characterization of DImC and DAmC.

Softwood kraft pulp (Domtar, Canada) was used as the starting material to synthesize DImF and DAmF. DAC was synthesized from pulp according to the procedure developed previously at our laboratory[22].The schematic of the reaction is shown in Scheme 4- 1. Aldehyde content of DAC fiber was determined to be 10.5 mmol g^{-1}. By reacting the aldehyde groups with ammonia to form imine bonds, DAC fiber was converted to diiminocellulose fibers (DImF). The amount of aldehyde converted to imine was determined by measuring the amount of residual aldehyde left in diiminocellulose fibre, which was found to be 0.5 mmol g^{-1}, hence imine content in DImF was 10.0 mmol/g. DAmF was synthesized by converting imine bonds to amine bonds in a reduction reaction with $NaBH_4$ as shown in Scheme 4- 1. Charge content of DAmF was determined to be 9.3 mmol g^{-1} by acid titration. Thus ~93% of the imines were converted to amines.

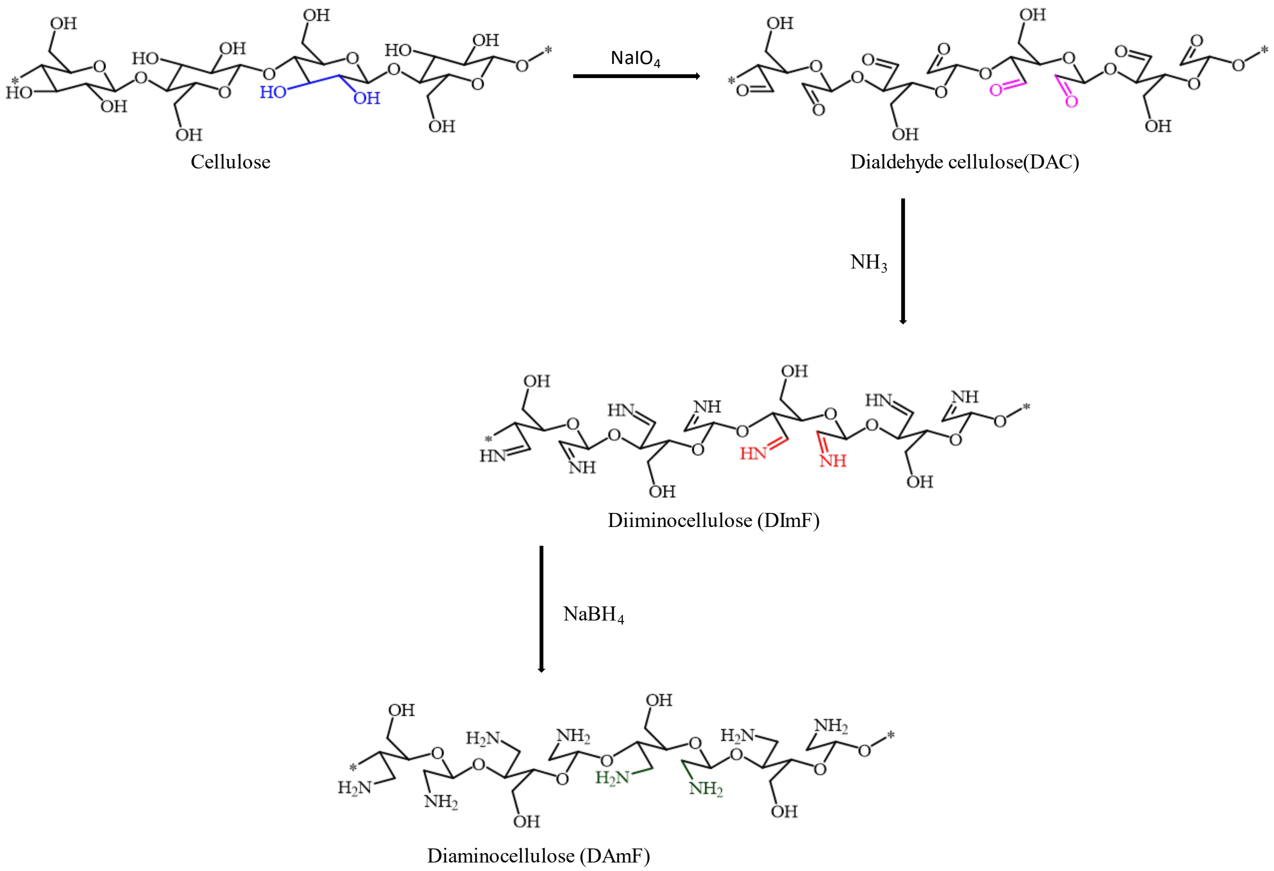

Scheme 4- 1. Schematic of conversion of cellulose to DImF and DAmF

4.3.1.1. Potentiometric titration of DImF and DAmF

The results gotten from the potentiometric titration of DImF and DAmF are presented in Fig. 4- 1. From the graph, DImF has pK_b values of 6.34 and 8.82 which translates to pK_a values of 5.18 and 7.66. For DAmF the values are 5.79 and 8.72 which translates to pK_a values of 5.28 and 8.21. Generally, amines are relatively more basic than imines, thus having a higher pK_a. This can be explained by molecular orbital theory and inductive effect[24]. The sp^2 orbitals of an imine nitrogen are approximately 67 % s character (1 part s, 2 parts p) while the sp^3 orbitals of an amine nitrogen are only 25% s character (one part s, three parts p). Sp^2 hybridization has a greater electronegativity than sp^3 hybridization because the s atomic orbital holds electrons in a spherical shape, closer to the nucleus than a p orbital. This implies that sp^2 nitrogen is less likely to donate electrons than sp^3 nitrogen, therefore it is less basic. For the inductive effect, more electronegative atoms absorb electron density more easily, leading to increased acidity. Protonated imines are more acidic than protonated amines, therefore imines are less basic.

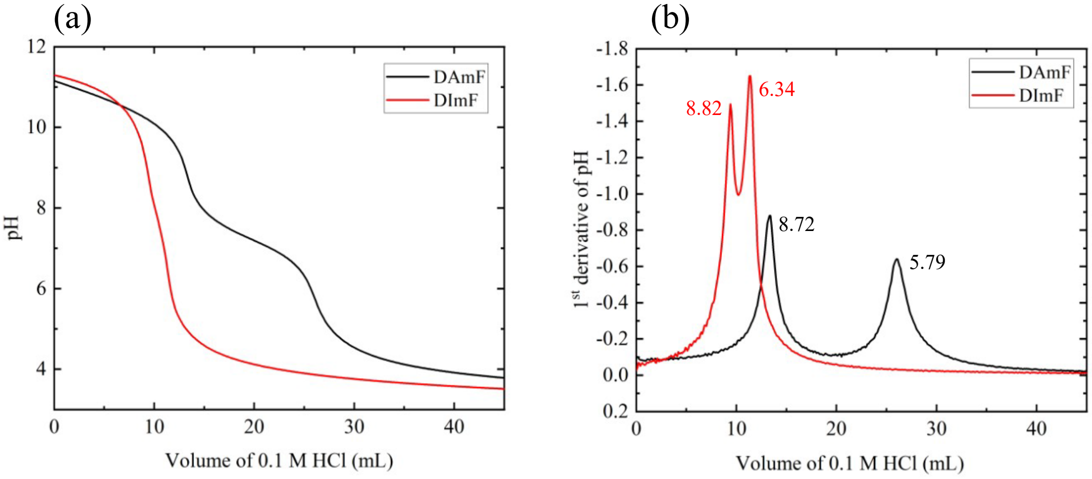

Fig. 4- 1- Potentiometric titration of DImF and DAmF using 10 mM HCl, amine content of DAmF was 9.3 mmol of -NH2 per gram of DAmF (a) volume of 10 mM HCl vs. pH (b) first derivative of pH titration curve indicating the maxima which are the points of inflection on the pH curves and hence, pKb values.

4.3.1.2. FT-IR spectroscopy

The FT-IR spectra of pulp, dialdehyde cellulose (DAC), diiminocellulose fiber (DImF), diaminocellulose fiber (DAmF), are shown in Fig. 4- 2a. The IR spectrum of the pure cellulose (Fig. 4- 2a) shows a strong broad band at 3310 cm^{-1}, and a band at 1644 cm^{-1} corresponding to the stretching and bending modes of the surface OH; the peak at 2884 cm^{-1} signifies the stretching vibration of C-H in a pyranoid ring, and the broad absorption peak 1059 cm^{-1} is attributed to the C-O-C stretching of β-glycosidic linkage[25]. DAC has a band at 1729 cm^{-1} which indicates the carbonyl (C=O) stretch of the aldehyde group. There was no significant difference between the IR spectra of DImF and DAmF, but we observed the disappearance of the carbonyl stretch on both DImF and DAmF IR spectra. The IR spectrum of DImF (Fig. 4- 2b) shows a peak at about 1597 cm^{-1} indicating the presence of C=N. The IR spectrum of DAmF shows a broad sorption peak at about 3249 cm^{-1} which originates from O-H or N-H stretching vibrations, and the peak at 1634 cm^{-1} could be attributed to the overlap of the N-H bending vibration and the absorbed H-O-H vibration band[26].

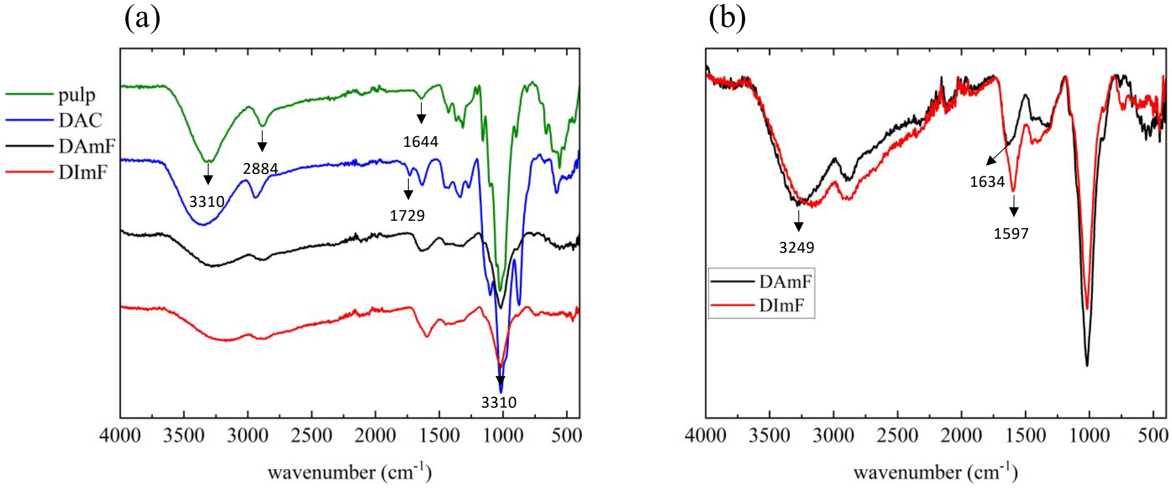

Fig. 4- 2. FT-IR spectra of (a) pulp, DAC fiber, DImF and DAmF (b) DImF and DAmF to display more clearly the differences between both of them.

4.3.1.3. Electrophoretic mobility (μ) and point of zero charge (PZC)

Electrophoretic mobility (μ) measurements of DImC and DAmC are plotted in Fig. 4- 3. From the graph, DImC and DAmC are positively charged until they reach the isoelectric point, which is a measure of the point of zero charge (PZC). PZC of DImC and DAmC are pH 8.0 ± 0.1 and 7.5 ± 0.1 respectively. Past the PZC, both polymers become negatively charged. At pH below the PZC, the imine and amine groups on DImC and DAmC are protonated, thereby acquiring a positive charge. From potentiometric titration, the two pK$_a$ values of DImF are 5.18 and 7.66, and 5.28 and

8.21 for DAmF. We would expect that at some pH greater than the pK_a values, DImC and DAmC should be neutral since the imines and amines would be deprotonated. But we observe negative values past the PZC ($\mu \cong -2\times10^{-8}$ $m^2V^{-1}s^{-1}$ for DImC at pH 9 and $\mu \cong -2.5 \times10^{-8}$ $m^2V^{-1}s^{-1}$ for DAmC at pH 10.5). This is likely due to deprotonation of hydroxyl groups naturally present in cellulose[27]. This result is comparable to that observed in Pereira, et. al. study in which cellulose was aminated with ethylenediamine[28]. The addition of imine and amine groups on cellulose results in positive and negative charge densities at pH below and above the PZC respectively.

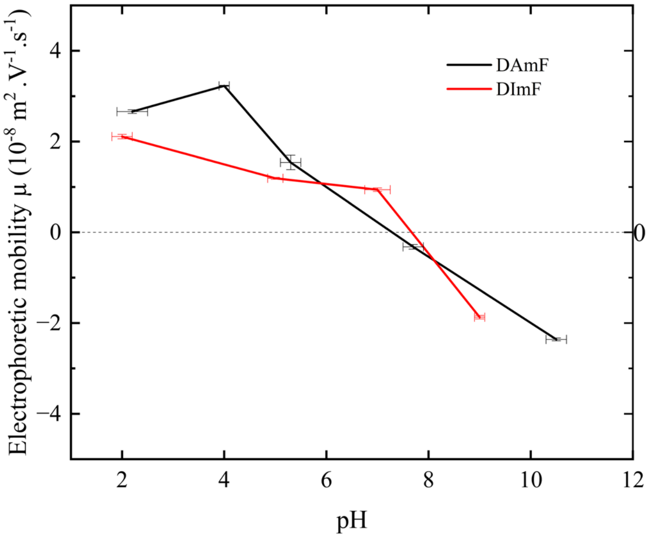

Fig. 4- 3. Electrophoretic mobility of DImF and DAmF. From the graph, the point of zero charge (PZC) of DImF and DAmF are 7.5 ± 0.1 and 8.0 ± 0.1 respectively. Error bars represent 2 standard errors of the mean (N=3)

4.3.1.4. XPS

As shown in Fig. 4- 4, X-ray photoelectron spectroscopy allows for the characterization of the surface of sorbents as well as their interactions with metal ions. Fig. 4- 4a shows the XPS survey of cellulose pulp, DAC fiber, DImF and DAmF. The prominent peaks, namely C1s, N1s, and O1s are observed at ~ 286.1 ± 0.1 eV, 399.9 ± 0.1 eV, and 532.3 ± 0.1 eV respectively, in the XPS spectra. The atomic percentages (AP) were calculated and displayed in Table 4- 1. Cellulose pulp has a greater C 1s and lower O 1s AP than theoretical 'pure cellulose' (see Table S4- 1 for the calculated values). This is likely due to impurities contained on the surface of cellulose fiber since there was no additional prep done on the fiber before measurements were taken (fiber was taken from cellulose sheet without washing or any chemical treatment). Calcium was also detected in cellulose at 352 ± 0.1 eV, most likely because of the presence of $CaCO_3$ retained in the fiber during the cooking stage of kraft pulping process[29]. The absence of calcium in DAC, DImF, and DAmF can be attributed to its likely dissolution during the chemical modifications conducted in water. C 1s and O 1s ap. on DAC is very close to the theoretical value at 55.2 ± 0.2 % and 44.5 ± 0.2 % respectively. DImF and DAmF have a new peak at 399.9 ± 0.1eV which is characteristic of nitrogen in an XPS spectrum. From Table 4- 1, the AP of C, N, O of DImF and DAmF are very similar (C 1s = 61.6 ± 1.1 %, 60.4 ± 0.7 %; N 1s = 14.7 ± 0.1 %, 14.7 ± 0.5 %; O 1s = 22.7 ± 0.7 %, 23.4 ± 0.1 % respectively). Pure DImF/ DAmF AP is calculated to be C 1s = 54.5 %, N 1s = 18.2 %; O 1s = 27.3%. The higher-than-expected C content in DImF and DAmF may be to surfactant-like impurities, adsorbed on to the positive charge of amine groups. Fig. 4- 4b and c also show the XPS curves for DImF and DAmF subjected to Pb^{2+} solutions: the presence of two doublets at 138/143 ± 0.1 eV corresponds to Pb $4f_{7/2}/4f_{5/2}$, respectively and 414/437 ± 0.1 eV corresponds to Pb $4d_{5/2}/4d_{3/2}$, respectively[30]. This confirms lead binding on the fibers. All fibers were found to contain trace amounts of silicon and fluorine. The presence of silicon is most likely attributed to contamination by airborne dust particles, while the presence of fluorine is likely a result of the water utilized in the studies (as non-washed cellulose pulp exhibited and absence of fluorine).

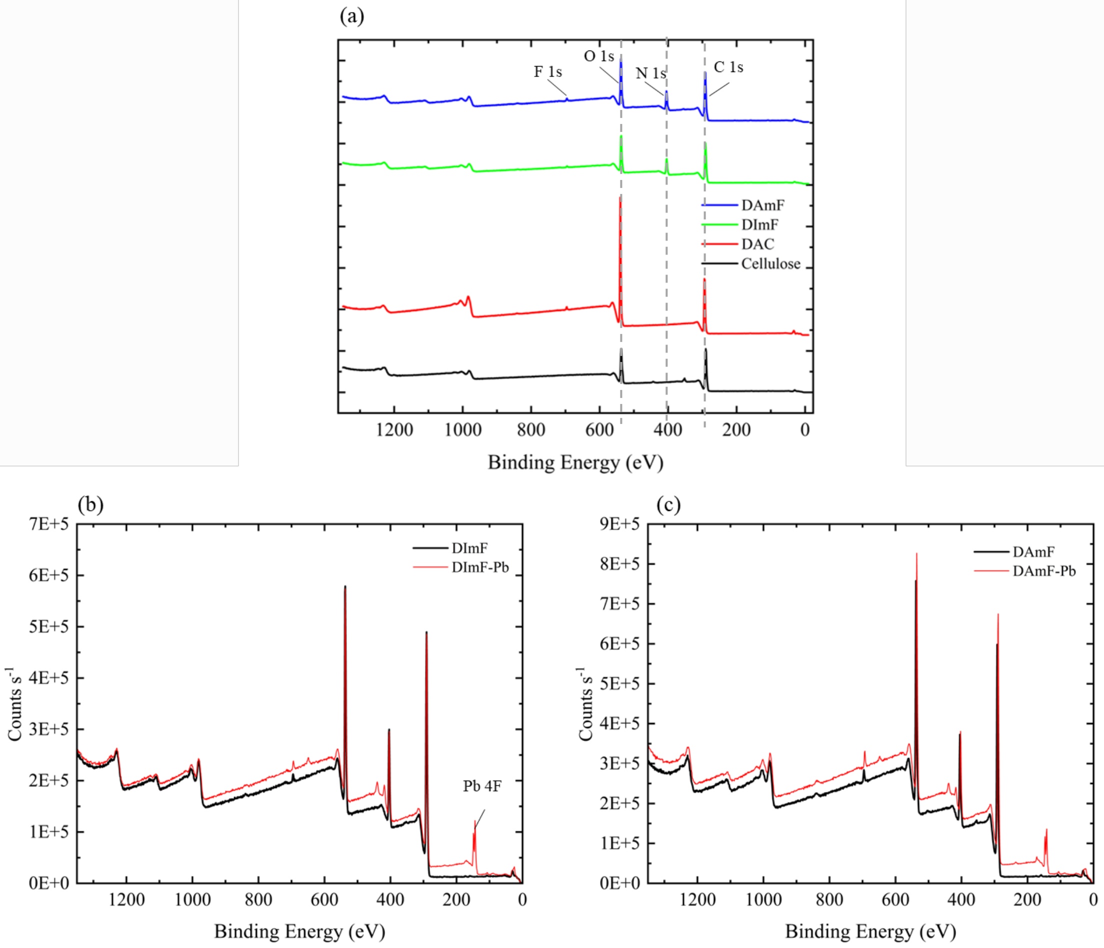

Fig. 4- 4. XPS survey of cellulose fibers (a) cellulose pulp, DAC, DImF and DAmF (b) DImF and DImF- Pb showing bands of C, N, O at 286.1 ± 0.1, 399.9 ± 0.1 and 532.3 ± 0.1 eV respectively and Pb 4F at 139 eV for the later (c) DAmF and DAmF-Pb showing bands of C, N, O at 286.1 ± 0.1, 399.9 ± 0.1 and 532.3 ± 0.1 eV respectively and Pb 4F at 139 eV

Table 4- 1. Atomic percentage by XPS of C, N, O, Ca, Pb, F and S of cellulose fibers. F and S are contaminants in the samples.

Elements	Cellulose	DAC	DImF	DImF-Pb	DAmF	DAmF-Pb
C (%)	68.2 ± 4.8	55.2 ± 0.2	61.6 ± 1.1	62.7 ± 0.2	60.4 ± 0.7	63.0 ± 0.7

N (%)	-	-	14.7 ± 0.1	14.0 ± 0.09	14.7 ± 0.5	12.2 ± 0.3
O (%)	30.7 ± 5.2	44.5 ± 0.2	22.7 ± 0.7	21.7 ± 0.2	23.4 ± 0.1	22.7 ± 0.4
Ca (%)	0.83 ± 0.36	-	-	-	-	-
Pb (%)	-	-	-	0.48 ± 0.01	-	0.40 ± 0.01
F (%)	-	0.42 ± 0.30	0.77 ± 0.07	0.84 ±0.09	1.09 ± 0.18	1.30 ± 0.06
Si (%)	0.26 ± 0.10	0.07 ± 0.05	0.29 ± 0.19	0.28 ± 0.02	0.34 ± 0.15	0.41 ± 0.02

Following the adsorption of Pb ions, DAmF exhibited a decrease in its N content, decreasing from 14.7 ± 0.1 % to 12.2 ± 0.3 %. It was assumed that the reduction in N content was attributed to Pb ion adsorbing on nitrogen and hence impeding the detection of emitted electrons from nitrogen. Depth profile analysis was performed on DAmF with adsorbed Pb ions (DAmF-Pb) to probe this assumption. The surface was subjected to 33 iterations of argon etching, resulting in the measurement of 34 distinct levels. The results are displayed in Fig. 4- 5 below. It was observed that Pb content increased from ~0.4 % to ~0.8 % by the third etch cycle and remained relatively constant throughout the etch cycle. Conversely, N1s % increased at first, then slightly decreased by the end of the experiment. C 1s % increased, while O 1s % decreased with each etching cycle. This is most likely due to damage of bonds containing O and N by Ar^+ bombardment. This is consistent with the observation made by Hofstetter, et. al.[31] The researchers noted that by etching organic polymers with the minimum energy of monatomic ions for a duration as little as 3 seconds, the resulting damage to the polymer material extended further into the bulk than the probing depth of XPS, which is 10 nm. Additionally, they showed that electronegative atoms, such as oxygen, fluorine, and nitrogen, are especially susceptible to damage when exposed to monatomic Ar^+ ions, resulting in an elevation of the C 1s peak. These bonds may be broken or weakened in a way that, when etched with a cluster argon source, they are selectively eliminated, resulting in a misrepresentation of the polymer's original composition. A more pronounced detrimental effect on oxygen compared to nitrogen or fluorine was observed in this study. The raw data is presented in Table S4- 2).

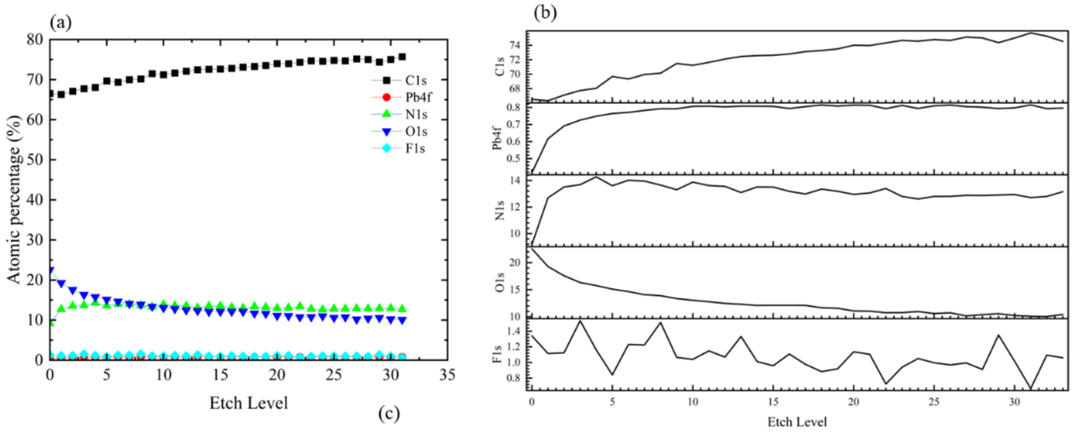

Fig. 4- 5. XPS depth analysis on DAmF with adsorbed Pb^{2+}, DAmF-Pb. (a) Atomic percentages of C, N, O, Pb and F of DAmF-Pb up to 33 etch levels. (b Stacked atomic percentage versus etch level.

From this data, it is assumed that amination reaction and adsorption of Pb ions was uniform across the fiber.

4.3.2. Pb^{2+} sorption studies

4.3.2.1. Effect of pH on Sorption

The sorption of Pb^{+} on DAmF and DImF adsorbents with amine and imine groups are affected by changes in pH due to competing sorption between heavy metals and H^{+} at low pH. Fig. 4- 6 depicts the effect of pH on the sorption of Pb^{2+} from water. At low pH, the imine and amine groups become protonated and electrostatic repulsion limits Pb^{2+} from approaching the active sites of the adsorbents, resulting in lower Pb^{2+} sorption. As pH increases, the amine/imine groups are deprotonated, reducing the electrostatic repulsion and these free groups can then operate as surface-bound ligands to efficiently bind to Pb^{2+} ions, resulting in an increase in sorption. It was observed that when the pH of solution is above 8, white precipitate formed. This is most likely due to the formation of $Pb(NO_3)_2.5Pb(OH)_2$ salt, and therefore experiments were performed at pH ≤ 8[32]. On the lower end, sorption experiments were not performed lower than pH 2.5 because the fibers dissolution is high at pHs < 2. All further sorption experiments were performed at pH 5.5 i.e., sorption experiments were done without pH adjustment.

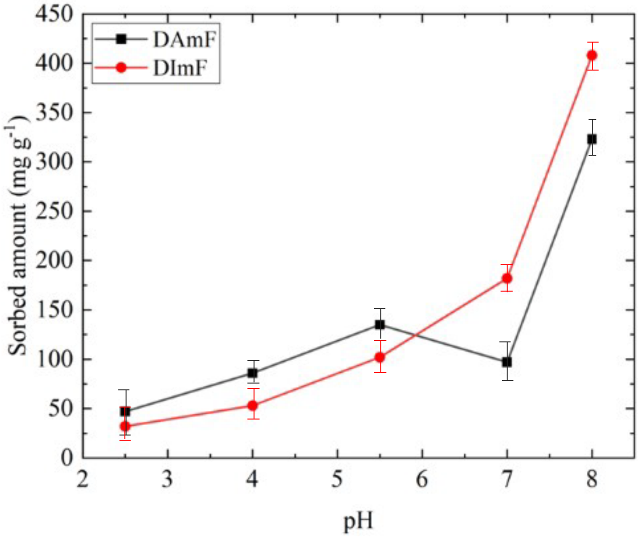

Fig. 4- 6. Effect of pH on sorption of Pb^{2+}. All experiments were performed using 10 mg of adsorbents, room temperature, no pH adjustment (5.5) and 10 ml of 1000 ppm Pb^{2+} . DAmF showed a higher sorbed amount at low pH (2.5 – 5.5) and DImF showed a higher sorbed amount at higher pH (7-8). Error bars represent 2 standard errors of the mean (N=3)

DAmF sorbed a larger amount of Pb^{2+} at acidic pH than DImF because amines are generally more basic than imines, therefore attracting both more H^+ and Pb^{2+} ions. At pH 7, DAmF shows a reduced sorption capacity likely due to an intramolecular H-bond formed when one of the amines is deprotonated and the other protonated. The schematic of this ring closure is shown in Scheme

4- 2 below. This ring closure is similar to the ring closure polystyrene maleic anhydride, here a H-bond is formed between the carboxyl groups of the (hydrolysed) maleic acid moieties at pH 7, when one is protonated and one dissociated[33].

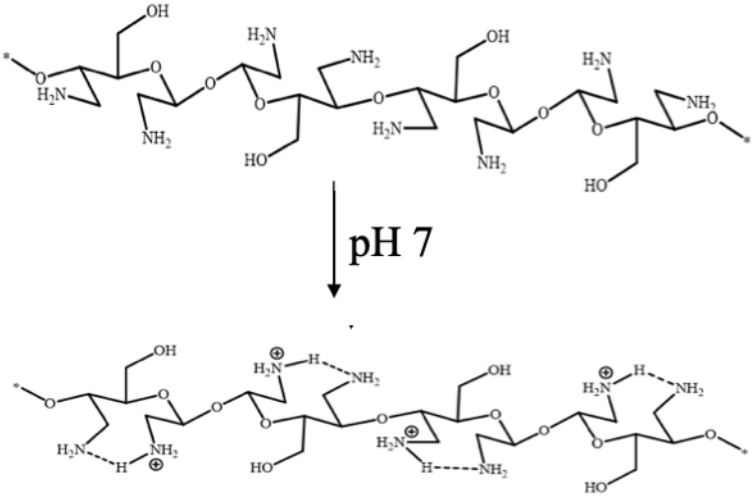

Scheme 4- 2. Proposed ring closure of DAmF. There exists a pH (pH 7.7) in which one of the amines is protonated and the adjacent is not, thereby resulting in creation of hydrogen bonding which leads to a close structure and destabilization of the solution.

Presumably no ring closure occurs in DImF due to the higher sorbed amount and above pH 8, the sorption of Pb^{2+} on DAmC approaches that of DImC.

4.3.2.2. Effect of initial concentration of Pb^{2+}

The initial concentration of Pb^{2+} as varied from 50 -1000 pm while the solution pH, contact time and adsorbent dosage were fixed at 5.5, 300 mins and 50 mg respectively. Fig. 4- 7a shows that as the amount of Pb^{2+} increased in solution, the sorbed amount (mg/g) increased, as typical in sorption experiments. No plateau was reached, due to the entering of Pb^{2+} ions in the pores of the fiber wall. The initial linear part of the curve corresponds to adsorption on the external surface. At higher concentrations, Pb^{2+} ions adsorb on sites in large pores, adsorption in nanopores is negligible on the time scale of the experiments. Because the adsorption in Fig. 4- 7a only consists of two linear parts, the data cannot be analyzed in terms of adsorption isotherms, which require an approach to a plateau value, which is not yet reached. As illustrated in Fig. 4- 7b, the percentage removal dropped after reaching a maximum, as the initial metal concentration increased. Throughout, DAmF showed a higher sorption because the pH was at 5.5 and DAmF has higher sorption at that pH.

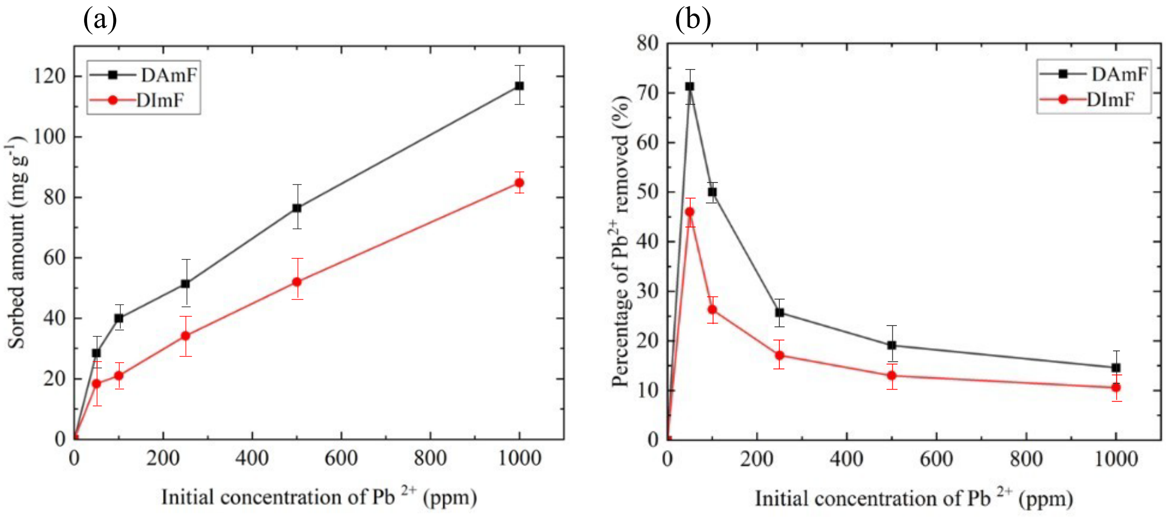

Fig. 4- 7. Effect of initial metal concentration. (a) amount sorbed metal ions versus initial concentration of metal ion (b) Percentage ion removal versus initial concentration. All experiments were performed using 50 mg of adsorbents, room temperature, no pH adjustment (5.5) and 40 mL of Pb2+ concentrations ranging from 50 – 1000 ppm. Error bars represent 2 standard errors of the mean (N=3)

*The measured maximum adsorption capacity of DImF and DAmF was limited due to the fact that the curve depicting the amount of sorbed material vs the concentration of Pb ion in Fig. 4- 7 did not approach a plateau. Consequently, the data could not be fitted to an isotherm, and as a result, q_{max} was not determined. The maximum adsorption capacity (q_{max}) observed for DImF and DAmF is comparable to that of the amine modified cellulose sorbent shown in Table 4- 2. Pb^{2+} sorbent with higher maximum adsorption also contained carboxylic acid groups which would induce negative charge density on the surface of sorbent that facilitates the adsorption of positive Pb ions.

Table 4- 2. Comparison of the maximum monolayer adsorption capacities of Pb ions on cellulose-based adsorbents. Modified form ref[34].

Bio-sorbents	Modification	Optimum pH	q_e (mg g^{-1})	Ref
Carboxylated cellulose (Cell-EDTA)	Modified pineapple leaf fiber with EDTA dianhydride at C-6 atom	6	41.2	[35]
Carboxymethyl cellulose (Cell-CM)	Modified pineapple leaf fiber with carboxymethyl group using sodium monochlorite and acetic acid C-6 atom	6	63.4	[35]
Schiff base cellulose (Cell-Hy)	$NaIO_4$ oxidation of cellulose pulp followed by acid-catalyzed condensation of dialdehyde cellulose with p-aminophenol	6	81.32	[36]
Schiff base cellulose (Gu-Mc)	KIO_4 oxidation of cellulose powder and condensation with alcoholic N-aminoguanidine hydrochloride in presence of triethylamine	6	52.0	[37]
Grafted cellulose (pAHA-cellulose)	Keto-alcohol free-radical initiation by CAN on cotton fibers, grafting with EMCA monomer followed by oximation	5.4	333.3	[38]

	with hydroxylamine and sodium hydroxide			
Grafted cellulose ($\text{PEI/SA-MCC}_{\text{MV}}$)	Grafting succinic anhydride on pretreated MCC with microwave H_2O_2 and then with polyethyleneimine	5	357.14	[39]
Cross-linked cellulose (PEI-RCSA)	Cross-linked cellulose–sodium alginate modified with polyethylene imine via glutaraldehyde cross-linking	5.5	234.2	[40]
Carboxylated cellulose (MMCC)	Modified MCC with BTCA at high temperature	5	1155.0	[41]
Diiminocellulose	$NaIO_4$ oxidation of cellulose pulp followed by s Schiff base reaction with NH_3	5.5	84.8 *	This work
Diaminocellulose	$NaIO_4$ oxidation of cellulose pulp followed by a Schiff base reaction with NH_3 and reduction with $NaBH_4$	5.5	116.8*	This work

4.3.2.3. Effect of adsorbent dosage

The effect of adsorbent dosage on the sorption of Pb^{2+} ion in aqueous solution as investigated by varying the adsorbents added from 5 mg to 100 mg for constant starting concentration, solution pH, and contact duration, 1000 ppm, 5.5, and 300 min, respectively. It was observed that as dosage of adsorbents increased, the percentage of Pb^{2+} sorbed from solution increased because there were more active sites that the metal ions can adhere to. Inversely, the sorbed amount is reduced because of equation Fig. 4- 8a, where there is an increment of the denominator (mass of adsorbent) when compared with the numerator values. we observed a drop from 208 mg g^{-1} (10.4 %) and 116 mg g^{-1} (5.8 %) at 5 mg of adsorbent to 40.4 mg g^{-1} (40.4 %) and 32.5 mg g^{-1} (32.5 %) at 100 mg adsorbent for DAmF and DImF respectively. The decrease in adsorption capacity with increasing adsorbent dose can also attributed to the high number of unsaturated adsorption sites, as well as overlap of adsorption sites and overcrowding of adsorbent particles[42].

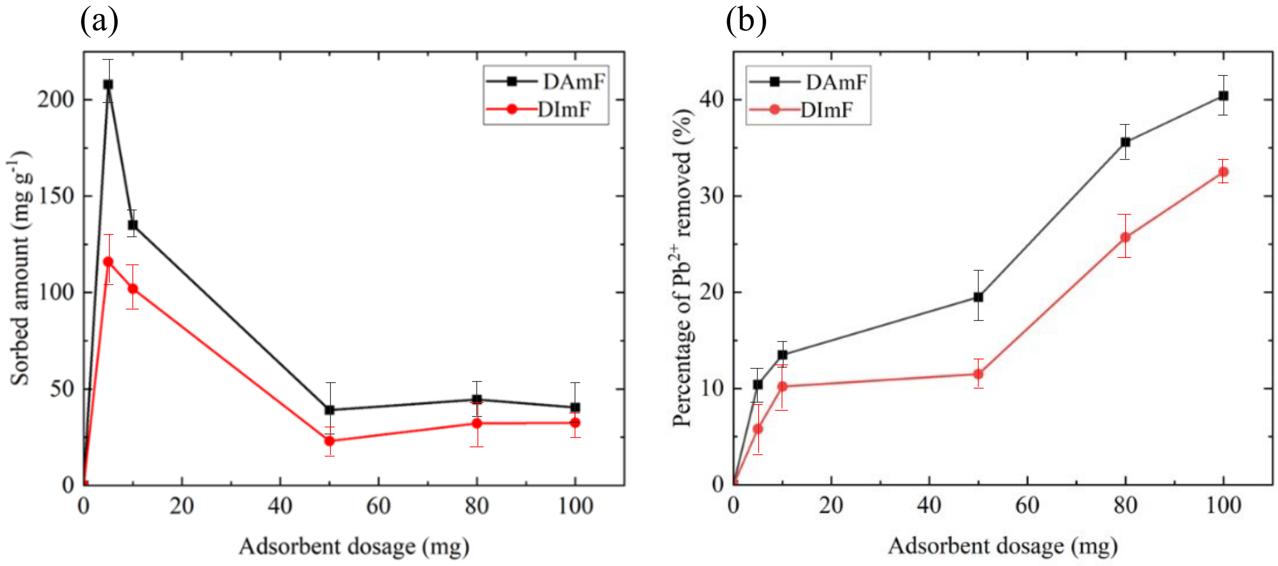

Fig. 4- 8. Effect of adsorbent dosage (a) dosage versus amount of metal removed (b) dosage vs. percentage removal. Error bars represent 2 standard errors of the mean (N=3)

4.3.2.5. Sorption kinetic study

The amount of Pb ions that sorbed on the DImF and DAmF increased as the reaction time increased. Therefore, we investigated the process of adsorption over time while keeping the amount of sorbent, the concentration of Pb^{2+}, and the volume of the solution constant at 50 mg, 50 - 1000 ppm, and 40 mL, respectively (see Fig. 4- 9). During the time interval of 0 to 50 minutes, there was a quick adsorption of Pb^{2+} due to the presence of an ample number of adsorption sites, hence the rapid increase in the sorption capacity. Nevertheless, as the reaction time increased, the rate of sorption declined due to a scarcity of adsorption sites, despite the rise in adsorption capacity. After a duration of 120 minutes, the rate of sorption of Pb reached a steady state.

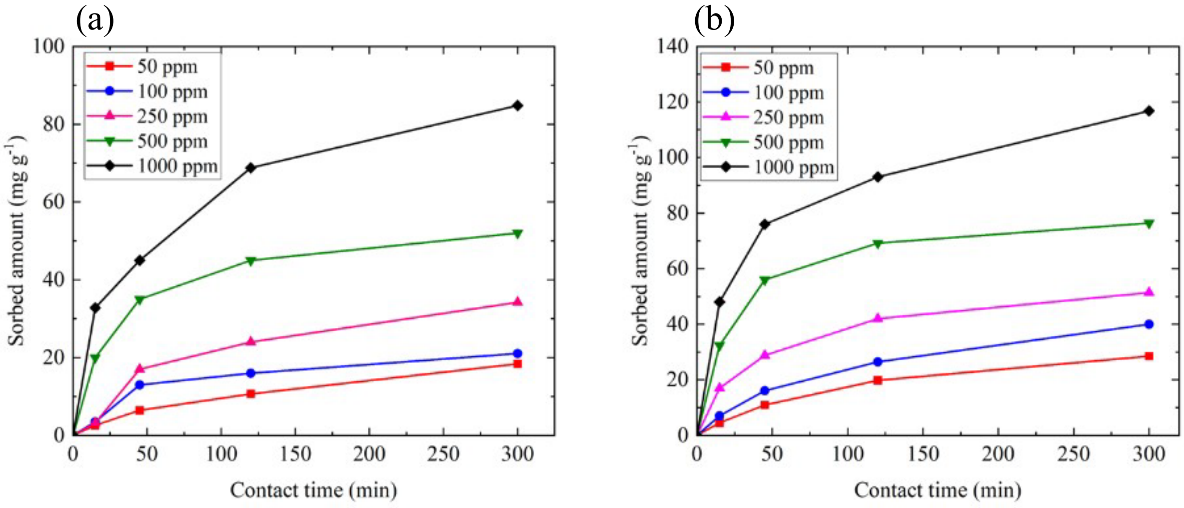

Fig. 4- 9. (a) Sorption kinetics of DImF (b) Sorption kinetics of DAmF (The initial Pb^{2+} concentration as varied from 50 to 1000 ppm (40 mL) at pH 5.5, while the DImF and DAmF dose as 50 mg (dry mass).

The initial slopes of the curve are approximately proportional to concentration. Initial slope is the adsorption on the external surface and absorption into large pores of the fiber. Pb^{2+} ions also diffuse into the lumen through pit holes in the fiber wall, but this process is relatively fast, and these ions are washed out in the desorption experiments. At pH less than 5, metals are mainly in their ionic form and in their hydrated form at higher pH. Pb^{2+} ionic radius is 0.112 nm, while its hydrated radius is 0.401 nm[43, 44]. These experiments are carried out at pH ~5.5 and Pb^{2+} is most likely in its hydrated state. Assuming Pb^{2+} can readily penetrate large pores, the accessible surface area and total surface area are approximately 15 m^2 and 300 m^2 per gram of fiber respectively[45]. The time of lumen loading can be estimated from

$$x^2 = 2Dt$$

where t is the time, x the root mean square distance (~ 15μm), D is the diffusion constant given by

$$D = \frac{kT}{6\pi\eta a} = \frac{4.1x10^{-21}}{6\pi \text{ x } 10^{-3} * 4.01x10^{-10}} = 5.4x10^{-11}\frac{m^2}{s}$$

where T, k, η and a are the absolute temperature, Boltzmann constant, solvent viscosity, and radius of a hydrated lead ion, which is 4.01 x10^{-10} m. Hence the time for lumen loading is approximately.

$$t = \frac{x^2}{2D} = \frac{(15x10^{-6})^2}{2 * 5.4x10^{-11}} \sim 2.1 \text{ s}$$

Thus, the time for an ion to diffuse into the lumen is very short, as is the time to diffuse out of the lumen during washing of the fiber. Hence, lumen loading plays no role in the adsorption experiments. If one Pb^{2+} ion is adsorbed per modified glucose group, the maximum adsorption capacity is 4.65 mmol g^{-1}, corresponding to 0.95 g g^{-1}. The adsorption capacity of external surface and large pores is about $\frac{15}{300}x0.95\ \frac{g}{g} = 475\ \frac{mg}{g}$, which is larger than 85 mg g^{-1} and 120 mg g^{-1}, the maximum adsorbed amount observed for DImF and DAmF respectively. 15 m^2 g^{-1} is the specific surface area of the large pores and the external area, and 300 m^2 g^{-1} is approximately the total specific surface area of cellulose fiber[46]. Of this, adsorption on the external surface is about 30 mg g^{-1}, which is reached for the highest Pb^{2+} concentration. Likely, the initial linear increase in adsorption is due to adsorption on the external surface of the fibers and the second linear increase is due to adsorption in large pores (micropores).

Modeling a fiber (of length 2 mm and diameter 30 μm) as a sphere with the same surface area, and a Pb ion as a sphere with a diameter twice its hydrated radius (0.401 nm), one can calculate the collision rate between fibers and lead ions from Smoluchowski (diffusion-controlled) kinetics, which leads to 3.5×10^{12} collisions of lead ions with a single fiber per second (the calculations are shown in the supplementary section - 4.6.1.). The maximum observed amount of lead ions for DAmF is 120 mg g^{-1} or about 1.2×10^{-4} mg per fiber, or 3.5×10^{14} lead ions per fiber. If each collision would be effective, an adsorbed amount of 120 mg g^{-1} would be reached in about 100 seconds. Instead, it takes 5 hours, showing that the kinetics is extremely slow. There are two reasons for this. One reason is that at pH 5 most amine and imine groups are protonated. This protonation is a dynamic process where protons continuously leave and re-associate. At a given time there is a distribution of protonated sites, with most neighboring amines or imine protonated, some having one protonated site and there are a very limited number non-protonated neighboring amine or imine sites. Pb^{2+} adsorption preferentially occurs on these non-protonated sites and thus is a slow process. This explains why adsorption on the external surface is slow. Another reason is that adsorption in pores is very slow as well. The pores have walls, which bare positively charged groups and it is difficult for cations to penetrate the pores. The distribution of cations inside the pores and in the bulk solution, is governed by a Donnan equilibrium. The concentration of cations in the pores can be orders of magnitude slower than in the bulk, again slowing down the kinetics substantially. After 6 hours, the sorption continues to increase, because we are far from saturation which is around 550 mg g^{-1} (assuming 1 Pb^{2+} per 2 amines/ imines) and little or no penetration has occurred yet in the nanopores.

4.4. Conclusions

DImF was successfully synthesized by periodate oxidation of cellulose pulp to produce DAC followed by a Schiff base reaction with ammonia. DAmF was synthesize by reducing the imine bonds (C=NH) in DImF to amine bonds (C-NH_2). Aldehyde content determination validated the conversion of pulp to DAC and the subsequent conversion of DAC to DImF, while conductometric titration confirmed the conversion of DImF to DAmF. At pH 5.5, the obtained fibers ere successfully employed for the sorption of Pb^{2+} ions from solution, with the maximum measured sorbed amounts of 84.8 and 116.8 mg g^{-1} for DImF and DAmF respectively. XPS was used to confirm that the sorption was facilitated by the coordination effect of N heteroatoms in the polymeric chain of the fibers with Pb^{2+} ions. Kinetics study showed that sorption was slow, and saturation was not reached during the time studied due to Donnan equilibrium, which limits the concentration of Pb ions in the pores.

4.5. REFERENCES

1. Fakhri, Y.; Saha, N.; Ghanbari, S.; Rasouli, M.; Miri, A.; Avazpour, M.; Rahimizadeh, A.; Riahi, S.-M.; Ghaderpoori, M.; Keramati, H., Carcinogenic and non-carcinogenic health risks of metal (oid) s in tap water from Ilam city, Iran. *Food and chemical toxicology* **2018,** *118*, 204-211.
2. Dehghani, M. H.; Afsari Sardari, S.; Afsharnia, M.; Qasemi, M.; Shams, M., Removal of toxic lead from aqueous solution using a low-cost adsorbent. *Scientific Reports* **2023,** *13* (1), 3278.
3. Kiani, G.; Soltanzadeh, M., High capacity removal of silver(I) and lead(II) ions by modified polyacrylonitrile from aqueous solutions. *Desalination and Water Treatment* **2014,** *52* (16-18), 3206-3218.
4. Arbabi, M.; Hemati, S.; Amiri, M., Removal of lead ions from industrial wastewater: A review of Removal methods. *International Journal of Epidemiologic Research* **2015,** *2* (2), 105-109.
5. Wani, A. L.; Ara, A.; Usmani, J. A., Lead toxicity: a review. *Interdisciplinary toxicology* **2015,** *8* (2), 55-64.
6. Swadźba-Kwaśny, M., Lead: Inorganic Chemistry. In *Encyclopedia of Inorganic and Bioinorganic Chemistry*, pp 1-24.
7. Rubin, R.; Strayer, D. S.; Rubin, E., The endocrine system. In *Rubin's pathology: clinicopathologic foundations of medicine*, 6th ed.; Rubin, E.; Strayer, D. S., Eds. Lippincott Williams & Wilkins: 2012.
8. Sokol, R. Z.; Berman, N., The effect of age of exposure on lead-induced testicular toxicity. *Toxicology* **1991,** *69* (3), 269-78.

9. Goel, J.; Kadirvelu, K.; Rajagopal, C.; Kumar Garg, V., Removal of lead(II) by adsorption using treated granular activated carbon: batch and column studies. *J Hazard Mater* **2005,** *125* (1-3), 211-20.

10. Vilar, V. J. P.; Botelho, C. M. S.; Boaventura, R. A. R., Influence of pH, ionic strength and temperature on lead biosorption by Gelidium and agar extraction algal waste. *Process Biochemistry* **2005,** *40* (10), 3267-3275.

11. Özacar, M.; Şengil, İ. A.; Türkmenler, H., Equilibrium and kinetic data, and adsorption mechanism for adsorption of lead onto valonia tannin resin. *Chemical Engineering Journal* **2008,** *143* (1), 32-42.

12. Zeng, Y.; Chen, Z.; Du, Y.; Lyu, Q.; Yang, Z.; Liu, Y.; Yan, Z., Microbiologically induced calcite precipitation technology for mineralizing lead and cadmium in landfill leachate. *Journal of Environmental Management* **2021,** *296*, 113199.

13. Pang, F. M.; Kumar, P.; Teng, T. T.; Mohd Omar, A. K.; Wasewar, K. L., Removal of lead, zinc and iron by coagulation–flocculation. *Journal of the Taiwan Institute of Chemical Engineers* **2011,** *42* (5), 809-815.

14. Berbar, Y.; Hammache, Z. E.; Bensaadi, S.; Soukeur, R.; Amara, M.; der Bruggen, B. V., Effect of functionalized silica nanoparticles on sulfonated polyethersulfone ion exchange membrane for removal of lead and cadmium ions from aqueous solutions. *Journal of Water Process Engineering* **2019,** *32*, 100953.

15. Tian, H.; Alkhadra, M. A.; Conforti, K. M.; Bazant, M. Z., Continuous and Selective Removal of Lead from Drinking Water by Shock Electrodialysis. *ACS ES&T Water* **2021,** *1* (10), 2269-2274.

16. Egbosiuba, T. C.; Egwunyenga, M. C.; Tijani, J. O.; Mustapha, S.; Abdulkareem, A. S.; Kovo, A. S.; Krikstolaityte, V.; Veksha, A.; Wagner, M.; Lisak, G., Activated multi-walled carbon nanotubes decorated with zero valent nickel nanoparticles for arsenic, cadmium and lead adsorption from wastewater in a batch and continuous flow modes. *Journal of Hazardous Materials* **2022,** *423*, 126993.

17. Asadi, F.; Shariatmadari, H.; Mirghaffari, N., Modification of rice hull and sawdust sorptive characteristics for remove heavy metals from synthetic solutions and wastewater. *Journal of hazardous materials* **2008,** *154* (1-3), 451-458.

18. Flora, S. J. S.; Pachauri, V., Chelation in metal intoxication. *International journal of environmental research and public health* **2010,** *7* (7), 2745-2788.

19. Akl, M. A.; Hashem, M. A.; Ismail, M. A.; Abdelgalil, D. A., Novel diaminoguanidine functionalized cellulose: synthesis, characterization, adsorption characteristics and application for ICP-AES determination of copper(II), mercury(II), lead(II) and cadmium(II) from aqueous solutions. *BMC Chemistry* **2022,** *16* (1), 65.

20. Júnior, O. K.; Gurgel, L. V. A.; de Freitas, R. P.; Gil, L. F., Adsorption of Cu(II), Cd(II), and Pb(II) from aqueous single metal solutions by mercerized cellulose and mercerized sugarcane bagasse chemically modified with EDTA dianhydride (EDTAD). *Carbohydrate Polymers* **2009,** *77* (3), 643-650.

21. Deghles, A.; Hamed, O.; Lail, B.; Azzaoui, K.; Obied, A.; Jodeh, S., Cellulose with Bidentate Chelating Functionality: An Adsorbent for Metal Ions from Wastewater. *BioResources* **2019,** *14*.

22. Alam Md, N.; van de Ven, T. G. M., An aqueous process for the separation of cellulose from biomass. *Journal of Science Technology for Forest Products and Processes* **2014,** *4* (3), 22-26.

23. Balaram, V.; Vummiti, D.; Roy, P.; Taylor, C.; Kamala, C. T.; Satyanarayanan, M.; Kar, P.; Subramanyam, K.; Raju, A.; Abburi, K.; Spectroscopy, A., Analysis of Geochemical Samples by Microwave Plasma-AES. *Atomic Spectroscopy* **2014,** *35*, 65-78.

24. Smith, J. G., Amines. In *Organic Chemistry*, 6 ed.; McGrall Hill Education 2017.

25. Jia, N.; Li, S.-M.; Ma, M.-G.; Zhu, J.-F.; Sun, R.-C., Synthesis and characterization of cellulose-silica composite fiber in ethanol/water mixed solvents. *BioResources* **2011,** *6* (2), 1186-1195.

26. Jin, L.; Li, W.; Xu, Q.; Sun, Q., Amino-functionalized nanocrystalline cellulose as an adsorbent for anionic dyes. *Cellulose* **2015,** *22* (4), 2443-2456.

27. Xing, X.; Han, Y.; Jiang, Q.; Sun, Y.; Wang, X.; Qu, G.; Sun, G.; Li, Y., Immobilization of laccases onto cellulose nanocrystals derived from waste newspaper: relationship between immobilized laccase activity and dialdehyde content. *Cellulose* **2021,** *28* (8), 4793-4805.

28. Pereira, A. R.; Soares, L. C.; Teodoro, F. S.; Elias, M. M. C.; Ferreira, G. M. D.; Savedra, R. M. L.; Siqueira, M. F.; Martineau-Corcos, C.; da Silva, L. H. M.; Prim, D.; Gurgel, L. V. A., Aminated cellulose as a versatile adsorbent for batch removal of As(V) and Cu(II) from mono- and multicomponent aqueous solutions. *Journal of Colloid and Interface Science* **2020,** *576*, 158-175.

29. Vegunta, V.; Senthilkumar, E. R.; Lindén, P.; Sevastyanova, O.; Vilaplana, F.; Garcia, A.; Björk, M.; Jansson, U.; Henriksson, G.; Lindström, M. E., High calcium content of

Eucalyptus dunnii wood affects delignification and polysaccharide degradation in kraft pulping. *Nordic Pulp & Paper Research Journal* **2022,** *37* (2), 338-348.

30. Neiber, R. R.; Galhoum, A. A.; El-Tantawy El Sayed, I.; Guibal, E.; Xin, J.; Lu, X., Selective lead (II) sorption using aminophosphonate-based sorbents: Effect of amine linker, characterization and sorption performance. *Chemical Engineering Journal* **2022,** *442*, 136300.

31. Hofstetter, Y. J.; Vaynzof, Y., Quantifying the Damage Induced by X-ray Photoelectron Spectroscopy Depth Profiling of Organic Conjugated Polymers. *ACS Applied Polymer Materials* **2019,** *1* (6), 1372-1381.

32. Pauley, J. L.; Testerman, M. K., Basic Salts of Lead Nitrate Formed in Aqueous Media1. *Journal of the American Chemical Society* **1954,** *76* (16), 4220-4222.

33. Malardier-Jugroot, C.; van de Ven, T. G. M.; Whitehead, M. A., Linear Conformation of Poly(styrene-alt-maleic anhydride) Capable of Self-Assembly: A Result of Chain Stiffening by Internal Hydrogen Bonds. *The Journal of Physical Chemistry B* **2005,** *109* (15), 7022-7032.

34. Kaur, J.; Sengupta, P.; Mukhopadhyay, S., Critical Review of Bioadsorption on Modified Cellulose and Removal of Divalent Heavy Metals (Cd, Pb, and Cu). *Industrial & Engineering Chemistry Research* **2022,** *61* (5), 1921-1954.

35. Daochalermwong, A.; Chanka, N.; Songsrirote, K.; Dittanet, P.; Niamnuy, C.; Seubsai, A., Removal of Heavy Metal Ions Using Modified Celluloses Prepared from Pineapple Leaf Fiber. *ACS Omega* **2020,** *5* (10), 5285-5296.

36. Saravanan, R.; Ravikumar, L., Renewable Modified Cellulose Bearing Chelating Schiff Base for Adsorptive Removal of Heavy Metal Ions and Antibacterial Action. *Water Environment Research* **2017,** *89* (7), 629-640.

37. Kenawy, I. M.; Hafez, M. A. H.; Ismail, M. A.; Hashem, M. A., Adsorption of Cu(II), Cd(II), Hg(II), Pb(II) and Zn(II) from aqueous single metal solutions by guanyl-modified cellulose. *International Journal of Biological Macromolecules* **2018,** *107*, 1538-1549.

38. Jiao, C.; Zhang, Z.; Tao, J.; Zhang, D.; Chen, Y.; Lin, H., Synthesis of a poly (amidoxime-hydroxamic acid) cellulose derivative and its application in heavy metal ion removal. *RSC advances* **2017,** *7* (44), 27787-27795.

39. Zhang, C.; Su, J.; Zhu, H.; Xiong, J.; Liu, X.; Li, D.; Chen, Y.; Li, Y., The removal of heavy metal ions from aqueous solutions by amine functionalized cellulose pretreated with microwave-H 2 O 2. *RSC advances* **2017,** *7* (54), 34182-34191.

40. Zhan, W.; Xu, C.; Qian, G.; Huang, G.; Tang, X.; Lin, B., Adsorption of Cu (ii), Zn (ii), and Pb (ii) from aqueous single and binary metal solutions by regenerated cellulose and sodium alginate chemically modified with polyethyleneimine. *RSC advances* **2018,** *8* (33), 18723-18733.

41. Hashem, A.; Fletcher, A.; Younis, H.; Mauof, H.; Abou-Okeil, A., Adsorption of Pb (II) ions from contaminated water by 1, 2, 3, 4-butanetetracarboxylic acid-modified microcrystalline cellulose: Isotherms, kinetics, and thermodynamic studies. *International journal of biological macromolecules* **2020,** *164*, 3193-3203.

42. Hashem, A.; Badawy, S.; Farag, S.; Mohamed, L.; Fletcher, A.; Taha, G., Non-linear adsorption characteristics of modified pine wood sawdust optimised for adsorption of Cd (II) from aqueous systems. *Journal of Environmental Chemical Engineering* **2020,** *8* (4), 103966.

43. Kadirvelu, K.; Goel, J.; Rajagopal, C., Sorption of lead, mercury and cadmium ions in multi-component system using carbon aerogel as adsorbent. *Journal of Hazardous Materials* **2008,** *153* (1-2), 502-507.

44. Faur-Brasquet, C.; Kadirvelu, K.; Le Cloirec, P., Removal of metal ions from aqueous solution by adsorption onto activated carbon cloths: adsorption competition with organic matter. *Carbon* **2002,** *40* (13), 2387-2392.

45. Alince, B.; van de Ven, T. G. M., Porosity of swollen pulp fibers evaluated by polymer adsorption. *Fundamentals of Papermaking Materials* **1997,** *2*, 771-788.

46. Alince, B.; van de Ven, T., Porosity of swollen pulp fibers evaluated by polymer adsorption. *Fundamentals of Papermaking Materials* **1997,** *2*, 771-788.

47. Antonsson, S.; Mäkelä, P.; Fellers, C.; Lindström, M. E., Comparison of the physical properties of hardwood and softwood pulps. *Nordic Pulp & Paper Research Journal* **2009,** *24* (4), 409-414.

48. Osińska, M., Removal of lead(II), copper(II), cobalt(II) and nickel(II) ions from aqueous solutions using carbon gels. *Journal of Sol-Gel Science and Technology* **2017,** *81* (3), 678-692.

4.6. Supplementary information

Table S4- 1. Theoretical atomic percentage calculated from molecular structure of cellulose and modified cellulose.

Elements	Cellulose	DAC	DImF	DAmF
C	54.5	54.5	54.5	54.5
N	-	-	18.2	18.2
O	45.5	45.5	27.3	27.3

Table S4- 2. Atomic percentage (ap) by depth profile analysis by XPS of DAmF-Pb for a total of 33 etch cycles.

Etch Level	C1s (%)	Pb4f (%)	N1s (%)	O1s (%)	F1s (%)
0	66.5	0.416	9.16	22.5	1.33
1	66.3	0.616	12.6	19.2	1.11
2	67.1	0.691	13.5	17.5	1.12
3	67.7	0.725	13.6	16.3	1.53
4	68.0	0.748	14.2	15.7	1.16
5	69.6	0.764	13.6	15.1	0.84
6	69.3	0.771	14	14.6	1.22
7	69.9	0.782	13.9	14.1	1.22
8	70.1	0.792	13.6	13.9	1.51
9	71.4	0.792	13.3	13.3	1.06
10	71.2	0.806	13.8	13.0	1.03
11	71.6	0.807	13.6	12.7	1.14

12	72.1	0.803	13.5	12.4	1.06
13	72.4	0.807	13.1	12.3	1.33
14	72.5	0.807	13.5	12.0	1.01
15	72.6	0.806	13.5	12.1	0.950
16	72.7	0.793	13.1	12.1	1.10
17	73.1	0.804	12.9	12.1	0.970
18	73.2	0.814	13.3	11.6	0.880
19	73.5	0.808	13.1	11.5	0.910
20	74.0	0.813	12.9	11.1	1.13
21	73.9	0.812	13.1	11.1	1.10
22	74.3	0.793	13.3	10.7	0.72
23	74.6	0.811	12.8	10.7	0.93
24	74.5	0.794	12.6	10.9	1.05
25	74.7	0.809	12.7	10.6	0.990
26	74.6	0.814	12.8	10.7	0.960
27	75.1	0.804	12.8	10.1	0.990
28	75.0	0.801	12.8	10.4	0.910
29	74.3	0.793	12.9	10.5	1.35
30	75.0	0.797	12.9	10.2	1.01
31	75.7	0.815	12.7	10.1	0.660
32	75.2	0.792	12.8	10.0	1.09
33	74.5	0.796	13.1	10.4	1.05

4.6.1. Calculation of rate of collision between Pb ions and DAmF.

The perikinetic aggregation for unequal sized spheres of species 1 (DAmF) of size much larger than species 2 (Pb ions) is given in equation 5 below.

$$J_{12} = \frac{2kTn_2}{3\eta}\frac{a_1}{a_2} \tag{10}$$

J_{12} is the number if Pb ions colliding with a single fiber per second, n_2 is the number of Pb ions per m^3, a_1 is effective radius of DAmF, a_2 is the radius of a solvated Pb ion, η is the viscosity of the solution, k is Boltzmann constant and T is temperature. The effective radius of the DAmF can be estimated from equation 6 below.

$$a_1^2 = \frac{2\pi RL}{4\pi} \tag{11}$$

Here, R is radius of the fiber (15 µm), and L is its length (about 2 mm)[47], hence a_1 is calculated to be 0.173mm. The radius of hydrated radius of Pb^{2+} is 0.401 nm[48], n_2 is the number of Pb ions per m^3 of solution and η = 1mPa.s (water). For a 40 mL 1000 ppm Pb^{2+} solution, concentration = 4.83×10^{-3} mol L^{-1}, therefore,

$$n_2 = 4.83\times10^{-3}\,\frac{\mathrm{mol}}{\mathrm{L}} * 1000\,\frac{L}{m^3} * 6.022\times10^{23}\,\frac{ions}{mol}$$

$$n_2 = 2.91\times10^{24}\,\frac{Pb\ ions}{m^3}$$

$$J_{12} = \frac{2 * 1.38\times10^{-23}\,\frac{Pa.m^3}{K.ions} * 298\,K * 2.91\times10^{24}\,\frac{ions}{m^3}}{3 * 0.001\ \mathrm{Pa.s}} * \frac{1.73\times10^5\ \mathrm{nm}}{0.401\,nm}$$

$$J_{12} = 3.48\times10^{12}s^{-1}$$

$$Time\ of\ aggregation\ (t) = \frac{1}{J_{12}}$$

$$t \cong 3.48 \times 10^{-19}\ s$$

Chapter 5

SYNTHESIS AND CHARACTERIZATION OF HAIRY AMINATED NANOCRYSTALLINE CELLULOSE

Preface

The literature review in chapter 2 highlights a clear need for the production of bio-based, biodegradable, and sustainable materials to be used in anti-bacterial applications. Furthermore, the emergence of antibiotic-resistant bacteria has limited the effectiveness of many conventional antibiotics. This chapter presents the possibility of animated hairy nanocrystalline cellulose (ANCC) as a viable antibacterial alternative, offering possibilities for the development of sustainable and efficient antimicrobial materials.

Chapter 5 has been published and was reproduced in this thesis with permission from Elsevier Inc.

Citation: Koshani, R.; Eiyegbenin, J. E.; Wang, Y.; van de Ven, T. G. M., Synthesis, and characterization of hairy aminated nanocrystalline cellulose. *J Colloid Interface Sci* 2022*, 607*, 134-144. DOI.org/10.1016/j.jcis.2021.08.172

5.1. Abstract

Hypothesis: The synthesis and characterization of aminated nanocrystalline cellulose (ANCC), a new member of the hairy nanocellulose family, is reported. Hairy nanocelluloses consist of a crystalline rod-like body with amorphous cellulose chains ("hairs") at both ends, on which various functional groups can be accommodated. In ANCC these groups are reactive primary amine groups, which are useful for bioconjugation- and Schiff base-centered modifications. We hypothesize that a two-step oxidation-reductive amination of cellulose fibers followed by hydrothermal treatment will result in the formation of rod-like hairy ANCC.

Experiments: ANCC was prepared by converting the aldehyde groups in cellulose, introduced by a periodate oxidation, to primary amines using ammonia and sodium borohydride, followed by a hot water treatment, during which diamine modified cellulose fibers were converted to ANCC.

ANCC was characterized by AFM, TEM, DLS, ELS, FTIR, NMR, XPS and conductometric titration. Antibacterial activity of ANCC was assessed by the viable cell counting method.

Findings*:* ANCC, with an amine content of 5.5 mmol g^{-1} is a bare nanocolloid (*i.e.* non-coated, without adsorbed polyelectrolytes or surfactants) which, as far as we know, has a positive charge density larger than any other bare cationic nanocolloid. It was observed that ANCC particles have a needle-like morphology with a width of ~5 nm and a length ~120 nm. DLS results proof that ANCC is hairy. Spectroscopic analysis confirmed the introduction of surface primary amine groups. ANCC showed promising bactericidal activities, against Gram-negative species due to their thinner and penetrable cell wall.

Keywords: hairy nanocrystalline cellulose; primary diamine modification; oxidation-reduction amination; hydrothermal treatment; antibacterial property

5.2. Introduction

Nanocelluloses owing to their unique rigidity, biocompatibility, biodegradability, renewable nature, and ease of chemical modification, have secured a respectable place among globally favorable nanomaterials. For decades, nanocrystalline celluloses (NCCs) have been produced by acid hydrolyzing the amorphous chains of hierarchical cellulose structures. These colloidal nanoparticles encompass mostly highly ordered segments of cellulose chains, impeding the physicochemical modifications of inner crystalline layers, which in turn restricts key colloidal properties, such as dispersion stability. To address these shortcomings, our group proposed the controlled oxidation of cellulose fibrils, which enables the partial disintegration of amorphous chains while keeping the crystalline body intact. This results in nanoparticles with a needle-like crystalline body sandwiched between two disordered cellulose regions (hairs), which we call hairy nanocelluloses (HNCs). The protruding soft biopolymeric hairs impart significant modifications to the colloidal properties of NCCs, such as ease of functionalization, introduction of high charge densities, leading to high stability in aqueous media. So far, via manipulating the functional groups of the hairs in the synthesis pathway, four different species have been developed, namely electrosterically stabilized nanocrystalline cellulose (ENCC) [1, 2], sterically stabilized nanocrystalline cellulose (SNCC) [3], bifunctional nanocrystalline cellulose (BNCC) [4] and cationic nanocrystalline cellulose (CNCC) [5] with a high quantity of carboxyl, aldehyde, carboxyl-aldehyde and quaternary ammonium groups, respectively (see Scheme 5- 1). Expanding the "hairy" cellulose nano-toolbox has given rise to significant advancements in the current applications of nanocelluloses *e.g.* anti-scaling agents [6], rheology modifiers [7], in vivo nanoscale carriers for bioactive molecules [8] and directed assembly [9].

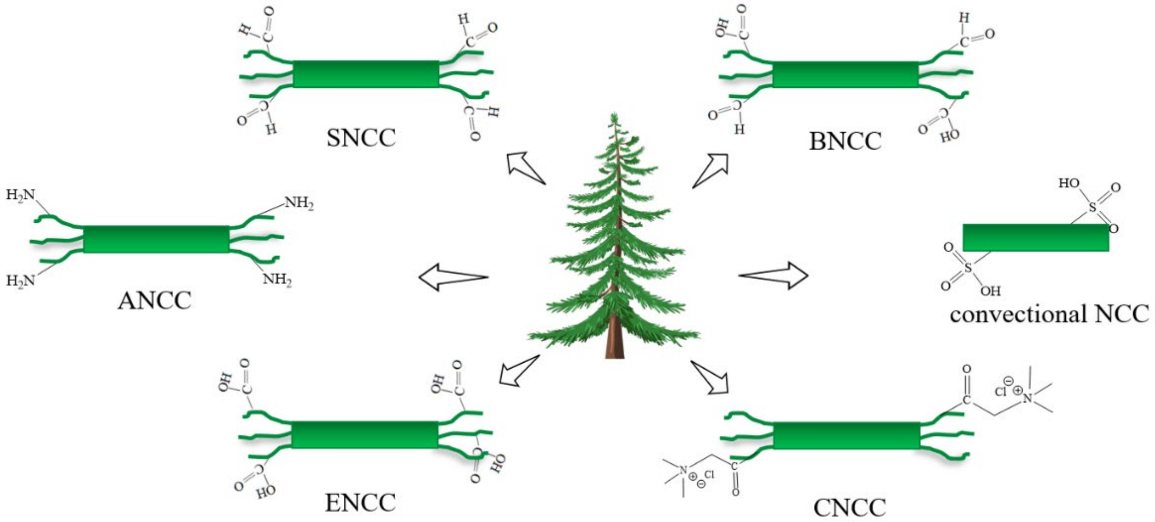

Scheme 5- 1- Common types of convectional and hairy nanocelluloses. Hairy nanocrystalline celluloses contain amorphous cellulose chains ("hairs") functionalized with carboxyl groups (ENCC), aldehyde groups (SNCC), aldehyde-carboxyl groups (BNCC), quaternary ammonium groups (CNCC) and primary amine groups (ANCC)

By taking advantage of reactive aldehyde groups of dialdehyde modified cellulose fibers (DAMF), we aimed at synthesizing hairy aminated nanocrystalline cellulose (ANCC) through a reductive amination reaction. Periodate oxidation of cellulose cleaves the C2–C3 bond in the glucose repeat units, forming 2,3-dialdehyde groups, yielding DAMF [10] (see Scheme 5- 2a). A Schiff base reaction between DAMF and ammonia forms imine bond and introduces secondary amine groups onto DAMF, referred to as diamine modified fiber (DAmMF), which reduce to primary ones using a reducing agent. This reaction is being used to prepare water-soluble aminated cellulose derivatives in our laboratory. It is worth noticing that different from CNCC, ANCC is only positively charged at low pH through the protonation of amino groups. A higher amine content is expected for ANCC as compared to CNCC, in which attaching the second quaternary ammonium groups to the same glucose unit is difficult due to steric hindrance and electrostatic repulsion. The primary amine groups of ANCC are highly active sites suitable for bioconjugation or Schiff base reactions. In addition, ANCC can be a green alternative to nano-chitosan for various medical and food applications for patients with shellfish allergies [11].

In this paper, we report the preparation of novel hairy nanocellulose with high density of primary amine groups by periodate oxidation and amination reduction of cellulose fibers, followed by a slightly acidic hot-water treatment. ANCC is hypothesized to have protruding hair-like aminated cellulose chains with a high charge/amine content, which exceeds the theoretical maximum surface charge content of conventional NCCs [1, 12]. This could likely prove that most of the charges are located in the hairs. Several techniques were employed to characterize hairy ANCC such as AFM, TEM, DLS, ELS, conductometric titration, FTIR, NMR and XPS. The antibacterial activity of ANCC was also tested using the CFU counting method.

5.3. Experimental section

5.3.1. Materials and chemicals

Q90 bleached softwood kraft sheets were provided by FPInnovations (Pointe-Claire QC Canada) and milled as starting cellulose material. Besides cellulose, the kraft sheets also contain hemicellulose and a low fraction of residual lignin. Sodium (meta)-periodate ($NaIO_4$), sodium chloride (NaCl), sodium hydroxide (NaOH), hydrochloric acid (HCl), ammonium acetate ($NH_4CH_3CO_2$), ammonia (NH_3), sodium borohydride ($NaBH_4$) and hydroxylamine-hydrochloride ($NH_2OH \cdot HCl$) were purchased from Sigma-Aldrich (Oakville, Canada). Isopropyl alcohol ($CH_3CHOHCH_3$) and uranyl acetate were purchased from Greenfield Global (Boucherville, Canada) and SPI Chemicals (West Chester, USA), respectively. Deionized (DI) water (resistivity ~10 MΩ cm) was used in all experiments, unless otherwise specified.

5.3.2. Periodate oxidation of cellulose fibers

According to our laboratory-developed protocol [1], 10 g of softwood pulp powder was added to a solution containing 13.2 g $NaIO_4$, 38.7 g NaCl and 625 mL DI water. The reaction beaker was wrapped with aluminum foil to avoid entry of any light. The pulp was stirred at room temperature for 42 hrs. Afterwards, to quench the reaction, 10 mL ethylene glycol was added into this mixture followed by stirring for an additional 15 min, which results in the consumption of the residual periodate. The DAMF were rinsed thoroughly with DI water 5 times by filtrating through a 4 µm pore size nylon cloth. Afterwards, to prepare DAMF for the reductive amination reaction, it should be fully dehydrated, because the remaining water in DAMF fibers can interfere in the amination reaction by hydrolyzing ammonia to ammonium and hydroxide. Dewatering the fibers was done through either drying the fibers at room temperature overnight or by solvent exchange. The solvent exchange was carried out by dispersing wet fibers in ethanol for 3 cycles. Each cycle includes stirring in ethanol for 10 hrs followed by filtration. A small amount of DAMF was taken for the aldehyde (-CHO) content determination before starting the amination reaction.

5.3.3. Reductive amination of DAMF

To synthesize DAmMF, 4 g of air-dried or solvent-exchanged DAMF (~8 mmol g^{-1} aldehyde groups), 2.5 g of $NH_4CH_3CO_2$ (3 mol per mol -CHO), and 80 mmol g^{-1} of NH_3 (10 mol per mol -CHO) were dispersed in 200 mL of anhydrous ethanol, and the slurry was stirred at 80 °C under reflux condition for 18 hrs. Then, the reaction was cooled with an ice bath and 0.46 g of $NaBH_4$ was gradually added followed by stirring for an additional 1 hr. The amount of $NaBH_4$ was calculated based on 1:0.5 molar ratio of the glucose units (~6.17 mmol g^{-1}): $NaBH_4$. In fact, one mole of $NaBH_4$ contains 4 hydride ions (H^-) that can participate in the reduction reaction. Finally, the aminated fibers were washed thoroughly 5 times with DI water. The dosage of chemicals used was based on the assumption that all the aldehydes would be converted to amine groups.

5.3.4. Isolation of hairy ANCC

Two grams of DAmMF were dispersed in 100 mL of DI water, the pH was adjusted to ~2.5 by 0.1 M HCl addition, in order to reach maximum protonation of amine groups, and the mixture was stirred thoroughly (15 min for solvent-exchanged fibers and 1 hr for air-dried fibers), to ensure fibers are well-dispersed. The DAmMF suspension was stirred at 60 °C in an oil bath for 1.5 hrs and subsequently centrifuged at 5000 rpm for 15 min to remove the non-fibrillated fibers. The supernatant containing ANCC was precipitated by adding propanol (1.5-2 times the weight of the supernatant), collected by centrifugation at 5000 rpm for 15 min, and stored at 4 °C for further examinations.

5.3.5. Characterization

5.3.5.1. Aldehyde content

The aldehyde content of DAMF before and after the amination reaction was measured by the procedure suggested by Kim et al. [10]. For this purpose, a known amount of sample (~30 mg) was resuspended in 10 mL DI water with pH adjusted to 3.5 by adding sufficient amounts of 0.1 M HCl solution. Then, $NH_2OH \cdot HCl$ (5 wt %) was added in excess to the suspension (10 mL). A 0.1 M NaOH solution was used as the titrator to compensate for the decrease in the pH as a result of HCl release after oxime formation. This protocol was repeated until the pH remained constant at 3.5, indicating the complete conversion of the dialdehyde groups to oxime compounds. The aldehyde content was calculated using the following equation (1):

$$Aldehyde\ content\ (mmol\ g^{-1}) = \frac{V_{NaOH} \times N_{NaOH}}{W} \qquad (1)$$

where V_{NaOH} is the volume of the consumed NaOH, N_{NaOH} is the normality of the NaOH, and W is the weight of fibers that were used for titration.

5.3.5.2. Amine content

The content of primary amine groups of ANCC was determined by conductometric titration with a standardized HCl solution on an 836 Titrando titrator (Metrohm, Switzerland). A certain volume of suspension of DAmMF fibers or ANCC particles was mixed with 100 mL of Milli-Q water. Afterward, the pH of the resulting suspension was adjusted to ~ 11.5 by drop-wise addition of 0.1 M NaOH while stirring. The protocol of titration was set on the addition of a 45 mL of 5 mM HCl solution with a rate of 0.1 mL min^{-1} to the dispersion up to a pH of ~ 3. The amine content in mmol per one gram of DAmMF or ANCC were calculated from the middle part of the titration curve representing the volume of the HCl solution to neutralize of the weak base.

5.3.5.3. Atomic force microscopy (AFM)

To morphologically characterize the ANCC particles, AFM images were acquired with an extended Multimode atomic force microscope with Nanoscope IIIa controller (Digital Instruments/Veeco, Santa Barbara, CA). A drop of ANCC suspension purified by dialysis was directly placed on freshly cleaved mica surface and allowed to dry at ambient air before imaging. Since the ANCC has positive charges, there was no need to pretreat the mica with poly-L-Lysine. Images were obtained in tapping mode using silicon cantilevers with a force constant of 37 N m^{-1}, a frequency range of 100−500 kHz and a nominal tip radius of 6 nm.

5.3.5.4. Transmittance electron microscopy (TEM)

To determine the size and shape of ANCC, TEM images were recorded using a Philips Tecnai 12, 120 kV, electron microscope equipped with a Gatan 792 Bioscan 1000×1000 wide angle multiscan charge-coupled device (CCD) camera. A 5 µL drop of suspension diluted to 0.05 wt. % was placed on a copper grid coated by a thin carbon film for 5 min and negatively stained using a drop of 2% uranyl acetate solution for 30 s, which enhances the contrast.

5.3.5.5. Particle size analysis by dynamic light scattering (DLS)

The effective diameter of ANCC particles was determined by a Brookhaven light scattering instrument BI9000 AT digital correlator. The concentration of ANCC suspension was kept at 0.1 wt %. The effect of various cosolvent concentrations ranging from 0 to 25 wt % and pHs of 1, 3, 5, 7, 9 and 11 on the size of ANCC particles was also studied. All experiments were carried out by monitoring the scattered light intensity at 90° scattering angle at 25 °C.

5.3.5.6. ζ -potential analysis by electrophoretic light scattering (ELS)

To study the effect of pH changes on ζ-potential of ANCC, the electrophoretic mobility of 0.1 wt. % nanoparticle suspension was measured using Zeta-sizer Nano ZS (Malvern Instruments Ltd., U.K.).

5.3.5.7. FTIR spectroscopy

To characterize the surface chemical properties of DAMF, DAmMF and ANCC, FTIR spectrometer (Spectrum Two, PerkinElmer, USA) with a single bounce diamond attenuated total reflectance (ATR) accessory was employed. Dried samples were placed on the ATR crystal. By lowering the tip of the pressure clamp, maximum pressure was exerted on the samples. The spectra were averaged from 32 scans at transmission mode from 400 to 4000 cm^{-1} with a resolution of 4 cm^{-1}.

5.3.5.8. Solid-state carbon-13 NMR spectroscopy

The data were acquired using a VNMRS-400 wide bore spectrometer operating at 399.9 MHz for ^{1}H and 100.5 MHz for ^{13}C in a 4 mm Varian Chemagnetics double-resonance probe. The recycle delay was 4 s. Samples were spun at 8 kHz with a CP contact time of 2 ms. For ANCC, 5188 scans (6 hrs) were collected, while for DAmMF, 16896 scans (18 hrs) were collected.

5.3.5.9. XPS spectroscopy

XPS was used to quantitatively determine the formation of primary amine groups onto the ANCC. Nanoparticles were characterized by K-Alpha™ XPS instrument (Thermo Scientific, USA) using monochromatic Al Kα radiation under a 10^{-8} mbar vacuum. To prepare a sample for XPS, an ANCC suspension was freeze-dried followed by drying under vacuum to ensure a moisture-free powder was obtained. Single survey scans with a pass energy of 200 eV were conducted to measure the elemental composition. High-resolution scans with a pass energy of 50 eV for N 1s peaks were recorded. In order to deconvolute the high-resolution scans to their constituent peaks, XPSPEAK41 software was used.

5.3.4. Evaluating antibacterial activity of ANCC using the colony-forming unit (CFU) method

5.3.4.1. Bacteria and culture condition.

Listeria monocytogenes ATCC 7644 and *Salmonella enterica* serotype Typhimurium SL1344 were chosen as Gram-positive and Gram-negative model bacteria, respectively. To prepare bacterial cultures, a small amount of the bacterial stock (maintained in frozen glycerol at -80 °C) was streaked onto plates of brain heart infusion agar (BHIA) for *L. monocytogenes* and of tryptic soy agar (TSA) for *S.* Typhimurium and incubated overnight at 37 °C. For each experiment, a few colonies from the plates were used and inoculated into 5 mL of broth and then incubated overnight at 37 °C at 120 rpm.

5.3.4.2. Bacterial cell reduction.

To assess the reduction of the number of viable bacterial cells after exposure to ANCC, the convectional CFU counting assay was performed. Initially, bacterial suspensions of *L. monocytogenes* and *S.* Typhimurium were diluted in broth to an OD_{600} of 0.3 and 0.5, equaling 10^9 CFU mL^{-1}, respectively. Afterward, the bacterial suspensions were serially diluted three times with steps of 10^{-1} and used for the test.

Two mL of ANCC suspensions at different concentrations were mixed with 1 mL of broth and 10 μL of bacteria suspension was added to the test tubes. After 3-hrs incubation at 37 °C, 10 µL of ANCC-bacterial suspensions was placed on agar plates, and incubated statically overnight at 37 °C. Then, the number of colonies was enumerated for each sample to calculate the percent of bacterial cell reduction according to the following equation 1:

$$Bacterial\ cell\ reduction = \frac{A - B}{A} \times 100 \qquad 1$$

Here A is the number of viable colonies in the absence of ANCC and B is the number of viable colonies after ANCC contact. All measurements were carried out in triplicates.

5.4. Results and discussion

5.4.1. Synthesis of hairy ANCC

The aldehyde content of DAMF was determined to be ~8 mmol g^{-1} after periodate oxidation of cellulose fibers (Scheme 5- 2 (a)). Assuming that the crystalline regions of cellulose nanofibrils have a cross-section of 5×5 nm (10×10 cellulose chains) and that the accessible cellulose molecules are located on the outer surface of the crystalline regions and in the amorphous regions, then an aldehyde content of 8 mmol g^{-1} corresponds to a full conversion (12.5 mmol g^{-1}) of the accessible cellulose molecules, if 30% of the cellulose is located in amorphous regions. (If x is the fraction of cellulose in the amorphous region, and 40% of the chains are located on the external surface, then $0.4 \cdot 12.5 + 12.5\ x = 8$, thus $x = 0.3$). This is consistent with the crystallinity of cellulose in kraft fibers, which is about 70% [13, 14]. Amination of DAMF was achieved through a Schiff base reaction to produce imine bonds between aldehyde groups of DAMF and amine groups of ammonia. This was followed by reducing the imine bonds to primary amines using $NaBH_4$ as reducing agent. The amination reaction steps are shown in Scheme 5- 2 (b). In addition to the ammonia, ammonium acetate ($NH_4^+CH_3COO^-$) was used which dissociated into ammonium (NH_4^+) and acetate (CH_3COO^-). The resulting ammonium protonates the formed imines, thereby releasing more ammonia into the reaction. ANCC was formed by adjusting the pH of the DAmMF suspension to acidic range (~2.5) and heating at 60 °C. The acidic pH of the solution resulted in the protonation of surface amine groups of DAmMF. Using the hot water treatment, aminated fibers were broken up into nano-scale structures by the electrostatic repulsion between the positively charged protonated amine groups. The acidic pH also helps in breaking the amorphous cellulose chains by hydrolysis. Moreover, at this pH, the solubility of the amine functionalized amorphous regions is enhanced at elevated temperatures. Consequently, the crystalline segments are released in the medium as individual nanorods with protruding hairs. Depending on whether we started with air-dried or solvent-exchanged DAMF, the weight of non-fibrillated DAmMF was found to be ~45% and < ~5%, respectively after hot-water treatment. A lower amount of non-fibrillated fibers implies that a higher nanocellulose content was obtained. For comparison, the weight fraction of sterically stabilized nanocrystalline cellulose (SNCC) was ~30% [3].

After removing the non-fibrillated fibers, isopropanol as cosolvent was used to isolate ANCC particles from the supernatant. Similar to other synthetic pathways for the formation of hairy nanocellulose [15, 16], besides nanoparticles (here ANCC), copolymers of dissolved diaminated cellulose derivatives (here DAmC) are formed. The yield of ANCC was ~25 % from air-dried DAMF and ~45-50 % from solvent-exchanged DAMF at the end of the reaction. In both cases, the remaining dissolved diaminated cellulose was ~10%. The amount of dissolved DAmC produced in the reaction is likely much larger than 10%. During dialysis of dissolved diaminated cellulose (DAmC), a fraction of it adsorbs on the surface of the dialysis bag and some of the DAmC passes through the pores of the membrane, either because DAmC contains small molecules as a result of hydrolysis under the acidic hydrothermal post-treatment conditions, and/or non-hydrolyzed DAmC could pass through the pores because the molecules are rod-like due to their high charge and can pass through holes which are much larger than their diameter.

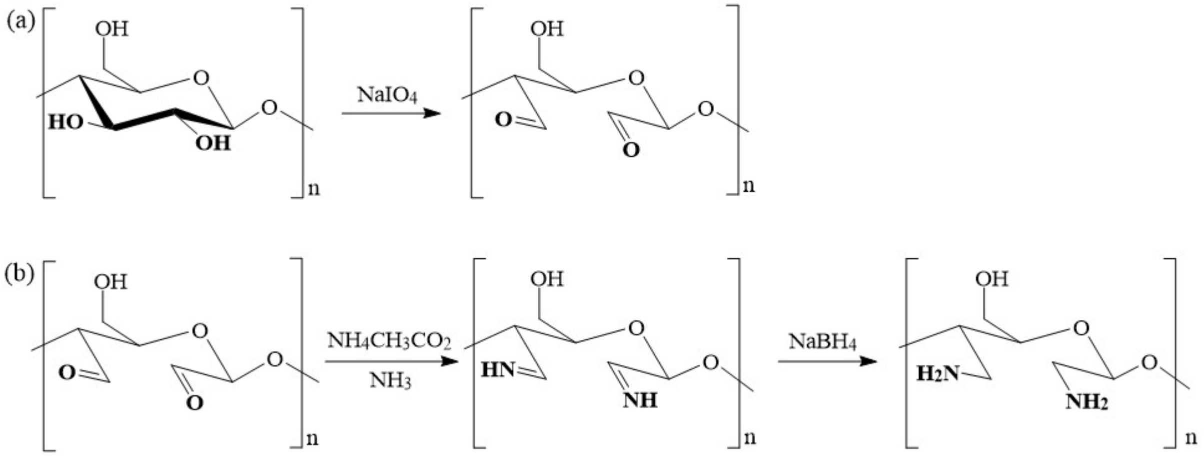

Scheme 5- 2. (a) Periodate oxidation of cellulose fibers to produce dialdehyde modified fibers (DAMF) and (b) reductive amination of DAMF, occurring in two successive steps. The first part is the nucleophilic addition to the carbonyl group of the aldehyde groups by ammonia to form an imine. The second part is the reduction of the imine to an amine using $NaBH_4$ as reducing agent. The final product is in the form of fibers, which are broken up by a hot acid water treatment.

5.4.2. Amine and aldehyde content

The content of primary amine groups of ANCC was measured by conductometric titration (Fig. 5-1a). During this reaction, a strong base (NaOH) is added first to fully deprotonate the amine groups, followed by titration with a strong acid (HCl) (Equations 2-3).

$$RNH_3^+ + NaOH \rightarrow RNH_2 + Na^+ + H_2O \tag{2}$$

$$RNH_2 + HCl \rightarrow RNH_3^+ + Cl^- \tag{3}$$

The amine content was determined to be ~3.5 mmol g^{-1} for ANCC from air-dried DAMF and ~5.5 mmol g^{-1} for ANCC from solvent-exchanged DAMF. The solvent-exchange method is to be preferred, as the air-dried fibers can retain up to 8% moisture, which might interfere with the amination reaction and the pores collapse as result of drying, thereby reducing the accessibility to the chemicals, which lowers the efficiency of the amination reaction. The resultant amine contents in both cases are less than the initial introduced aldehyde groups (~8 mmol g^{-1}). This can be explained by the high charge of the cellulose chains, which likely results in the dissolution of the cellulose chains located on the outer surface of the crystals. If all the chains on the outer surface were to dissolve, the amine content would be $0.3 \cdot 12.5 = 3.8$ mmol g^{-1}, which is lower than the observed value (5.5 mmol g^{-1}). Thus, likely only a fraction of the outer surface goes into solution. Another possible explanation is that the ends of the crystal segment are being converted into amorphous chains with a rate faster than the rate on the external surface (Scheme 5- 3). This results in a higher content of amorphous domains, thereby obtaining more than 3.8 mmol g^{-1} amine content. In a previous study [17], we showed that an oxidative modification enhances the solubility of cellulose chains at the crystal surface of NCC to the extent that they dissolve and detach from the crystal. At the same time, it was shown that the oxidation reaction proceeded faster at the ends of the crystal than on the outer surface, resulting in amorphous regions at the ends of the crystal. The same shortening of the crystalline regions might have occurred during the reduction reaction used for the synthesis of ANCC. To account for a charge density of 5.5 mmol g^{-1}, the amount of cellulose in the amorphous parts must have increased from 30 to 40%.

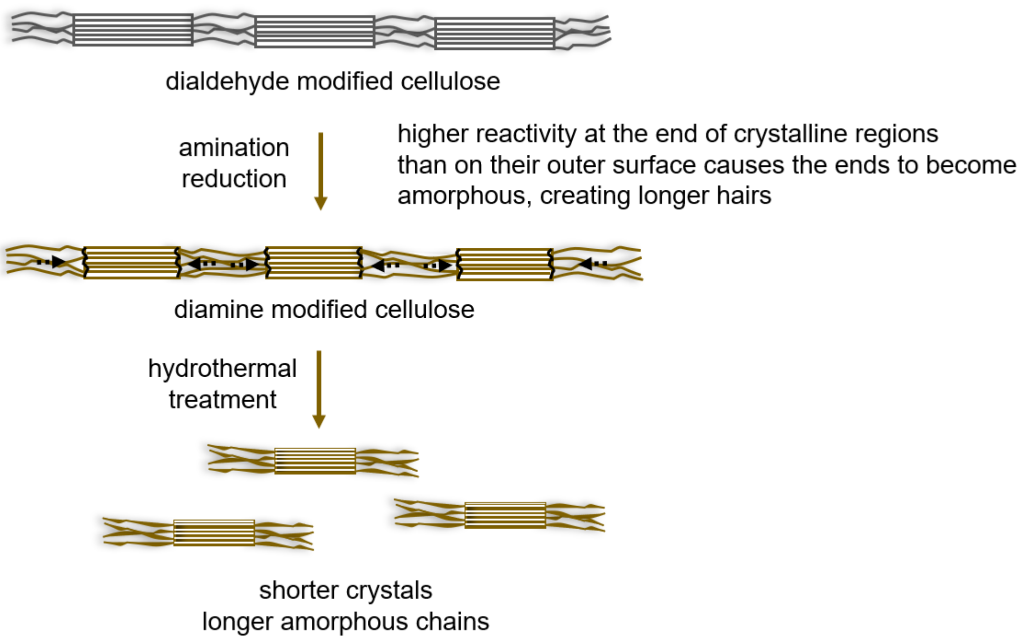

Scheme 5- 3. Schematic representation of creating ANCC with shorter crystalline region and longer protruding amorphous chains through converting part of crystalline segment into amorphous chains. Crystalline regions have higher reactivity at the end than their outer surface. The advancing reaction front is indicated by black vertical wiggles.

To examine the efficiency of the reductive amination reaction, the aldehyde content of fibers before and after amination reaction was measured. The intact DAMF showed a ~8 mmol g^{-1} aldehyde content, while after amination reaction this value was reduced to ~2.5 and 0 mmol g^{-1} for DAmMF obtained from air-dried and solvent-exchanged DAMF, respectively. This indicates that using solvent exchange of DAMF from water to ethanol, a 100% conversion is achieved, consistent with a charge content of 12.5 mmol g^{-1} in the accessible chains.

ANCC containing diamino groups shows two different pK_b values through conductometric titration, resulting from the amination of C2 and C3 on the glucose units.

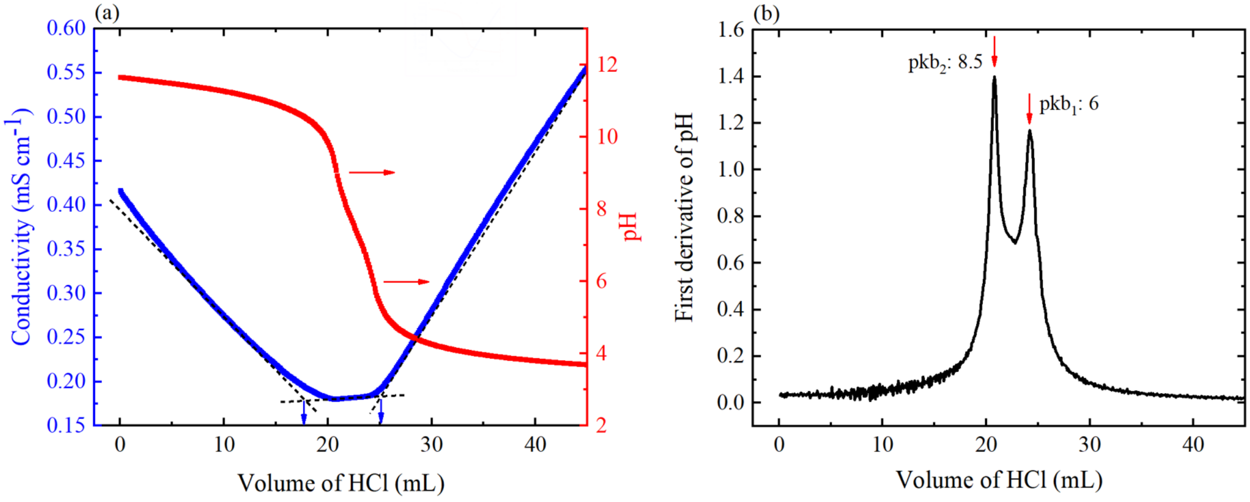

Fig. 5- 1. (a) Conductometric titration of ANCC using a strong acid (HCl, 0.01 M), indicating that ~7.5 ± 1 mL of acid (shown with blue arrows) is required to neutralize all the weak base, implying a functional group content of ~5.5 mmol of -NH_2 per gram of ANCC with two pK_b values shown with red arrows; (b) first derivative of pH titration curve indicating the location of pK_b values.

The following characterizations were conducted on ANCC from solvent exchanged DAMF due to its higher amine content, which is more favorable for future applications.

5.4.3. Morphology of ANCC

To investigate the morphology of the developed ANCC particles, AFM and TEM images were captured and the results are shown in Fig. 5- 2. As shown in the AFM image (Fig. 5- 2a), the nanoparticles are in the shape of typical rod-like nanosized cellulose particles, which is consistent with those of previous NCCs isolated via an oxidation reaction [2, 3] and acid hydrolysis [18]. We refer to these rod-like nanoparticles as aminated nanocrystalline cellulose (ANCC).

The dimensions of rod-like ANCC prepared by oxidation-reductive amination reaction were determined by TEM images, an example of which is shown in Fig. 5- 2b. The length and diameter of nanoparticles were, on average, ~120 nm and ~5 nm, respectively. The length is consistent with the value obtained from DLS measurements (~140 nm). The DLS size of ANCC is smaller than that of hairy ENCC in previously reported studies [1, 2]. This might be due to the acidic heat-treatment in the synthesis process, carried out at pH of ~2.5, which causes a shortening of the hairs as a result of heat-catalyzed acid hydrolysis. In the ENCC synthesis pathway, this step is implemented at neutral pH.

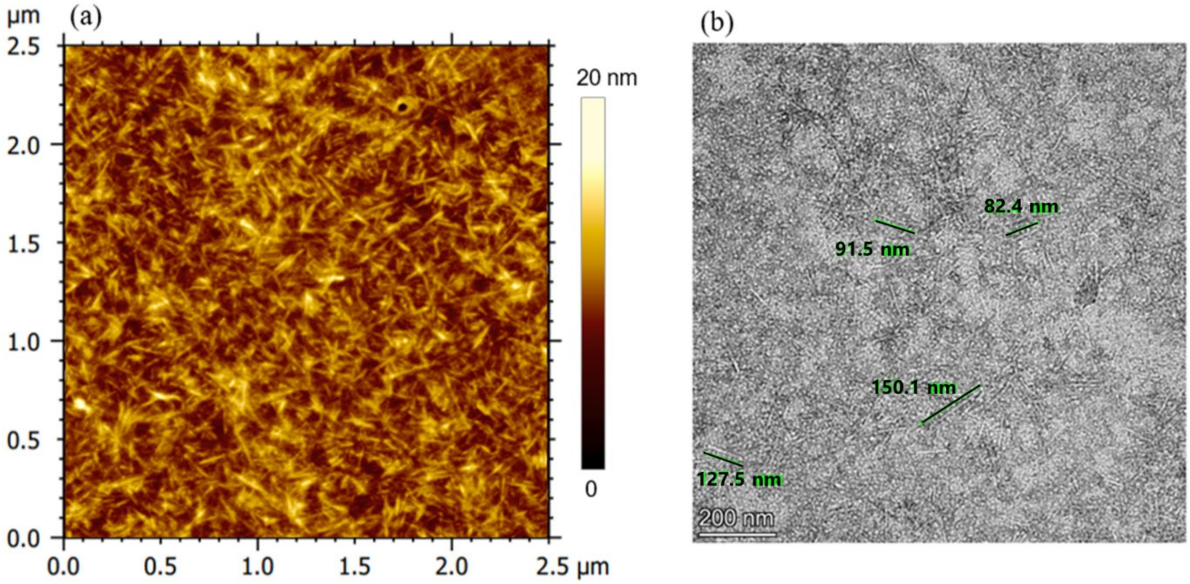

Fig. 5- 2. (a) AFM height image and (b) TEM image of ANCC.

5.4.4. Effects of cosolvent and pH on particle size and charge density of ANCC

This experiment was performed to verify the presence of the hairs protruding from the crystalline segment of ANCC and to investigate the stability mechanism of the corresponding suspension.

Fig. 5- 3a shows the particle size changes of ANCC due to cosolvent addition. Diaminated cellulose chains (hairs), protruding from the poles of crystalline segments, do not dissolve in isopropanol. Therefore, by adding isopropanol to hairy ANCC suspension, the Flory–Huggin's polymer–solvent interaction parameter (χ) is increased. When it reaches the value of 0.5, steric

repulsion between ANCC particles is eliminated and at the same time the electrostatic repulsion is reduced due to a reduction in dielectric constant, resulting in ANCC aggregation. Before reaching this value, the solvent (water/isopropyl alcohol mixture) becomes progressively poorer, leading to a contraction of the hairs. Accordingly, the size of ANCC, measured by DLS, first showed a slight decrease with isopropanol addition due to the contraction of the hairs, and then an increase due to the flocculation of ANCC particles. The equivalent hydrodynamic diameter of ANCC decreased from ~140 nm to 130 nm in the presence of 1% cosolvent. This is proof that ANCC is sterically stable as a result of the protruding hairs. As we show below, the nanoparticles are also subject to electrostatic repulsion (at low pH), hence they are electrosterically stable.

The effects of pH on particle size and ζ-potential of ANCC were also studied (Fig. 5- 3b). By decreasing the pH from 5 to 3, an increase in the particle size from ~135 nm to ~145 nm was observed. This is likely due to the expansion of the hairs as a result of increasing electrostatic repulsion among the protonated amine groups. Outside the pH range 3-5, the particle size changes drastically, implying ANCC aggregation, which correlates with the changes in ζ-potential. The ζ-potential of ANCC was found to be +10 ± 0.7 mV at pH ~5, proving that amine groups are present on ANCC, inducing positive charges. Since negatively charged impurities in water, which are difficult to eliminate completely, can be easily adsorbed on amine groups, we purified ANCC suspension using DOWEX 1X4-50 ion-exchange resin (Sigma-Aldrich-Canada). After contacting the suspension with resins for 1 hr, the ζ-potential value of ANCC at the same pH increased by 10 mV, proving the presence of surface-active impurities. The presence of surface-active impurities in DI has also been seen in SNCC suspensions, where they change the surface charge from zero to negative.[3] As seen in Fig. 5- 3b, the charge density of amine groups greatly depends on the solvent pH.

At pH ~3, the amine groups undergo maximum protonation ($-NH_2 \rightarrow -NH_3^+$), which results in a ζ-potential of +34 mV leading to highest stability. The lower the pH, the higher the amount of the protonated amine groups. At pH ~1.5, the ζ-potential value is lowered due to the increase in ionic strength as a result of excess addition of HCl which screens the charges. This leads to the reduction in the electrophoretic mobility [19]. By increasing the pH toward the alkaline range, the ζ-potential shifts to negative values (-4 mV at pH ~7 and -31 mV at pH ~10). At pH 7, the negative charges are likely due to the presence of anionic impurities, present in the water. The effect of impurities on ζ-potential was previously reported for SNCC, which showed a negative value at lower SNCC concentration and approached zero at higher concentrations, for which there were far fewer impurities per particle [3]. At a pH around 10, the deprotonation of the amine groups ($-NH_3^+ \rightarrow -NH_2$) and hydroxyl groups on C6 of cellulose chains ($OH \rightarrow O^-$) results in higher negative values. The deprotonation and the increasing ionic strength from NaOH addition results in ANCC aggregation, as shown in Fig. 5- 3c. large aggregates formed at pHs above 7, were beyond the detection limit of DLS.

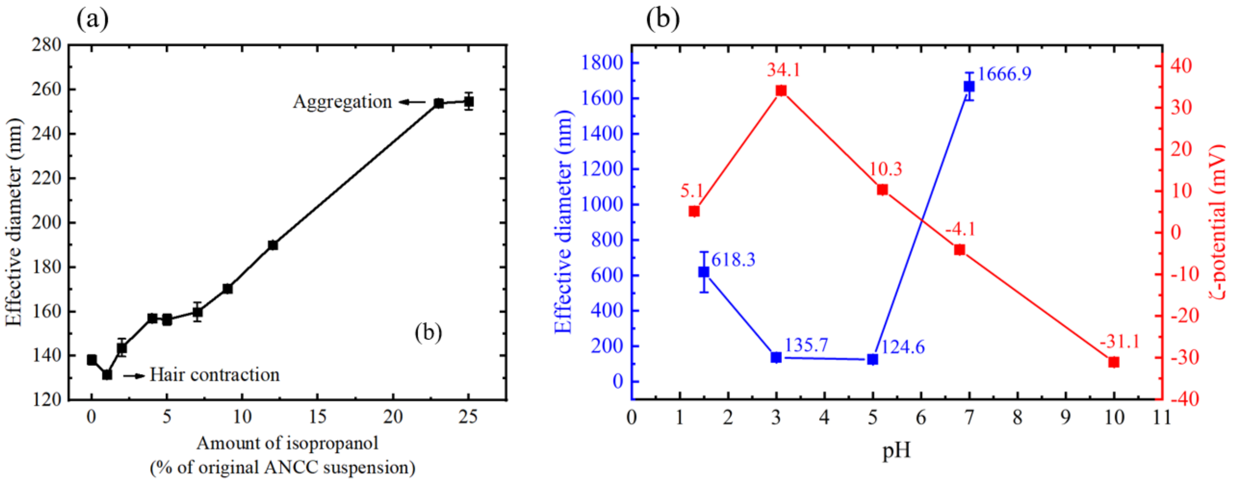

Fig. 5- 3. (a) Equivalent spherical diameter of ANCC measured by DLS as a function of cosolvent addition at pH ~5; (b) equivalent spherical diameter and ζ-potential of ANCC under different pH conditions, measured at T~22 °C by DLS and electrophoretic light scattering, respectively.

5.4.5. FTIR and solid-state ^{13}C NMR spectroscopy

To investigate the surface chemistry of the developed ANCC and confirm the introduced primary amine groups, ATR-FTIR and CP/MAS ^{13}C NMR were performed, and the spectra are shown in Fig. 5- 4.

In the FTIR spectrum of ANCC (Fig. 5- 4a), the absorption peaks of primary amine groups, typically appearing around 3400-3250 cm^{-1}, overlapped with the stretching vibrations of O─H in its cellulosic structure. The peaks at 3300 and 2900 cm^{-1} in all cellulosic samples are due to O─H and C─H stretching vibrations[23]. Thus, the amine groups cannot be clearly detected; instead, ANCC indicates a broad sharp peak at 1635 cm^{-1} for the C─NH_2 bending vibrations. Also, disappearance of the two characteristic peaks of aldehyde groups at 1726 cm^{-1} and 878 cm^{-1} implies the conversion of the aldehyde to amine groups.

In the NMR spectra (Fig. 5- 4b), DAMF shows a broad peak spanning from 105 to 85 ppm with a trace of the peak from carbonyl groups appearing at around 200 ppm. The absence of carbonyl signals demonstrates that the aldehyde groups of DAMF have formed hemiacetal linkages with primary O─H groups on DAMF chains [22]. ANCC shows multiple peaks appearing from 105 to 55 ppm, displaying the carbons of glucose units in the cellulose structure, specified as: 65 ppm for C6, 80-70 ppm for C2, C3, C5, 90 ppm for C4 and 105 ppm for C1 [20, 21]. The absence of the broad peak at 200 ppm in the ANCC spectrum indicates the conversion of aldehyde groups. Also, the sharp peak of C4 itself signifies the formation of the crystalline nanoparticles. The C4' peak, which typically appears at ~85 ppm in the intact cellulose structure, is not detectable for ANCC; thus, strengthening the claim of shortening the hairs as a result of the heat-catalyzed acid hydrolysis.

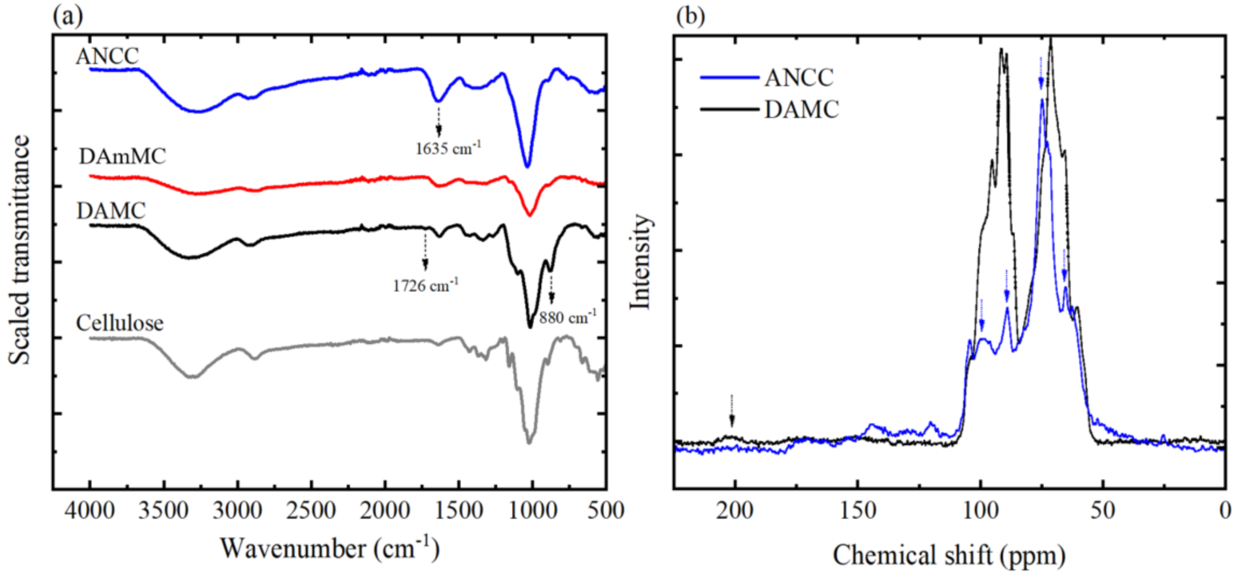

Fig. 5- 4. (a) FTIR spectra of cellulose pulp, DAMF, DAmMF and ANCC and (b) solid-state ^{13}C CP/MAS NMR spectra of DAMF and ANCC.

5.4.6. XPS analysis

To further examine the amine formation, XPS was performed on freeze-dried ANCC and the spectra are shown in Fig. 5- 5. The spectrum of ANCC indicates a N1s peak at about 400 eV which is mostly due to the presence of amine groups in the chemical structure of ANCC, confirming its successful amination reduction reaction. From XPS analysis (Fig. 5- 5a), the ANCC has 8.5 % nitrogen, corresponding to 5.7 mmol g^{-1} amine content, consistent with conductometric titration (5.5 mmol g^{-1}).

To better comprehend the nature of the carbon and nitrogen bonding in ANCC, C1s and N1s peaks were deconvoluted into their constituent sub-peaks, as shown in Fig. 5- 5b and Fig. 5- 5c, respectively. For C1s (Fig. 5- 5b), the peaks at 284.8 ± 0.1, 286.1 ± 0.1, and 287.3 ± 0.1 eV are correlated to sp^3 (C-C), glycosidic bond (C-O-C), amine bond (C-N) and hydroxyl group (C-O), respectively [5, 22]. For N1s (Fig. 5- 5c), the peaks at 399.1 ± 0.2, 400.3 ± 0.2, and 401.1 ± 0.2 eV correspond to primary amine, secondary amine, and protonated nitrogen, respectively [23, 24].

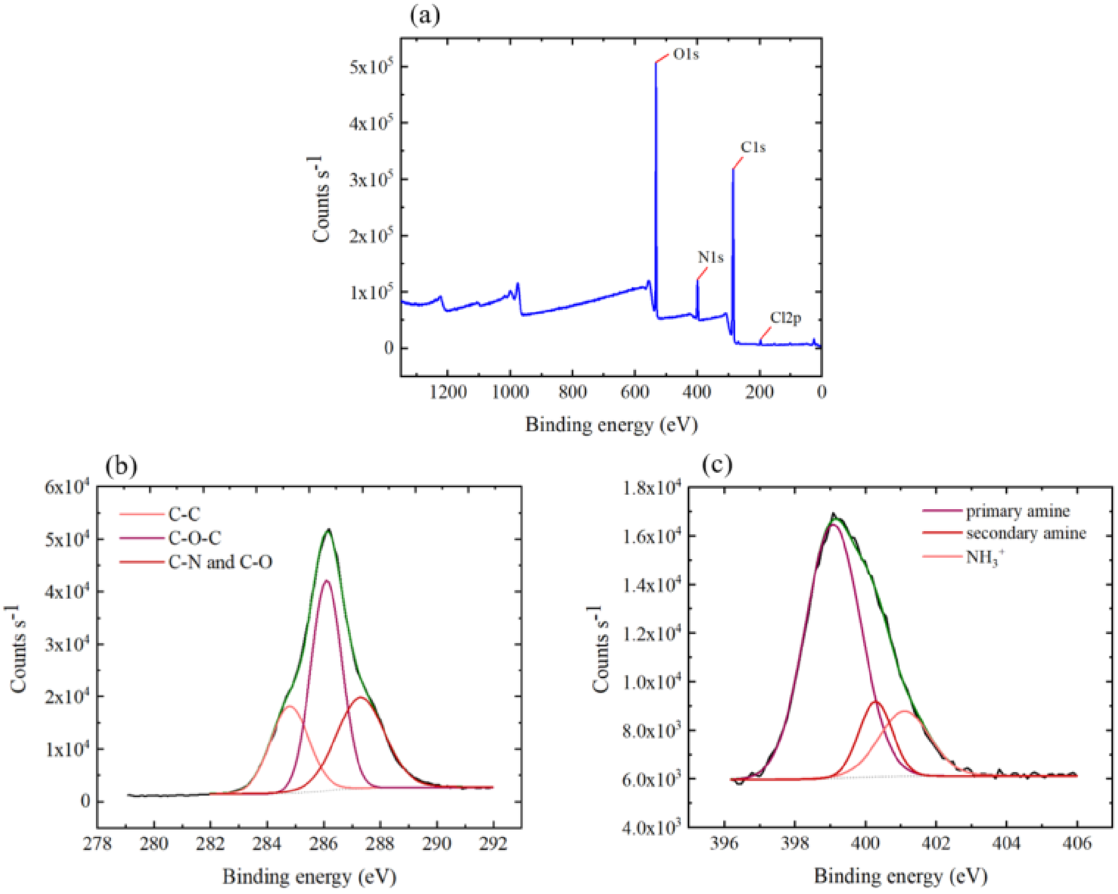

Fig. 5- 5. (a) XPS spectrum of ANCC; (b) C1s deconvoluted into C-O-C, C-N, C-O and C-C; (c) N1s peaks deconvoluted into protonated amine, primary and secondary amine groups.

5.4.7. Evaluating antibacterial activity of positively charged ANCC.

Hairy ANCC bearing a high local density of amine groups is a promising candidate for inducing antibacterial activity. We hypothesize that, similar to other cationic antibacterial compounds like chitosan[25], ANCC can electrostatically attack the negatively charged cell membrane of bacteria.

To prove our hypothesis, we tested the viability of *L. monocytogenes* and *S.* Typhimurium after 3-hrs exposure to ANCC particles with 3.5 mmol g^{-1} and 5.5 mmol g^{-1} amine content. The results, expressed as the percentage of bacterial cell reduction (see Equation 1), are shown in Fig. 5- 6.

As observed in Fig. 5- 6a, ANCC with 3.5 and 5.5 mmol g^{-1} amine groups started killing *L. monocytogenes* at concentrations of 1000 ppm and 150 ppm, respectively. At lower concentrations, no antibacterial activity was observed for ANCC against this Gram-positive bacterium. ANCC with 5.5 mmol g^{-1} started its antibacterial activity at significantly lower concentrations compared to its homologue with 3.5 mmol g^{-1} amine content implying that the higher amine content results in higher antibacterial activities. By the selected CFU counting protocol, increasing the ANCC concentration to above 1500 ppm resulted in gel formation in the bacteria suspension, causing difficulty in plating.

The antibacterial activities of ANCC against Gram-negative *S.* Typhimurium are shown in Fig. 5-6b. Similar to the Gram-positive bacteria, the higher the amine content of ANCC, the higher its antibacterial activity. The antibacterial effect of ANCC is more significant against Gram-negative *S.* Typhimurium than against Gram-positive *L. monocytogenes* which is likely due to the thicker and more rigid cell wall of the Gram-positive bacteria. The mechanism of ANCC bactericidal action is likely similar to cationic biocides, such as chitosan. It consists of adsorption onto the negatively charged cell surface and damaging the outer membrane of bacteria by electrostatic interaction, increasing cell wall permeability. Cationic biocides also reduce the biosynthesis of adenosine triphosphate (ATP), responsible for energy transport within the cell essential for many processes in bacteria.[26]

At concentration of 1500 ppm, the two ANCC particles show a similar antibacterial activity against both bacteria. It could be that, besides the effect of amine groups, ANCC particles likely coat the bacterial cells, thereby limiting their access to nutrients, leading to cell death.

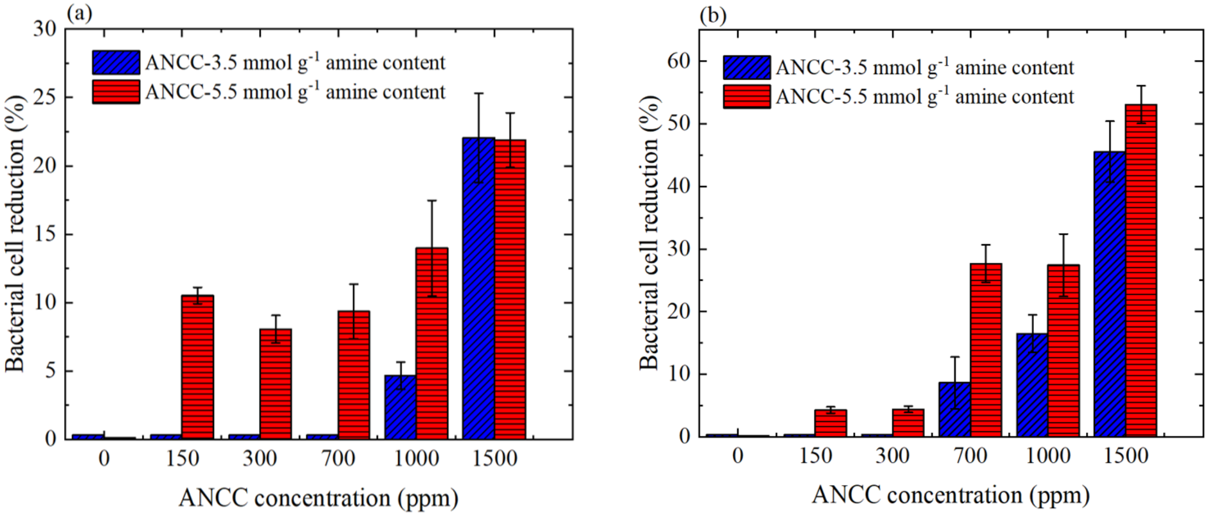

Fig. 5- 6. Evaluation of the antibacterial activity of hairy ANCC particles carrying 3.5 mmol g^{-1} and 5.5 mmol g^{-1} primary amine groups against (a) Gram-positive *L. monocytogenes* and (b) Gram-negative *S.* Typhimurium through reduction in viable colonies after 3-hrs contact. The error bars represent the standard deviation of three independent replicates.

5.5. Conclusions

Exploring new members of colloidal hairy nanocelluloses family, easily tunable in terms of size and surface functional groups, continues to attract widespread interest. Hairy nanocellulose consists of a rod-like nanocrystal with hairs protruding from both ends, which are more accessible than the crystalline segment for chemical reactions and which also enhance colloidal stability, both sterically and electrosterically. It was previously shown that hairs provide an extensive platform for the accommodation of carboxyl [1], aldehyde [3], carboxyl-aldehyde [4] and quaternary ammonium groups [5]. Also, by chopping off the dangling amorphous hairs via the controlled acid hydrolysis, a variety of hairy nanocelluloses with different sizes were developed [2].

Here, we have presented a methodology to synthesize amine-functionalized hairy nanocellulose by periodate oxidation and reductive amination of cellulose fibers, followed by acidic hot-water treatment. Introducing positively charged amine groups onto DAMF, greatly improves the efficiency of fibrillation of DAMF into nanosized structures under aqueous thermo-treatment. ANCC has a width of 5 nm and a length of about 120 nm, an amine content of ~5.5 mmol g^{-1} and a ζ-potential of ~+35 mV at pH 3. The amine content was verified with conductometric titration and XPS. The successful functionalization of primary amine groups onto nanocellulose was confirmed by FTIR, solid carbon-13 NMR and XPS analysis. It was shown that ANCC is electrosterically stabilized. Moreover, ANCC shows antibacterial activity, significantly higher against Gram-negative bacteria than Gram-positive ones.

ANCC can readily be further functionalized using bioconjugation or Schiff base reactions to find applications in a variety of fields including drug delivery, wastewater treatment, packaging and many more. As an example, by covalently linking a type of carboxyl-bearing photosensitizer to the primary amine groups of ANCC, we have developed biodegradable photo-bactericidal surfaces suitable for food packaging [27].

5.6. References

1. Yang, H.; Alam, M. N.; van de Ven, T. G. M., Highly charged nanocrystalline cellulose and dicarboxylated cellulose from periodate and chlorite oxidized cellulose fibers. *Cellulose* **2013,** *20* (4), 1865-1875.

2. Koshani, R.; van de Ven, T. G. M., Electroacoustic characterization of trimmed hairy nanocelluloses. *Journal of Colloid and Interface Science* **2020,** *563*, 252-260.

3. Yang, H.; Chen, D.; van de Ven, T. G. M., Preparation and characterization of sterically stabilized nanocrystalline cellulose obtained by periodate oxidation of cellulose fibers. *Cellulose* **2015,** *22* (3), 1743-1752.

4. Yang, H.; Sheikhi, A.; van de Ven, T. G. M., Reusable green aerogels from cross-linked hairy nanocrystalline cellulose and modified chitosan for dye removal. *Langmuir* **2016,** *32* (45), 11771-11779.

5. Yang, H.; van de Ven, T. G. M., Preparation of hairy cationic nanocrystalline cellulose. *Cellulose* **2016,** *23* (3), 1791-1801.

6. Sheikhi, A.; Kakkar, A.; van de Ven, T. G. M., Nanoengineering colloidal and polymeric celluloses for threshold scale inhibition: towards universal biomass-based crystal modification. *Materials Horizons* **2018,** *5* (2), 248-255.

7. Sheikhi, A.; Yang, H.; Carreau, P. J.; van de Ven, T. G. M., Colloidal nano-toolbox for molecularly regulated polymerization: chemorheology over 6 decades of viscoelasticity. *Materials Horizons* **2017,** *4* (6), 1165-1170.

8. Hosseinidoust, Z.; Alam, M. N.; Sim, G.; Tufenkji, N.; van de Ven, T. G. M., Cellulose nanocrystals with tunable surface charge for nanomedicine. *Nanoscale* **2015,** *7* (40), 16647-16657.

9. Tavakolian, M.; Lerner, J.; Tovar, F. M.; Frances, J.; van de Ven, T. G. M.; Kakkar, A., Dendrimer directed assembly of dicarboxylated hairy nanocellulose. *Journal of colloid and interface science* **2019,** *541*, 444-453.

10. Kim, U.-J.; Kuga, S.; Wada, M.; Okano, T.; Kondo, T., Periodate oxidation of crystalline cellulose. *Biomacromolecules* **2000,** *1* (3), 488-492.

11. Zivanovic, S.; Davis, R.; Golden, D., Chitosan as an antimicrobial in food products. In *Handbook of Natural Antimicrobials for Food Safety and Quality*, 2015; Vol. 20, pp 153-181.

12. Sheikhi, A.; Yang, H.; Alam, M. N.; van de Ven, T. G. M., Highly stable, functional hairy nanoparticles and biopolymers from wood fibers: towards sustainable nanotechnology. *JoVE (Journal of Visualized Experiments)* **2016,** (113), e54133.

13. Mahrous, F.; Koshani, R.; Tavakolian, M.; Conley, K.; van de Ven, T. G. M., Formation of hairy cellulose nanocrystals by cryogrinding. *Cellulose* **2021**, 1-17.

14. Moradian, M.; Islam, M. S.; van de Ven, T. G. M., Insoluble Regenerated Cellulose Films Made from Mildly Carboxylated Dissolving and Kraft Pulps. *Industrial & Engineering Chemistry Research* **2021,** *60* (15), 5385-5393.

15. Sheikhi, A.; van de Ven, T. G. M., Colloidal aspects of Janus-like hairy cellulose nanocrystalloids. *Current Opinion in Colloid & Interface Science* **2017,** *29*, 21-31.

16. van de Ven, T. G. M.; Sheikhi, A., Hairy cellulose nanocrystalloids: a novel class of nanocellulose. *Nanoscale* **2016,** *8* (33), 15101-15114.

17. Conley, K.; Whitehead, M.; van de Ven, T. G. M., Chemically peeling layers of cellulose nanocrystals by periodate and chlorite oxidation. *Cellulose* **2016,** *23* (3), 1553-1563.

18. Koshani, R.; van de Ven, T. G. M., Carboxylated Cellulose Nanocrystals Developed by Cu-Assisted H2O2 Oxidation as Green Nanocarriers for Efficient Lysozyme Immobilization. *Journal of Agricultural and Food Chemistry* **2020,** *68* (21), 5938-5950.

19. Safari, S.; Sheikhi, A.; van de Ven, T. G. M., Electroacoustic characterization of conventional and electrosterically stabilized nanocrystalline celluloses. *Journal of Colloid and Interface Science* **2014,** *432*, 151-157.

20. Groszewicz, P. B.; Mendes, P.; Kumari, B.; Lins, J.; Biesalski, M.; Gutmann, T.; Buntkowsky, G., N-Hydroxysuccinimide-activated esters as a functionalization agent for amino cellulose: synthesis and solid-state NMR characterization. *Cellulose* **2020,** *27* (3), 1239-1254.

21. Koshani, R.; van de Ven, T. G. M.; Madadlou, A., Characterization of carboxylated cellulose nanocrytals isolated through catalyst-assisted H2O2 oxidation in a one-step procedure. *Journal of Agricultural and Food Chemistry* **2018,** *66* (29), 7692-7700.

22. Ly, B.; Thielemans, W.; Dufresne, A.; Chaussy, D.; Belgacem, M., Surface functionalization of cellulose fibres and their incorporation in renewable polymeric matrices. *Composites Science and Technology* **2008,** *68* (15-16), 3193-3201.

23. Ravi, S.; Zhang, S.; Lee, Y.-R.; Kang, K.-K.; Kim, J.-M.; Ahn, J.-W.; Ahn, W.-S., EDTA-functionalized KCC-1 and KIT-6 mesoporous silicas for Nd3+ ion recovery from aqueous solutions. *Journal of Industrial and Engineering Chemistry* **2018,** *67*, 210-218.

24. Tavakolian, M.; Munguia-Lopez, J. G.; Valiei, A.; Islam, M. S.; Kinsella, J. M.; Tufenkji, N.; van de Ven, T. G. M., Highly Absorbent Antibacterial and Biofilm-Disrupting Hydrogels from Cellulose for Wound Dressing Applications. *ACS Applied Materials & Interfaces* **2020,** *12* (36), 39991-40001.

25. Kim, C. H.; Choi, J. W.; Chun, H. J.; Choi, K. S., Synthesis of chitosan derivatives with quaternary ammonium salt and their antibacterial activity. *Polymer Bulletin* **1997,** *38* (4), 387-393.

26. Marinelli, L.; Di Stefano, A.; Cacciatore, I., Carvacrol and its derivatives as antibacterial agents. *Phytochemistry Reviews* **2018,** *17* (4), 903-921.

27. Koshani, R.; Zhang, J.; Lu, X.; van de Ven, T. G. M.; Wang, Y., Modified hairy nanocrystalline cellulose as photobactericidal nanofillers for food packaging application. *ACS Sustainable Chemistry and Engineering* **2021,** *DOI: 10.1021/acssuschemeng.1c02289*.

Chapter 6

CONCLUSIONS AND FUTURE WORK

6.1. Conclusions

A new protocol for synthesizing a new type of cellulose derivative was developed in this thesis. This gave rise to the successful fabrication of various forms of aminated cellulose including diiminocellulose fiber (DImF, diaminocellulose fiber (DAmF), diaminocellulose (DAmC) and aminated nanocrystalline cellulose (ANCC) and some of their potential applications were explored. The preparation methods for these celluloses are summarized in Fig. 6- 1. The physical properties and applications explored in this thesis are summarized in Table 6- 1. These new aminated celluloses are not only additions to the growing family of cellulose derivatives but have very promising industrial and medical applications.

DImF was prepared by complete oxidation of OH groups in the C2 and C3 position by periodate. After reaction, DImF is the form of fibers. In chapter 4, DImF was used in absorbing Pb ions for water.

DAmF was prepared by complete oxidation of OH groups in the C2 and C3 position by periodate, followed by a reductive amination reaction. DAmF is insoluble at room temperature and pH above 2. DAmF was used to adsorb negatively charged dye (PR), it showed high and fast adsorption at pH 2. Complete desorption of dye occurred at pH 10 and the fibers were intact and performed well after 5 cycles. This makes it an excellent reusable green adsorbent for anionic dyes. The fibers were also used in the sorption of positively charged lead ions. Maximum sorption occurred at pH 8 but it also shows good adsorption at pH 5.5 when pH was not adjusted. This was made possible by coordination between the amine groups and Pb^{2+} ions.

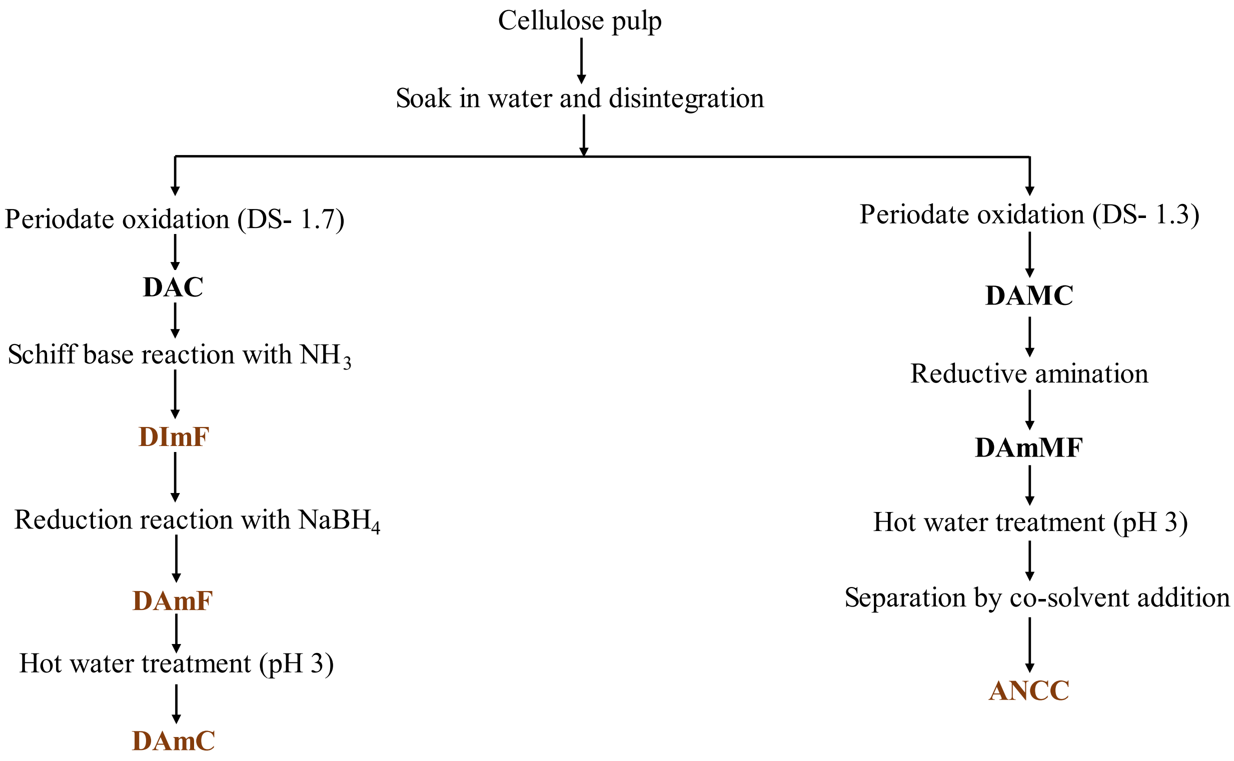

Fig. 6- 1. Preparation of various aminated cellulose including DAmF, DAmC and ANCC

Table 6- 1. Summarization of physical properties of aminated cellulose

	Physical form	Amine content (mmol g^{-1})	Application
DImF	Fibers	9.5	Lead removal from solution
DAmF	Fibers	9.5	Dye and lead removal from solution
DAmC	Polymeric chains (soluble)	9.5	Dye removal from solution
ANCC	Nanocellulose	5.5	Anti-microbial activity

DAmC was produced by subjecting DAmF to a hot water treatment at pH 3. DAmC is electrosterically stable and remain in solution when cooled to room temperature. DAmC was stable across all pH except 7, at which half of the amine groups on the ring is protonated and the other is non protonated. This leads to the closure of the rings in the polymer via hydrogen bonding which in turn leads to destabilization. DAmC was used in removing dye (PR) from solution. DAmC was rapidly and efficiently flocculated by the dye, leading to its removal from solution.

ANCC was prepared by subsequent partial periodate oxidation and reductive amination of cellulose fibers, followed by an acidic hot water treatment. ANCC has a width of 5 nm, a length of about 120 nm, and a ζ-potential of ~+35 mV at pH 3. It was shown that ANCC is electrosterically stabilized and ANCC shows antibacterial activity, significantly higher against Gram-negative bacteria than Gram-positive ones.

6.2. Future Works

- DAmF can be used as an adsorbent in a multi-metal system of divalent cations (Co^{2+}, Ni^{2+}, Zn^{2+}, Cd^{2+} and Pb^{2+}) to study its selectivity for any of the heavy metals. Also, the reusability of the fibers in this system could be explored by performing desorption reactions.
- For DAmC, it could be useful to investigate the molecular weight and also study the effect of the degree of substitution on the molecular weight. It has been reported that chlorite oxidation reduces the degree of polymerization of cellulose derivative, dicarboxyl cellulose (DCC)[1], it will be advantageous to know if the same happened for the reductive amination reaction.
- DAmC, DAmF and ANCC have a high amount of amine groups that can be further functionalized and utilized. Since amine groups can participate in bioconjugation or Schiff

base reactions, they can be employed as cross-linkers in gels and thin film applications used for drug delivery, food packaging and many more.

- DAmC and ANCC can be used for capturing atmospheric CO_2.

1. Singh, O., Kinetics and mechanism of hypochlorite oxidation of cellulose. *Textile Dryer & Printer* **1982**, 35-38.